MUSiC - A Model Unspecific Search in CMS based on 2010 LHC data

Von der Fakultät für Mathematik, Informatik und Naturwissenschaften der RWTH-Aachen University zur Erlangung des akademischen Grades eines Doktors der Naturwissenschaften genehmigte Dissertation

vorgelegt von

Diplom-Physiker

Holger Pieta

aus Eschweiler

Berichter:
Universitätsprofessor Dr. Thomas Hebbeker
Universitätsprofessor Dr. Christopher Wiebusch

Tag der mündlichen Prüfung: 20.06.2012

Abstract

A Model Unspecific Search in CMS (MUSiC) is presented in this work, along with its results on the data taken in 2010 by the Compact Muon Solenoid (CMS) at the Large Hadron Collider (LHC). This analysis shows a sensitivity to various models for new physics and provides a broad view at the data, due to its minimal theoretical bias. Events are classified with respect to their reconstructed objects: Muons, electrons, photons, jets and missing transverse energy. Up to three kinematic variables in each of these classes are systematically scanned for continuous bin regions deviating significantly from the predictions by the Standard Model of particle physics. No deviations beyond expected fluctuations are observed, when taking systematic uncertainties into account. The sensitivity of the analysis to certain models beyond the Standard Model is demonstrated.

Contents

1. Introduction

With the first large scale data taking of LHC in 2010 a new energy regime of particle physics opened up. Even with a comparatively low integrated luminosity of 36.1 pb^{-1}, the large increase in centre of mass energy, from 2 TeV at the Tevatron to 7 TeV allows to probe energy regions that were out of reach before.

A large number of theories predicts how new physics may manifest itself, and many of them are tested by dedicated analyses. As of now, no new physics has been detected, but limits have been determined. Thus any existing new physics must either be hidden below the currently achievable precision or it is realised in a way not yet considered. To avoid missing something that sits in plain sight, but no-one had a look at yet, we implemented a *Model Unspecific Search in CMS*: "MUSiC"[1, 2].

Analyses with similar strategies have been used successfully at other experiments[3, 4, 5, 6, 7, 8]. At CDF and D0 the SLEUTH algorithm checks the high energy tails for an excess of events. It has been modified at H1 to include regions that do not necessarily run to the end of the distributions. On the other hand the VISTA algorithm at CDF employs a global fit to determine a set of nuisance parameters, which are covered in terms of uncertainties in the other algorithms. It then looks at the global agreement of some kinematic variables, but does not identify deviating regions.

MUSiC compares measured data to the Standard Model expectation by systematically scanning kinematic distributions of many final states. In contrast to its predecessors it is also sensitive to deficits. By not applying any model-specific selection it is sensitive to a large number of signs for new physics and provides a global overview. However, this also causes it to be less sensitive to specific models than a dedicated analysis. An additional application of the algorithm could be to verify and improve the simulation of the Standard Model.

The analysis identifies and rates deviations, but an additional interpretation is needed to determine their causes, be it new physics, detector effects or a lack of understanding in the simulation.

2. The Standard Model and beyond

2.1. Standard Model

During the last century the current best understanding of matter and interactions has been condensed into a single model, aptly called *Standard Model*. In the Standard Model a small number of fundamental particles and an even smaller number of force fields are needed to describe most of what is currently known about the microscopic world. Using this approach one is able to predict the outcome of all experiments conducted so far, with some notable exceptions that will be covered in Section 2.2. Introduced by Weinberg, Glashow and Salam, it first only covered electroweak interactions[9, 10, 11], but was later extended to also describe the strong force[12]. Detailed descriptions of the Standard Model can e.g. be found in[13]; some key features are summarised in the following sections.

In the Standard Model all matter is build from fundamental, point-like particles without any known internal structure. Interactions between those particles can be described by an exchange of other point-like particles. The former are particles carrying a spin of $1/2$, and are called Fermions as they behave according to Fermi-Dirac statistics. The latter on the other hand are called bosons, because they follow the Bose-Einstein statistics as they carry an integer spin, which is usually 1. The number of matter particles in conserved, though due to the existence of anti-particles, they can be produced and annihilated in pairs. Force carrying particles, the bosons, on the other hand can be produced and annihilated at will, as long as the charge is conserved. Anti-particles posses the same properties as their respective normal particle, e.g. the mass, but all conserved quantum numbers are inverted, e.g. the charge.

2.1.1. Matter particles

The fermions are split into two groups: The leptons, which do not participate in the strong force, and the quarks, which do.

Leptons exist in a charged and an uncharged form, the latter being called neutrinos. Currently three families of one charged and one uncharged lepton are known: The electron, the muon and the tauon; each with its respective neutrino. The most important one is the electron, which is to be found in the shells of atoms. The number of particles are usually conserved for each family separately, i.e. it is possible to change an electron into an electron neutrino, but it is not possible to change an electron into a muon. Generation or annihilation of particles of one family is only possible with the associated production or annihilation of anti-particles. However, due to a mixing phenomenon observed in the neutrinos, it is possible to change the family[14, 15, 16].

All quarks are charged, either carrying $2/3$ or $-1/3$ of the lepton charge; anti-quarks carrying $-2/3$ or $1/3$, respectively. Non-integer charges can not be observed in free particles, because stable quarks only exist in bound states, called hadrons, of either two (called mesons) or three (called baryons) quarks. The quarks are also grouped into three families, each containing one $2/3$ charged quark and one $-1/3$ charged quark. The most important quarks are the up and the down quark, which can be found in the two most important

	Family	1	2	3
up-type Quarks	Name	Up (u)	Charm (c)	Top (t)
	Mass	≈ 2.5 MeV	≈ 1.3 GeV	≈ 173 GeV
down-type Quarks	Name	Down (d)	Strange (s)	Bottom (b)
	Mass	≈ 5 MeV	≈ 100 MeV	≈ 4.2 GeV
charged Leptons	Name	Electron (e)	Muon (μ)	Tau (τ)
	Mass	511 keV	106 MeV	1.78 GeV
uncharged Leptons	Name	e-Neutrino	μ-Neutrino	τ-Neutrino
	Mass	$\mathcal{O}$(eV)	$\mathcal{O}$(eV)	$\mathcal{O}$(eV)

Table 2.1.: *Fermions in the Standard Model, compiled from[19].*

Force	Relative strength	Range [m]	Carrier	Mass [GeV]
Gravity	10^{-40}	∞	Graviton	0
Weak force	10^{-2}	10^{-13}	$W^{\pm}/Z^0$	80/91
Electromagnetic	10^{-2}	∞	Photon (γ)	0
Strong force	1	10^{-15}	8 Gluons	0

Table 2.2.: *Range, strength (at energy scales close to the Z mass) and mass of fundamental forces and their carriers, compiled from[19].*

baryons: The proton and the neutron, which make the cores of atoms. Similarly to the leptons, the number of particles of each family is usually conserved, favouring reactions transforming quarks within their families, but mixing of the families is still possible[17, 18].

Table 2.1 summarises the known fermions.

2.1.2. Force carriers

Classically the forces between matter particles are described by force fields. In quantum mechanics, particles are associated to the fields. Then the forces can be described by the exchange of these particles. Currently four forces are known, which are summarised in Table 2.2.

Gravity does play an important role on large scales, where all participating objects are neutral in respect to the charge of all other forces. However, in reactions found at colliders, participating objects are not neutral and thus the other forces are far stronger than gravity, which can hence be ignored. If gravity can be described by quantum mechanics, its carrier is the graviton, though this particle has not been observed yet. All left-handed particles are affected by the weak force, which is besides its name still strong enough to be important when describing particle collisions. On macroscopic scales the weak force is visible in some radioactive decays, but due to the mass of its carriers its range is limited. The electromagnetic force is not limited in its range and can be observed in everyday physics. In microscopic physics it is responsible for the shells of atoms and for binding molecules. It only couples to particles carrying an electric charge. As described later, the carriers of the weak and electromagnetic force mix into each other, generating the unified electroweak force with the carriers γ, Z^0 and $W^{\pm}$. The strong force is indeed the strongest, but it is only active on very small scales. This is due to the force carrier itself possessing colour, which is the strong force equivalent of the charge. This means that the strong force couples to its own carriers, and thus it does not get weaker with increasing distance like the other forces, but instead the potential increases. This is the cause of the so called confinement,

not allowing any free coloured particles to exist. Thus on larger scales all objects are colour-neutral and no macroscopic effects of the strong force can be seen. It does however play the important role of binding the nucleons in the atom core.

2.1.3. Gauge theories and symmetries

Most predictions of the Standard Model are based on symmetries, which introduce conserved physical properties, e.g. the translation symmetry of space introduces momentum conservation. In quantum dynamics particles exist as excitation of the quantum fields. Mathematically speaking, the propagation of particles in space and time is defined by quantum wave functions $\Psi(x)$. If these functions are changed by certain transformations U, as shown in Equation 2.1, the fundamental equations of physics, e.g. the equation of motion, should not be changed.

$$\Psi(x) \to \Psi'(x) = U\Psi(x) \tag{2.1}$$

If the adjoint operator $U^\dagger$ of U equals the inverse operator $U^{-1} = U^\dagger$ for a transformation, it is connected to a symmetry. Symmetry groups collect all transformations a physical system is invariant under.

Symmetries introduce conserved properties, e.g. in Quantum Electrodynamics (QED) transformations of the group $U(1)$ lead to conserved electromagnetic charges and currents in the theory. To also introduce forces acting between charges, the global transformation U must be made local, i.e. space and time dependent:

$$U \to U(x) \tag{2.2}$$

Then the wave functions must be extended by a vector field A to keep the fundamental equations invariant under the transformations. The fields transform like:

$$\Psi(x) \to \Psi'(x) = e^{i\alpha\chi(x)}\Psi(x), \qquad A_\mu \to A'_\mu = A_\mu - \partial_\mu\chi(x) \tag{2.3}$$

The constant α and the scalar function $\chi(x)$ can be chosen arbitrarily, a process called gauging, which is why it is called a gauge theory. A particle is associated to each field, which is in this case the photon. The photon is a boson, because vector fields are associated to spin 1 particles.

2.1.4. Electroweak unification

Interactions of charged particles can be described with the fields introduced by the $U(1)$ symmetry group, but the uncharged neutrinos interact as well. The next complex symmetry group $SU(2)$ introduces three exchange particles, two of them can be linearly combined to the observed W bosons:

$$W^\pm = \frac{1}{\sqrt{2}}(W_1 \mp iW_2) \tag{2.4}$$

The associated charge is called the weak isospin T, which is associated to left-handed fermions, but not to right handed fermions. This matches the observation of W bosons coupling only to left-handed particles.

While two of the $SU(2)$ bosons do describe the couplings of the observed W boson, one important fact is missing: Bosons introduced by symmetry transformations must be massless, otherwise the invariance under gauge transformations is broken. This can be solved by introducing another scalar field with a non-vanishing ground state, which breaks

Particle	Charge	Weak isospin		Weak hypercharge
	Q	T	T_3	Y
ν_L	0	1/2	1/2	−1/2
ν_R	0	0	0	0
l_L	−1	1/2	−1/2	−1/2
l_R	−1	0	0	−1
q_L^u	2/3	1/2	1/2	1/6
q_L^d	−1/3	1/2	−1/2	1/6
q_R^u	2/3	0	0	2/3
q_R^d	−1/3	0	0	−1/3

Table 2.3.: *Charge, isospin and hypercharge of fermions.*

the local symmetry. The field couples to all other fields, including itself. Being part of the $SU(2)$ group, this field has four degrees of freedom, of which three are used to give mass to the three bosons. This process is called the Higgs-mechanism. The fourth degree of freedom manifests itself as an additional spin 0 boson, the Higgs particle, which has not been confirmed experimentally.

The remaining third boson W^3 of the $SU(2)$ group is massive as well, thus it cannot be the photon. Also it couples only to left-handed fermions, contradicting measurements of the Z boson. Weinberg, Glashow and Salam solved this by combing electromagnetic and weak force, called the GSW model. In the combined symmetry group $SU(2) \times U(1)$ the remaining massive $SU(2)$ boson W^3 and the massless $U(1)$ boson B can mix:

$$\gamma = \cos\Theta_W \cdot B + \sin\Theta_W \cdot W^3 \tag{2.5}$$

$$Z = -\sin\Theta_W \cdot B + \cos\Theta_W \cdot W^3 \tag{2.6}$$

The mixing angle Θ_W is called the weak mixing angle or Weinberg angle. The B boson couples to the weak hypercharge Y, which is connected to the electromagnetic charge Q and the third component of the weak isospin T_3 via $Q = T_3 + Y$. In the end the mixed bosons γ and Z match the observed properties of the photon and the Z boson. Table 2.3 summarises the various charge properties of all fermions.

2.1.5. Quantum chromodynamics

In some physical processes quarks and leptons are basically equivalent, e.g. $Z/\gamma \to f\bar{f}$ with f being any fermion. Experimental evidence shows that the decay into quarks is three times more frequent than expected from the coupling constants and the ratio of the number of quark flavors to the number of lepton flavours[20, 21]. Thus another quantum number is needed which allows to distinguish three different kinds for each of the six quarks, i.e. the total number of quarks states must be 18. The next complex symmetry group $SU(3)$ provides a system including a three-state charge. All quarks carry an additional charge, whose states are conveniently called *Red*, *Green* and *Blue*, which is the reason why this charge is also called *colour*. Anti-quarks carry anti-colour. The $SU(3)$ groups contains eight transformations which are usually referred to as rotations, thus eight additional vector fields are introduced which interact with the colour charge. The quanta of these fields are the eight coloured gluons, which in contrast to the quarks always carry two colour charges, linearly combined from one colour and one anti-colour, thus the field particles of this interaction are themselves affected by the field. This causes the strength of the interaction to increase with increasing distance, resulting in the confinement effect:

Coloured particles can never be free; a system of quarks must always be colour neutral on larger scales. When two coloured particles are pulled away from each other, more and more energy is added to the system. At some point the energy in the system is large enough to create additional particles which restore colour neutrality. On the other hand the shape of the strong potential also causes *asymptotic freedom*: Strongly interacting particles appear to be unbound on scales smaller than the proton radius.

In a stable system colour neutrality can be achieved in two ways: First by combining a coloured quark with another anti-quark carrying the anti-colour, which is realised in mesons. Second the combination of all three colours also results in a colour-neutral system, realised in baryons.

2.1.6. Parton Distribution Functions

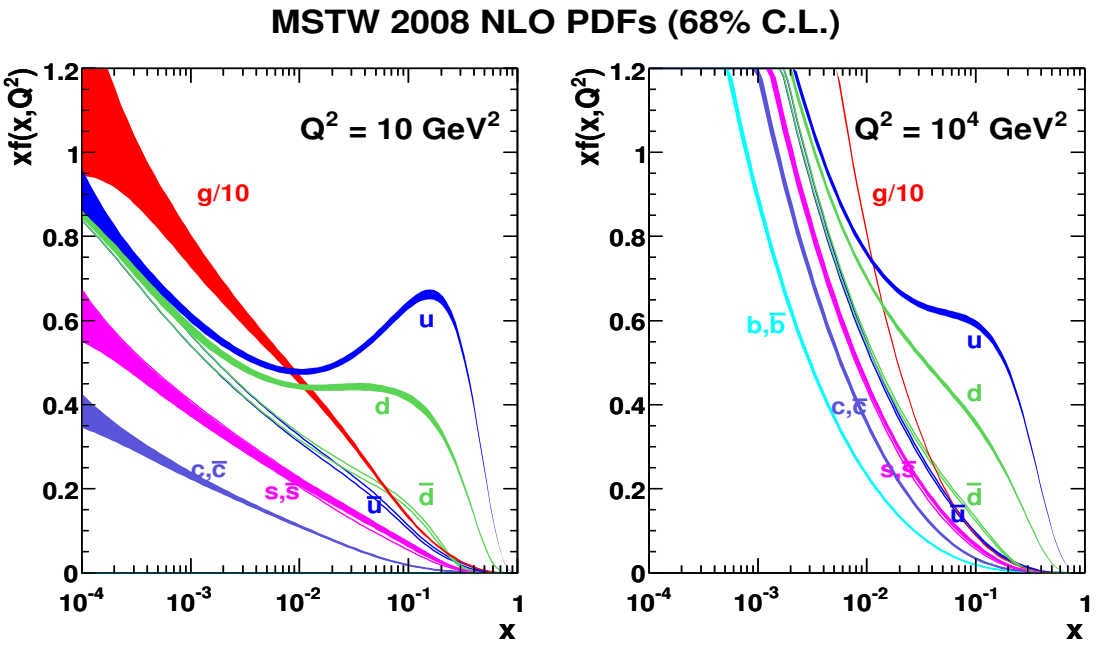

Figure 2.1.: *PDFs for protons derived[22] by the MSTW group for two different values of Q. The bands represent the uncertainties. The actual PDFs, here donated as $f(x, Q^2)$, are scaled by the momentum fraction x for better presentation.*

The Standard Model provides rules to calculate what happens if two quarks collide. One can for instance compute the cross section of two partons p_i and p_j producing X: $\sigma(p_i p_j \to X)$. But due to the properties of QCD it is currently not possible to predict from basic principles what happens if two protons collide, i.e. which of the various partons in the proton actually take part in the interaction. Thus Parton Distribution Functions (PDFs) have been introduced. Details can be found e.g. in [23].

PDFs encode phenomenologically the probability of finding a parton p (quark or gluon) carrying a fraction x of the total proton momentum in its rest frame, if during the interaction a momentum transfer Q takes place: $PDF(p, x, Q^2)$. Given the partonic cross sections $\sigma(p_i p_j \to X)$ for a combination of two partons p_i and p_j, this allows to calculate

the total cross section in proton-proton (PP) collisions:

$$\sigma(PP \to X) = \sum_{i,j} \int_0^1 \int_0^1 dx_1\, dx_2\, PDF(p_i, x_1, Q^2)\, PDF(p_j, x_1, Q^2)\, \sigma(p_i p_j \to X) \quad (2.7)$$

Here i and j run over all partons p_i that contribute to σ_{ij}.

A special procedure, the DGLAP equations, allows to calculate $PDF(p_i, x_1, Q^2)$ at any Q as long as it is known at a specific $Q_0 \neq Q$. The form of the $PDF(p_i, x_1, Q_0^2)$ cannot be calculated from first principles, thus suitably chosen smooth functions are fitted to experimental data, e.g. acquired at lepton-hadron colliders like HERA. These fits are performed by various groups, if which in this analysis CTEQ, MSTW and NNPDF are used. Figure 2.1 shows the results of the MSTW group as an example.

2.2. Beyond the Standard Model

Observations of gravitational effects in galaxies suggest a much higher amount of matter in the universe than visible[24]. The Wilkinson Microwave Anisotropy Probe[25] measured about 4% of the total energy density in the universe to be matter, plus 23% *dark matter* and the rest is mostly *dark energy*. Neither dark matter nor dark energy can be explained by the Standard Model.

Besides this obvious deficit of the Standard Model, there are some flaws that are more aesthetic than fundamental: The measurable mass of the Higgs boson depends on a fundamental mass parameter and on radiative corrections involving other bosons. Extrapolating this to the Planck scale, a correction in the order of 10^{36} GeV^2 results. This must be compensated by the mass parameter to a precision of about 10^{-32} to reach a measurable Higgs mass in the order of 100 GeV, which is suggested by theoretical[26] and experimental[27] hints. There is no mechanism to explain this precise cancellation, called *fine tuning*, in the Standard Model[1].

While the electromagnetic and weak force are unified in the $SU(2) \times U(1)$ gauge group, the strong force is treated independently in the $SU(3)$ gauge group. Similar to the fine tuning problem, nothing forces one to believe in a *Grand Unified Theory*, but it could provide further insight. And last but not least the Standard Model does not provide any explanation of the fermion mass hierarchy or why there are e.g. only three lepton families. Also only left-handed neutrinos are described in the Standard Model, which cannot acquire mass using the Higgs field. Experimental evidence[28] has however shown that neutrinos can oscillate between families, which can only happen with massive neutrinos.

Some or all of these drawbacks can be solved by extending the Standard Model in one way or another. These extensions then need to be tested experimentally to validate or exclude them. For a conventional analysis at CMS one would now choose a specific extension and devise a way to maximise the sensitivity of CMS for this model, i.e. maximise the chance that a CMS measurement can either verify or exclude the model in question. This is not the apprach of MUSiC. However, as described in Section 8.2, it is still useful to select a few models to judge the sensitivity of MUSiC to certain kinds of deviations.

[1] It might be pure chance, but this would be a rather inelegant explanation.

2.2.1. Heavy neutral vector boson

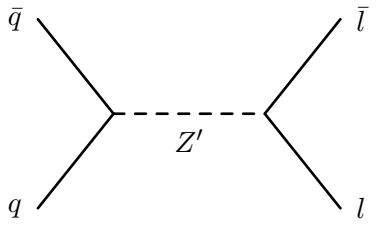

(2.8)

The Standard Model knows four force carrying vector bosons, plus the Higgs boson. However, there is no fundamental reason why there cannot be more, and indeed many theories beyond the Standard Model predict additional bosons. One possible extension of the Standard Model is hence an additional vector boson behaving similar to the Z boson, but possessing a much higher mass. It is commonly called Z'[29]. The high centre of mass energy of the LHC allows to look for such bosons at masses higher than those probed at previous accelerators.

Various models predict additional $U(1)$ symmetry groups, which come with additional vector bosons. Here the *Sequential Standard Model* is used, which assumes the same fermion couplings as the SM Z boson. Thus the cross section calculations are the same as in the Standard Model with a higher mass parameter. It should hence be visible in e.g. the di-lepton mass over a background dominated by Drell-Yan lepton pairs ($pp \to \gamma/Z \to l^+l^-$; see Figure 2.8). This model serves as a benchmark to see if MUSiC or other analyses are sensitive to deviations in the di-lepton mass.

2.2.2. Excited leptons

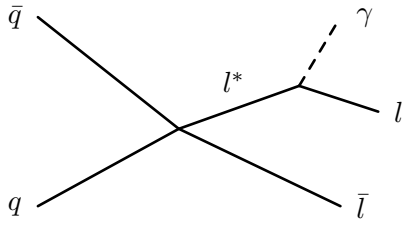

(2.9)

In the Standard Model leptons are assumed to be fundamental and pointlike, but a substructure is not ruled out experimentally. The discovery of a substructure would be a clear sign of physics beyond the Standard Model. The LHC allows to probe smaller substructures than excluded by existing limits.

If leptons are indeed made from other, smaller particles, one consequence would be excited leptons: Higher excitation states of the bound substructure resulting in new leptons with the same properties but a higher mass. These excited states can spontaneously decay into the ground state and a photon, thus they show up in the combined mass spectrum of a lepton and a photon (see Figure 2.9). The coupling between excited leptons and SM particles can be described as a contact interaction[30]. The cross section of this interaction depends on a scale below which the interaction takes place:

$$\sigma \propto \Lambda^{-4} \tag{2.10}$$

By choosing Λ the cross section can be varied in a large range for a given mass of the excited lepton. If the cross section σ_0 has been calculated at a given scale Λ_0, the cross

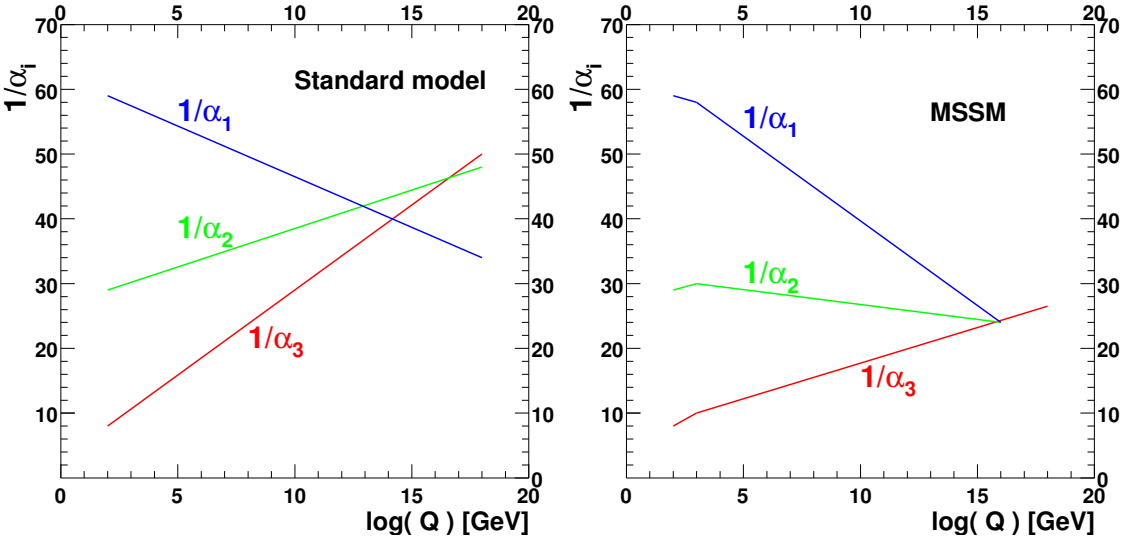

Figure 2.2.: *Couplings of the Standard Model compared to those in the MSSM. No unification at high energies occurs in the SM, but can be achieved in the MSSM. Plots adapted from [32]*

section can simply be adjusted to a scale Λ_1:

$$\sigma_1 = \sigma_0 \cdot \left(\frac{\Lambda_0}{\Lambda_1}\right)^4 \tag{2.11}$$

2.2.3. Supersymmetry

In the Standard Model, matter consists of fermions, and bosons are force carriers, thus one possible extension is to introduce matter bosons and force carrying fermions. This introduces a fundamental boson-fermion symmetry and is commonly called Supersymmetry. The symmetry must however be broken to allow the Supersymmetric partners of the Standard Model particles to be heavier, explaining why they have not been observed yet. More details can be found in [31].

Whether a particle is part of the Standard Model or an additional supersymmetric particle is encoded in a quantum number, the R-parity, which may or may not be conserved. The R-parity does not change when the number of supersymmetric particles is changed in units of two. Thus if R-parity is conserved, supersymmetric particles can only be produced and annihilated in pairs. If one of the additional particles is stable, i.e. R-parity is conserved, and only weakly interacting, then it is a dark-matter candidate. Also the fine-tuning problem can be solved naturally in supersymmetric models, though additional Higgs-like particles are needed.

Even minimal Supersymmetry[2] introduces over 100 new free parameters, e.g. the masses of the new particles. Thus it is not feasible as a benchmark model, because even little changes in some of the parameters can change the model signatures quite drastically. However, by assuming a grand unification close to the Planck scale (see Figure 2.2) and conserved R-parity and by introducing a graviton to mediate the soft Supersymmetry breaking, the number of free parameters can be reduced to five. This is called *Constrained*

[2]One additional particle for each Standard Model particle

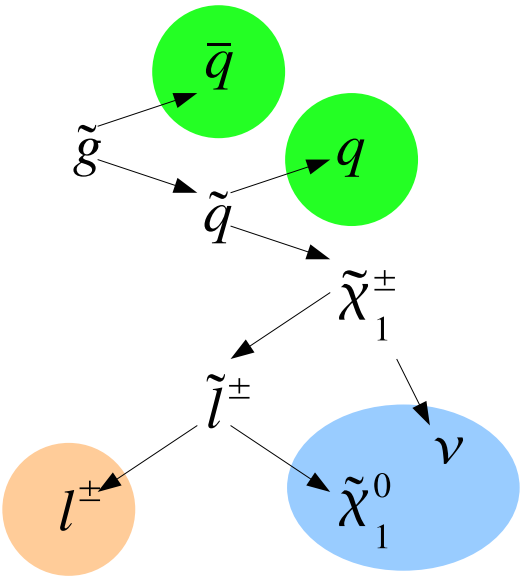

Figure 2.3.: *Example[33] of a supersymmetric cascade decay. Leptons are shown in red, jets in green and $\not{E}_T$ in blue.*

Minimal Supersymmetric Standard Model or *Minimal Supergravity*. The five free parameters are:

- m_0: Mass of spin 0 particles at the unification scale
- $m_{1/2}$: Mass of spin 1/2 particles at the unification scale
- A_0: Unified coupling constant
- $tan\beta$: Ratio of the vacuum expectation values of the two Higgs fields at the electroweak scale
- $sign(\mu)$: Sign of the unified mass term of Higgs-like particles at the electroweak scale

The properties of the supersymmetric extension can still vary strongly depending on the actual values of these parameters, but it still allows to define benchmark points where analyses and experiments can be compared.

In the chosen benchmark points heavy supersymmetric particles are produced in pairs and then each of them undergoes cascade decays as shown in Figure 2.3. The excepted signature is thus invisible energy combined with a number of leptons and jets.

3. CMS at LHC

3.1. Large Hadron Collider

Physics beyond the Standard Model is expected to show up either in small deviations in low energy precision measurements or in the high energy domain. The former is covered by e.g. b-factories like KEKB, the latter by colliders at the energy frontier, e.g. LEP and Tevatron. The closer the centre of mass energy of a collider is to the mass scale of a certain physics process, the higher is the probability of this process taking place in a collision. To probe the high energy domain of physics beyond the Standard Model the centre of mass energy needs to be as high as possible. This is particularly true for a hadron collider, where only fractions of the centre of mass energy of the hadron system are available at the parton level. But the cross section can still be small even at high centre of mass energies, thus the collider also needs to provide a high instantaneous luminosity to produce enough events in a moderate time span. It takes a long time to plan, develop and build a new collider, thus the next generation machine was already being planned while Tevatron and LEP were still being operated. In 1994 CERN decided to build the *Large Hadron Collider* LHC in the tunnel of LEP after this collider went out of operation, which happened in 2000.

The LHC is a proton-proton collider[1], which allows much higher centre of mass energies than an electron collider due to a greatly reduced synchrotron radiation. On the other hand only a fraction of the proton-proton centre of mass energy is available for interactions at the parton level. The remaining longitudinal momentum of both protons is mostly lost into the beam pipe, thus the rest frame of the interaction is not known. Using only protons no time consuming anti-proton generation is needed, which limits the luminosity of Tevatron, but requires the installation of two systems for the two counter-rotating beams.

The LHC had been designed to collide protons with a centre of mass energy of 14 TeV. To reach such a centre of mass energy in a tunnel of nearly 27 km the beam-bending dipoles need a field strength of more than 8 T. However, technical challenges limit the field strength to about 4 T and thus the centre of mass energy to 7 TeV until the end of 2011. In this mode LHC delivered 47 pb^{-1}[34] to CMS and ATLAS in 2010. CMS and ATLAS are the two general purpose detectors that are part of the LHC project, while LHCb and ALICE focus on b-physics and heavy ion physics, respectively. Most of the collisions were delivered with 368 bunches per beam with a minimal distance of 150 ns at a peak luminosity of 200 $\mu\mathrm{b}^{-1}\mathrm{s}^{-1} = 2 \cdot 10^{32}\ \mathrm{cm}^{-2}\mathrm{s}^{-1}$. This causes on average 2.7[35] relevant collisions per bunch crossing, that is collisions with enough activity to be visible in the CMS detector.

More details about the LHC can be found in [36, 37, 38].

[1] Other modes of operation, e.g. lead-lead collisions, are possible as well but of no interest for this analysis.

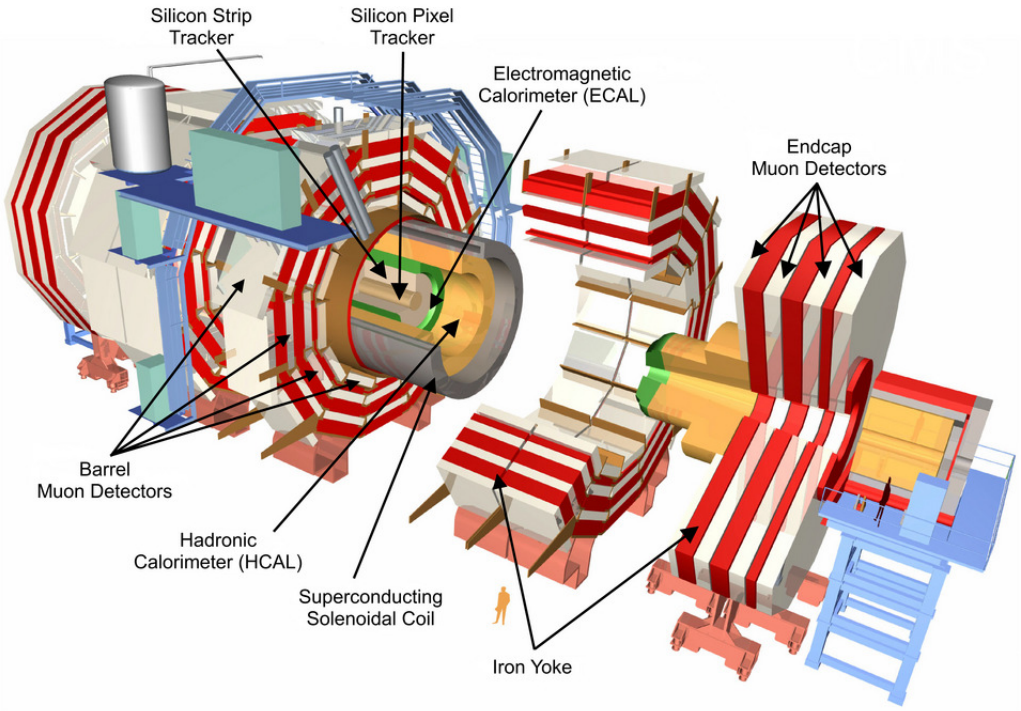

Figure 3.1.: *Perspective view of the CMS detector[40].*

3.2. Compact Muon Solenoid

Both beams in LHC have the same energy, thus a symmetric detector layout is recommendable for general purpose detectors. A spherical design put up technical difficulties, thus a cylindrical shape wrapped around the beams has been chosen by CMS and ATLAS. The barrel parts of those detectors are then closed at both ends by so called endcaps. In such a layout a solenoid[2] is the obvious choice for the magnet that allows to measure the momentum of charged particles flying away from the interaction point. To measure the various properties of different particles multiple detectors are needed, which are layered around the interaction point. Both CMS and ATLAS have a similar general structure:

- The innermost layer provides points in space where charged particles passed through, allowing to reconstruct their trajectory and momentum.
- The next layer provides calorimetric measurements of the energy of most particles.
- The outer layer again measures the position of charged particles that managed to pass through all previous detector parts.
- One or more magnets provide the field needed to measure the momentum of charged particles.

A brief tour through the CMS detector from the inside out follows, more details can be found in [39]. A conceptual view of the CMS detector and its components can be seen in Figure 3.1. The coordinate system used by CMS is defined in Appendix A.1.

[2] ATLAS also uses a toroid magnet in the muon system

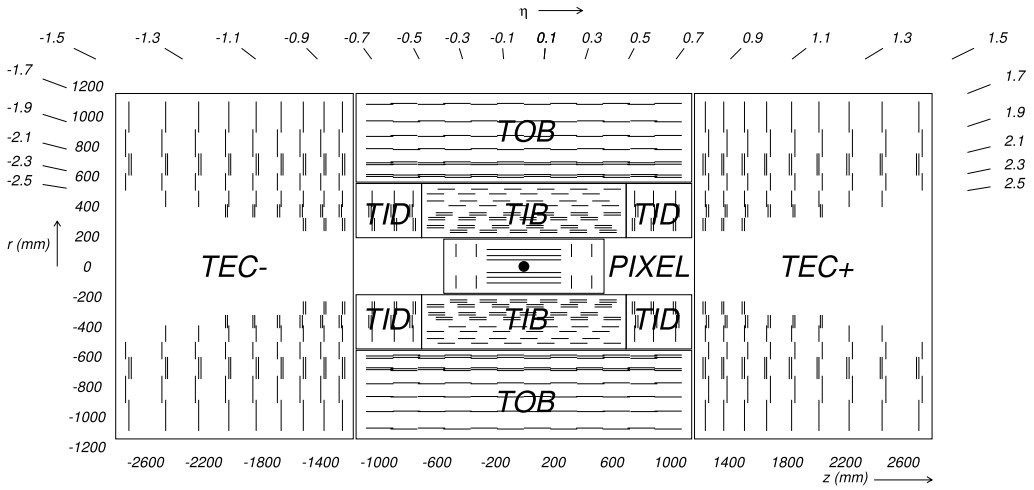

Figure 3.2.: *Layout of the CMS inner tracking detector[39].*

3.2.1. Inner tracking system

The first thing to be encountered by a particle is the beam pipe, which is needed to sustain the required vacuum for the circulating beams, but a nuisance from a detector standpoint. It has been made from beryllium, which minimises the effect on passing particles.

The first sensitive part of the detector in a particle's path are the three layers of the silicon pixel detector, mounted at radii between 4.4 and 10 cm. It is enclosed by two discs at each end, giving the pixel detector a total length of 93 cm. Electrically charged particles passing the layers are measured with a spatial resolution of the order of 10 µm. Combined with the acceptance in pseudorapidity[3] of up to $|\eta| < 2.5$ this allows an excellent localisation of both collision vertices and secondary vertices from particle decays.

A typical particle crosses ten layers of silicon strip detectors located between 0.2 and 1.2 m from the interaction point. Together with twelve discs in the endcaps the whole structure is 5.4 m long and also covers up to $|\eta| < 2.5$. Some modules are so called stereo modules which consists of two layers right on top of each other, but one tilted slightly. This allows to also measure the position of a hit along the strips. The strips provide a spatial precision of down to 15 µm in ϕ direction, allowing a momentum resolution of

$$\frac{\Delta p_T}{p_T} = 0.15 \frac{p_T}{\text{TeV}} \oplus 0.5\% \tag{3.1}$$

in a magnetic field of 3.8 T, when the detector is fully aligned. The spatial precision is better than the pixel or strip spacing, because the deposited charge is spread over multiple adjacent pixels or strips, and thus a charge centroid can be calculated.

Figure 3.2 shows the layout of the silicon tracking detectors in CMS.

3.2.2. Calorimeter

Most particles are absorbed in the next two layers of the detector, the electromagnetic (ECAL) and the hadronic (HCAL) calorimeter, which measure the deposited energy. Figure 3.3 shows the position of the calorimeters outside of the tracker and inside of the coil.

[3]See Appendix A.1 for the definition of the CMS coordinate system.

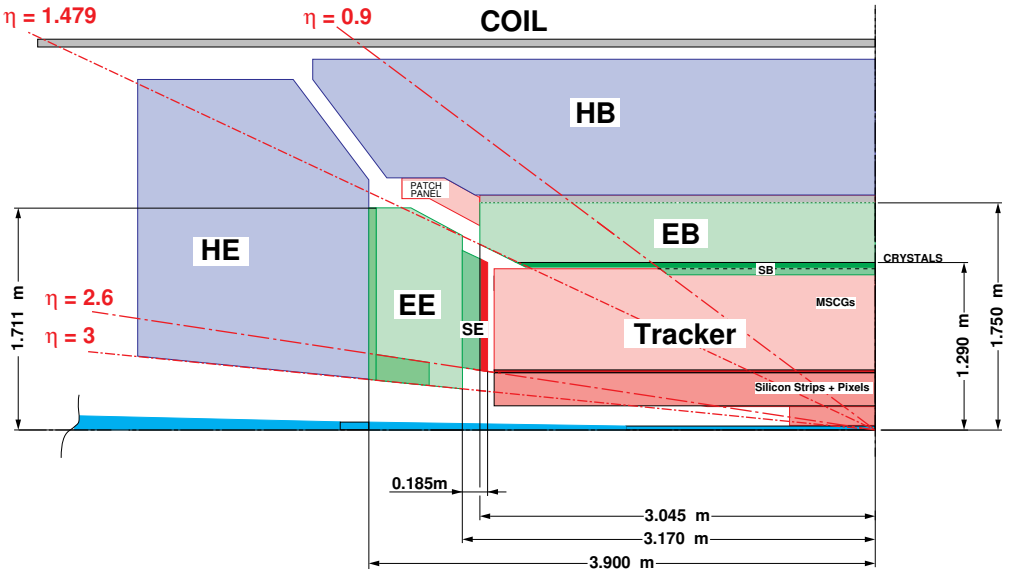

Figure 3.3.: *Schematic view of the layout of the tracker and calorimeter of CMS [41].*

Lighter objects that interact electromagnetically, i.e. electrons and photons, are absorbed in the first layer of the calorimeters, creating electromagnetic showers. During the shower process atoms in the ECAL material are excited, emitting scintillation light, which is measured using Avalanche Photo Diodes (APDs) in the barrel and Vacuum Phototriodes (VPT) in the endcaps. The ECAL is made from lead-tungstate crystals ($PbWO_4$). This material provides about 26 radiation lengths in a crystal length of 23 cm in the barrel. It also has a small Moliere radius, allowing a good spatial granularity of 0.0174×0.0174 in $\eta \times \phi$ in the barrel. Barrel and endcap together cover a pseudorapidity range of $|\eta| < 3$. A preshower detector at the inside of the endcaps, made from two layers of lead absorbers and silicon detectors, improves the spatial resolution. Test beam measurements show an energy resolution of:

$$\frac{\Delta E}{E} = \frac{2.8\%}{\sqrt{\mathrm{E}\ /\mathrm{GeV}}} \oplus \frac{0.12}{\mathrm{E}\ /\mathrm{GeV}} \oplus 0.3\% \tag{3.2}$$

Hadrons interact with the nucleons of the calorimeter materials. However, the nuclear interaction length is larger than the radiation length, thus they are absorbed deeper in the material and the developing showers penetrate further. A crystal calorimeter of sufficient thickness would have been prohibitively expensive, thus the next detector layer after the ECAL is a sandwich of brass absorbers and plastic scintillators, the HCAL. A total of 14 barrel layers of this sandwich provide five to ten nuclear interactions lengths, depending on the angle of impact. Similarly 17 layers in the endcaps add up to ten interaction lengths if the ECAL is included. The barrel HCAL covers up to $|\eta| < 1.3$ with a segmentation of $\Delta\phi \times \Delta\eta = 0.087 \times 0.087$. The endcaps extend the range to $|\eta| < 3$ with a granularity of 0.087×0.087 to 0.17×0.17. Another scintillator layer just outside of the magnet uses the coil as an absorber for additional interaction lengths. The HCAL has been designed to reach a resolution of[42]

$$\frac{\Delta E}{E} = \frac{100\%}{\sqrt{\mathrm{E}\ /\mathrm{GeV}}} \oplus 4.5\% \tag{3.3}$$

Additional forward calorimeters located at 11 m distance along the beam are used to extend the range to $|\eta| < 5$. They consists of quarz fibres in a steel absorber to detect

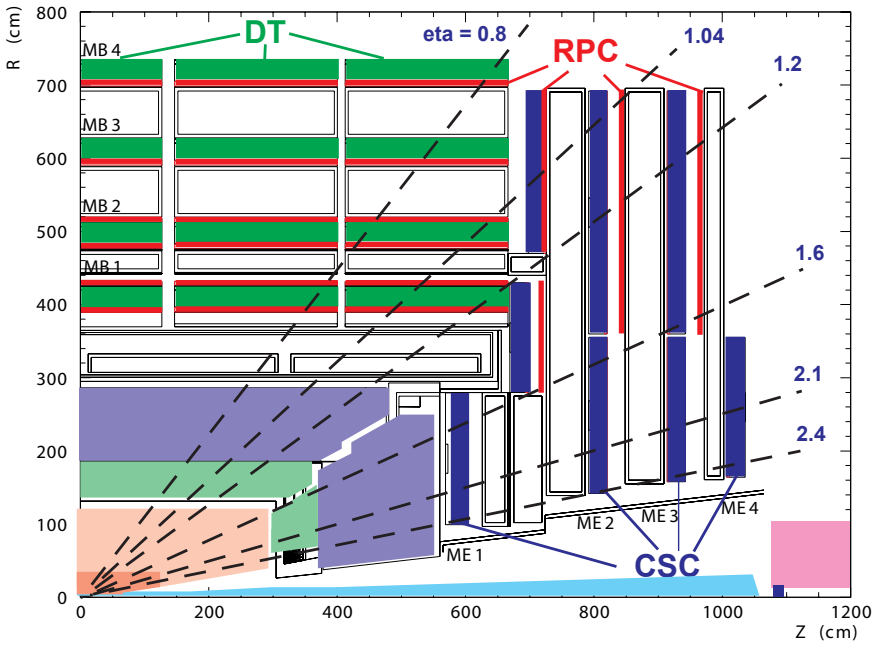

Figure 3.4.: *One quadrant of the CMS detector with tracker, calorimeters and muon system[43].*

the Cherenkov radiation of shower particles. Separate fibres at different depths allow to distinguish between showers generated by hadrons and by electrons or photons.

3.2.3. Magnet coil

The magnetic field needed to measure the momentum of charged particles is provided by a superconducting solenoid of 12.5 m length and 5.9 m open bore. It is located just outside of the HCAL and generates a field of 3.8 T in the inside. Placing the calorimeters inside of the magnet reduces the amount of absorbing matter in front of the calorimeters, improving their energy resolution, though it requires the use of detectors tolerant against very high fields. A solenoid provides a very homogeneous field in its inner volume, but a rather complicated one at its ends and on the outside. The outside field is controlled and bundled using iron discs and wheels interleaved with the muon system. This reduces the field outside of the detector to a strength tolerable by normal electronics, while at the same time providing a strong field to the muon system, thus allowing the muon system to not only identify, but also to help in measuring the muon momenta.

3.2.4. Muon system

The last sensitive detector part to be passed by particles is the muon system. It consists of four layers of gas-based detectors interleaved with three layers of iron return yoke. The iron bundles the field, providing up to 1.6 T in its inside, again bending the trajectories of charged particles and allowing momentum measurements. Figure 3.4 shows the location of the muon system.

Muons are the only particles able to pass through copious amounts of matter but still be visible in the tracking detectors. Sometimes hadronic showers pass through the ECAL, HCAL and the coil, hitting the first layer of the muon system. This shower is then stopped in the iron layers, while the muons continue their way and are thus easy to identify.

In the barrel all but the outermost of the four layers of muon detectors, called *stations*, are made from twelve layers of drift tubes (DT). They are aligned in both ϕ and η direction, providing information for both flight direction and momentum determination. The outermost station contains only eight layers providing position measurements in the ϕ direction for momentum determination. Each drift tube is a rectangular tube with a central anode wire, allowing to measure the distance to the wire of a charged particle passage to a precision of 250 µm.

In the endcaps a non-uniform magnetic field and the higher rate of passing particles rules out the use of drift tubes. Instead *cathode strip chambers* (CSC) are employed, which are multi-wire proportional chamber with their cathode walls split into strips with a width of 8.4 to 16 mm. The anode wires and the cathode strips are mounted perpendicular to each other, allowing a two-dimensional measurement in one chamber. The position along the strips can only be determined to a precision of a few millimetres, but by weighting the charge distribution of several adjacent strips, a precision of about 150 µm can be achieved perpendicular to the strips. Thus the CSCs are mounted in the endcaps with the strips pointing along the radial axis, providing the precision needed for momentum measurements.

Both the DTs and the CSCs are sandwiched between *resistive plate chambers* (RPC). A high voltage between two conductive plates causes an avalanche discharge when a charged particle passes the RPC. The high resistance of the plates stops the avalanche before the whole chamber is discharged. A striped design similar to the CSCs gives a reasonable precision along the ϕ direction, but the main reason for the RPC is the fast response and high timing resolution much better than the minimal LHC bunch crossing distance of 25 ns. This allows to assign hits to bunch crossings and to trigger quickly.

The muon system allows to identify muons, but also improves the momentum measurement at high p_T, e.g. at 1 TeV the resolution is improved to about 10%, compared to the inner tracking system alone.

3.2.5. Trigger

Reading out 100 million analogue channels every 25 ns[4] is not possible and wasteful, because most of the time the majority of channels will show only noise.

The first decision whether to read out the data in the electronics is made by the *Level 1 Trigger*. In this step custom-built hardware does a very basic reconstruction in isolated parts of the detector. The muon trigger system combines correlated hits into segments and segments into tracks, which then need to pass thresholds in terms of curvature and η. The ECAL trigger system groups 5×5 crystals and sums up their measured values. Energy measurements of adjacent groups are combined to apply thresholds on E_T and isolation. The applied selection thresholds reduce the rate of events actually read out to about 10 to 100 kHz.

Once the L1 trigger has tagged an event to be read out, the measurements of the various detectors are combined in the event builder network to form a complete picture. The *High Level Trigger*, or *Event Filter* then performs basic reconstructions taking into account all detectors to decide whether the event is worth to be written out to the mass storage systems. It is based on software running on a general purpose computer farm. The muon HLT performs a track fit over hits in the muon system to determine the p_T and applies isolation criteria. The photon trigger reconstructs energy clusters and applies isolation and quality criteria. The electron trigger additionally matches the cluster to tracking

[4]LHC design conditions

information. In the end the HLT reduces the number of events written to the storage system to a few hundreds per second.

3.3. Computing and the grid

The reconstruction described in Section 3.4, the simulation described in Section 4.2 and the analysis itself need large amounts of computing power to be finished in time. It is not feasible to concentrate all the needed infrastructure in one place, generating a single point of failure and forcing most people to work remotely. Thus the *Worldwide LHC Computing Grid* (WLCG) has been invented: A number of batch computing systems are located at institution and universities that are part of the CMS collaboration. Central workload management systems allow the users to define jobs that are automatically send to available computing centres that host the required data.

Depending on their importance and function, the computing centres are grouped into *tiers*.

- The *Tier 0* (T0) is located at CERN. Its main task is to reconstruct the data coming from CMS. It also provides long term storage for this data.

- Eleven *Tier 1* (T1) centres are located in Europe, North America and Asia, of which seven are used by CMS. Re-reconstruction of the data is performed at the T1s. They also provide long term storage for Standard Model simulations. The distribution of CMS data to the T2 is also routed through the T1s to reduce the load on the T0.

- About 150 *Tier 2* (T2) centres are distributed all over the world, of which about 50 are used by CMS. Their main task is to provide computing power to the users, allowing them to perform their analyses. The SM simulation is also performed at the T2s and the output transferred to and stored at the T1s. For the user analyses the data stored at the T0 and the T1s needs to be replicated at the T2s, with each individual sample usually stored at a handful of T2s to provide redundancy.

- All user interactions with the grid resources are performed from local computing resources, which are commonly known as *Tier 3*, though formally these resources are not a part of the grid.

The three steps of the MUSiC analysis (see Section 6.1) are performed at T2s and on local computing resources at the RWTH Aachen university. Prior to the classification step (see Section 6.1.1) both measured and simulated data is *skimmed*, i.e. stripped of information not needed in this analysis. The jobs performing this task are run on the T2s that host the needed data, and the output is send to and stored at the RWTH Aachen T2. Given that each event can be considered independently, parallelisation of this task is straight forward. The classification step is performed at the RWTH Aachen T2, storing output on the local RWTH Aachen resources. At the end of 2011 this step can be performed in parallel for the individual measured and simulated samples, but work is ongoing to allow parallelisation at the event level. The least step in MUSiC, the scanning for deviations (see Section 6.1.2), is performed on local RWTH Aachen computing resources. The algorithm is able to scan multiple distributions at once, but only on a single computer. Thus to reduce the time needed for this step, a single computer with a high number of CPU cores is needed.

3.4. Reconstruction

Advanced algorithms are employed to translate the raw data coming from CMS detector electronics into information that can be interpreted by a physicist. Ideally the resulting information is as close as possible to how we currently think of the underlying physics, e.g. in terms of Feynman diagrams. This procedure is called reconstruction. The reconstruction algorithms are based on both the properties of particular particles as well as on the way the detector is expected to respond to them.

3.4.1. Tracking

A particle hitting the silicon detector generates free charges which can be detected. These charges spread over multiple adjacent strips or pixels. After calculating the charge centroids of adjacent pixels or strips the silicon detectors deliver two- or three-dimensional positions in space. Two[5] or three of those points in the pixel detector and the first layers of the strip tracker are combined into a first estimate of the particle trajectory[44]. This trajectory is then extrapolated to the next tracker layers using a Kalman-filter[45] technique taking into account the magnetic field and the material budget. If an appropriate hit is found close to the extrapolated position the track fit is updated. At the end a last fit is performed over all hits associated to this trajectory.

Once a fit was successful, all hits associated to this track are removed. The full procedure is repeated a number of times with increasingly loose thresholds for the seed and fit quality.

3.4.2. Muons

The reconstruction of tracks in the muon system alone works in a fashion very similar[46] to the procedures in the silicon detectors. Hits in the individual layers of one station are combined to form segments, which already provide a rough estimate of the trajectory. The track estimate is then extrapolated to the innermost muon station, from where a first filtering step is performed to make a track. It is then refined by running the final filter from the outside in, resulting in a so called *standalone muon*.

A *global muon* is formed by first matching the standalone muon to a track in the silicon detectors. The hits associated to the tracks in both detectors are then used to perform a global fit of the trajectory.

3.4.3. Electrons and photons

Particles incident on the ECAL produce electromagnetic showers which in turn cause several adjacent crystals to scintillate. Thus the first step is to combine the signals in adjacent crystals into a cluster which ideally contains all the signals generated by a single particle. The ECAL reconstruction is mainly aimed at electrons and photons. Electrons usually radiate bremsstrahlung in the magnetic field of the solenoid. Due to the material of the tracker, which amounts to about one radiation length, the electromagnetic show can start before the ECAL is reached. In case of photons this effect is called *conversion*, when one photon converts into an electron-positron pair. In both cases the total energy is spread in ϕ due to the magnetic field and must be recombined to get the energy of the original particle. In η no spread is expected due to the magnetic field, leaving only the size of the shower, which is not expected to exceed five crystals.

[5] In case of two positions the interaction point is used as an additional constraint.

In the barrel region the crystal grid is arranged along η and ϕ, thus the clustering is straightforward[47]. Starting from the crystal with the highest energy entry, a region of five crystals in η and a width of 0.6 in ϕ is defined centred on this crystal. The *supercluster* is formed by combining all energy entries in the search region, if they exceed certain thresholds. The procedure is then repeated with all crystals removed that are already part of a cluster to form more superclusters. Local energy maxima in the superclusters are used as local clusters.

In the endcaps the crystal grid is arranged along the vertical and the horizontal axis and not along η and ϕ, thus a different algorithm is used. Squares of 5×5 crystals are centred on local energy maxima to form local clusters. A supercluster is formed by combining all local clusters in a window of $\eta \times \phi = 0.14 \times 0.6$ centred on the local cluster with the highest energy. More superclusters are formed by repeating the procedures on all local clusters not already part of a supercluster.

Any supercluster may be a photon, thus selection criteria (see Section 5.2.3) need to be applied to increase their purity and suppress misidentified hadrons. Electrons on the other hand are also visible in the form of a supercluster, but they are charged and thus are expected to leave signals in the tracking detector. The cluster position is used to determine a window in the pixel detector to look for track seeds[48]. The default track reconstruction uses averaged assumptions about bremsstrahlung and multiple scattering which are useful for all kinds of particles. Electrons however are expected to radiate a lot more than hadrons and muons, thus a special *Gaussian sum filter*[49] algorithm is used to take into account bremsstrahlung and the material budget. Any supercluster loosely matched to a GSF-reconstructed track is considered to be an electron, thus additional selection criteria need to be applied, as described in Section 5.2.2.

3.4.4. Particle Flow Reconstruction

All previously described reconstruction algorithms focus on a specific part of the detector or on the properties of a specific kind of particle. They do not, however, take into account other parts of the detector or objects which may have been reconstructed elsewhere. The *Particle Flow Reconstruction* (PF) [50] on the other hand tries to reconstruct the event as a whole, combining the information of all detector parts. In this analysis it is used for reconstruction of $\not\!\!E_T$ and jets, where it provides a better resolution than the default algorithms.

The basic idea of the PF algorithm is the *linking*, that is looking for measurements of the same particle in multiple detectors. For instance one would expect an entry in the calorimeters for each reconstructed track, but with different amounts of energy of different kinds of particles. In case a link is found, the combination of the measurements improves the resolution and in some cases reduces the impact of needed corrections. Accidentally counting the same particle twice is also avoided once the link is made. The PF algorithm uses the following basic particles:

- Muons: A track in the inner tracking system matched to a track in the muon system, with little or no calorimeter entries, compatible to minimally ionising particles.
- Electrons: A track in the inner tracking system matched to entries in the ECAL but without matched entries in the HCAL. Bremstrahlung is also considered while reconstructing the electron.
- Photons: A cluster in the ECAL without a track nearby and without matching entries in the HCAL.

- Charged hadrons: A track with matching entries in both ECAL and HCAL.
- Neutral hadrons: Matching entries in ECAL and HCAL without a matched track.

The resulting set of objects can then be used or combined into other objects.

The $\not{E}_T$ is constructed by taking the negative vector sum of all objects. Jets are constructed by applying a clustering algorithm to the reconstructed objects. Compared to jets constructed from calorimeter entries alone, this jets require smaller corrections to account for e.g. lost energy and non-linear response.

3.4.5. Jets

Coloured particles emerging from the interaction undergo fragmentation and hadronisation, that is they radiate additional coloured particles, which are combined into hadrons to form a burst of colourless particles. Compared to the masses of all resulting objects the initial particles carry a lot of momentum, at least in interactions of interest for this analysis. Thus the system is highly boosted and all particles in the final state move roughly in the same direction. The information of interest, i.e. the momentum of the initial particles, is preserved at this point, but to reconstruct it the outgoing particles need to be combined again. This is done by jet clustering algorithms which try to revert the process of fragmentation and hadronisation.

In this analysis the anti-k_T sequential recombination algorithm[51] is used with a size parameter of $R = 0.5$. Sequential recombination algorithms try to undo the fragmentation process to reconstruct the properties of the initial particle. They work by defining a distance d_{ij} between two objects i and j. The two objects with the smallest distance are removed from the list of objects in consideration and combined into a new object, which is then again part of the list. If the distance d_{iB} to the beam is smaller than any remaining d_{ij} the object is classified as a complete jet and not considered anymore. Algorithms working in this fashion are infrared safe[6] and collinear safe[7]. Due to the particular definition of d_{ij} of the anti-k_T algorithm jets are also nearly cone-shaped, which is beneficial for jet corrections. Any object, e.g. also isolated muons, are at the end part of the jet collection, thus cleaning criteria need to be applied to only select hadronic jets.

The cluster algorithm may miss same objects which came from the fragmentation of a specific particle, or they may pick up an object which came from somewhere else, e.g. another jet. Also the calorimeters do not react linearly to particles of all energies. This causes the energy of the reconstructed jet to deviate from the energy of the initial particle. By comparing jets reconstructed in simulated events to the underlying generator information correction factors are devised[52], which depend on p_T and η. They are verified using the p_T balance of di-jet and photon+jet events. Nevertheless there might be a difference between jets reconstructed in simulated events and those in data events, thus uncertainties on the corrections need to be taken into account, the jet energy scale uncertainties.

3.4.6. Luminosity measurement

Besides the centre of mass energy there is one other value of crucial importance for the Standard Model prediction: The integrated luminosity for one experiment. It can be

[6] A random distribution of soft objects in the detector does not change the outcome of the clustering algorithm.

[7] Splitting of one particle into two collinear particles does not change the outcome of the clustering algorithm

inferred from the beam parameters using Equation 3.4.

$$\mathcal{L} = \frac{f_{BX} N_b^2}{4\pi\sigma_x\sigma_y} \tag{3.4}$$

The inputs to this equation are: The number of bunch crossings per time f_{BX}, the number of protons per bunch N_b and the horizontal and vertical beam widths σ_x and σ_y assuming a Gaussian distribution of protons in the beam. The parameters f_{BX} and N_b are known with a sufficient precision, but σ_x and σ_y need to be determined using *Van der Meer* scans[53], which provide detailed information about the radial beam profiles. The scans interrupt the normal running of the accelerator and can thus only be performed a couple of times per year. During routine operation the above equation only allows a precision of worse than 10 %.

To increase precision, the luminosity is monitored online using the forward calorimeters (HF)[54]. One approach is to determine the fraction of the HF that did not measure energy entries in a collision. Another approach uses the linear relation between the average energy in the HF and the instantaneous luminosity. The measurements are later refined using offline methods, such as the number of reconstructed vertices per event. All methods use variables which are correlated to the instantaneous luminosity, but the precise relations need to be calibrated using Van der Meer scans. After calibration, the methods reach a precision of about 5 %.

4. Analysis input

4.1. Data

During the 2010 runs LHC delivered an integrated luminosity of 47 pb^{-1}[34] to CMS. Of this total amount of data, CMS was able to record 36.1 pb^{-1} with all subdetectors running and fully functional. These data have been certified to be suitable for physics analysis and are hence used in this analysis. This amounts to about $3.5 \cdot 10^{12}$ proton-proton collisions with a total cross section of 98.3 mb[55], which took place in the CMS detector.

During the course of data taking the CMS online system has be run using a number of evolving software versions, which reflected the understanding of the detector at the time of running. After the end of the data taking the evolution converged and all the data was reconstructed again using the newest version of the CMS software package, which at that time was 3.9.7. Thus all available data is reconstructed in a consistent way. The data used in this analysis is included in the re-reconstruction campaign known as *December 22*.

The data are written into so called streams[1] depending on the High-Level triggers that accepted the specific event. Events that fire e.g. any of the muon triggers are stored in the muon stream, while events firing electron triggers are stored in the electron stream. In case an event fires both muon and electron triggers, it ends up in both streams and is effectively stored twice. MUSiC analyses events from muon, electron and photon streams and is thus in danger of using the same event twice or even three times. Hence events from the electron stream are excluded, if they also fire muon triggers, and events from the photon stream are excluded if they also fired any of the muon or electron triggers. A total of about $150 \cdot 10^6$ events ended up in the streams used by MUSiC and are analysed. This number includes events counted more than once, whose duplicates are removed later on.

4.2. Standard Model Prediction

Analyses like MUSiC need a reliable prediction of what the experiment is expected to measure, supposed the Standard Model is a valid description. The Standard Model as described in previous sections is a mathematical model of the fundamental physics, but it does not provide a detailed description of the measured data in experiments like CMS. To make that link the following procedures are used:

4.2.1. Cross sections

Given the Standard Model or models of new physics, it is possible to determine the differential cross sections for various processes. For event generation purposes[2] this differential cross sections are determined from Feynman diagrams at leading order (LO), that is for most processes tree-level diagrams without any loops. Diagrams with higher number of particles and loops contain higher powers of the coupling constants in the calculations and are hence called *higher orders*. They provide better precision when calculating cross

[1] Technically the streams correspond to different files.
[2] Explained later in this section

sections. Usually the coupling constants are smaller than 1 and thus the effect of higher orders is lower and can be treated as corrections. To determine the total cross section of a process the differential cross section needs to be integrated, which most of the time can only be done numerically using Monte-Carlo techniques.

Differential cross sections at leading order usually give a reasonable estimate of the kinematic properties, but the total cross sections offer limited precision. Higher order calculations are available at next-to-leading-order (NLO) and next-to-next-to-leading-order (NNLO). For many processes used in this analysis higher order cross section calculations are available, but no higher order event generation is used, because for technical reasons there is currently only a small number of higher order generators available in the CMS software framework. In this case it is a common approach to take the leading order events, but normalise their weights to higher order calculations. The ration between the weight using a LO cross section and the weight of a higher order calculation is called a *k-factor*. Details can be found in the sections describing the respective samples.

Most NLO and NNLO calculations take into account higher orders in α_s, that is the strong coupling, but not in the electroweak coupling α. Usually higher order corrections in α_s show a higher effect, because the coupling constant is closer to 1.

In order to compare with CMS data, each event in a sample needs to be weighted by $w = \frac{k\sigma L}{N_{MC}}$ with σ being the estimated cross section, L the integrated luminosity and N_{MC} the number of generated events in this sample. Ideally this weight is below 1, but if σ is too high, not enough events can be generated due to limited computing resources.

4.2.2. Event generation

During the numerical integration of the differential cross section information about energy, momentum and direction of the participating particles can be obtained as well. The result is a set of events that resemble the underlying truth of the physical processes happening in collisions. The core of the generators only work at parton level, that is they use Parton Distribution Functions (PDFs, see Section 2.1.6) to choose one parton from each incoming proton and then use the respective differential cross section to calculate the collision of these two partons and the result is a small set of outgoing partons or leptons. In case some of these particles posses a very short lifetime, their decays are also simulated.

For a full description of what happens at a proton-proton collision, some more steps need to be performed. Both incoming and outgoing particles can radiate more particles, e.g. all strongly interacting partons tend to radiate off additional gluons and charged particles can radiate photons. All of the described events are presumed to take place on a very small scale and thus quarks and gluons can be considered as free particles. However, once these strongly interacting partons begin to move outwards and leave the range of asymptotic freedom, they need to be turned into colour-neutral objects. This step is called *hadronisation*, as the coloured partons are combined with spontaneously generated partons to form colour-neutral hadrons. In case these hadrons are not stable, they will again undergo decay simulation. Other outgoing particles with a sufficiently short lifetime are forced to decay at this point, too. The remnants of the two protons undergo interactions as well, producing more outgoing particles.

At the LHC not only single protons, but bunches of protons are brought to collision. If the density of protons in the bunches is high enough, there is a high probability of not only one pair, but multiple pairs of protons to interact. The consequence of this effect is called *pile-up*, because of a number of potentially interfering collisions is piled upon the collision of interest. Due to the construction of the detector it is usually not possible to completely

separate the collision of interest and the pile-up. To interfere with the measurement there must be at least some measurable activity in the active areas of the detector in the pile-up collisions. Those interactions are usually called *minimum bias*. In the CMS simulation this includes single and double diffractive events, low-p_T interactions and all processes with $p_1p_2 \to p_3p_4$ with p_i being any quark or gluon[3]. For each simulated event a varying number of additional interactions randomly chosen from the above processes is added. The number of additional collisions is drawn from a distribution that is similar to the data[35].

All stable particles left in the end are handed over to the detector simulation. Stable in this context means a sufficiently long lifetime to travel at least one centimetre undecayed.

Some generators, like PYTHIA 6[56], can only be used for processes involving two incoming and two outgoing particles in the matrix element, though the subsequent decay of the outgoing particles can produce more. An additional module, usually called *parton shower* takes care of the aforementioned radiation of strongly interacting partons or photons. This module uses empirical models about the frequency and kinematic properties of this radiation. While these models are usually tuned to match the data, they may underestimate the number and energy of the additional particles. More advanced generators like MadGraph[57] or Alpgen[58] can handle more outgoing particles and are thus able to include at least some of the radiated partons in the initial process. The parton shower is still needed, as the number of additional partons is usually limited, but the effect of uncertainties in the shower models are greatly reduced.

4.2.3. Detector simulation

While the result of the generation step gives a picture of the underlying physics, it still does not show what CMS is expected to measure. Thus a simulation of the detector response is needed to convert the list of particles into the expected electrical signals. First the list of stable particles is handed over to GEANT 4[59, 60], which simulates the interactions between generated particles and materials in the CMS detector. Combining knowledge about particles, detector geometry and properties of matter, GEANT is able to predict the reaction of the detector material to passing particles and the reaction of the particles while crossing the detector, e.g. the production of light when a charged particle crosses a piece of scintillator.

In a second step the response of the detector and read-out electronics is simulated to generate a set of data that is as close as possible to the data delivered by the experiment.

4.2.4. Reconstruction

As the simulated detector response is in the same format as the real data, it can be put through the same reconstruction algorithms, described in section 3.4.

4.2.5. Monte-Carlo samples

Simulated samples to be compared with data need to be produced and reconstructed in a way that is close to how the data were reconstructed. The MC samples used in this analysis belong to the *Fall 2010* production campaign, which has been generated, simulated and reconstructed using the CMS software package in version 3.8.4.patch2. Changes in the software between this version and the one used for the data are not expected to affect reconstruction, as they just contain modifications in response to technical problems in the data.

[3]PYTHIA[56] processes 11-13, 28, 53, 68, 92-95

The following Standard Model processes have been used in this analysis. Due to the selection criteria (see Section 5) MUSiC needs events containing leptons and photons, but not hadrons alone. However, due to the finite probability of hadrons being reconstructed as leptons or photons, some purely hadronic samples are used as well. In total $2 \cdot 10^8$ simulated events are used in this analysis. A summary table of this information can be found in Appendix B.

W boson with associated jets

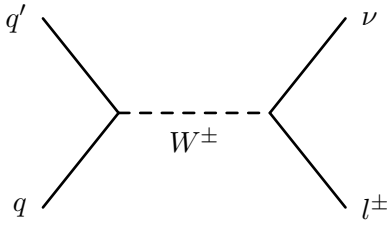

(4.1)

The electroweak process with the highest cross section predominantly shows up with one charged lepton and missing energy as shown in Figure 4.1. The W boson can also decay into jets, but this process is not expected to be visible in MUSiC due to the requirements described in Section 5. Additional jets can be radiated off the two incoming quarks. This sample has been generated using MadGraph[57] with all multiplicities of additional particles grouped into one sample according to their respective relative frequencies. The cross section of 31.3 nb[61] has been calculated at NNLO using FEWZ[62]. Due to the high order of the calculation, a small uncertainty of only 5% is applied to the cross section.

Drell-Yan with associated jets

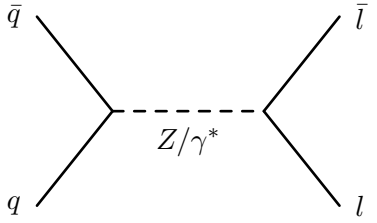

(4.2)

The electroweak Drell-Yan process (Figure 4.2) is dominant in events containing two leptons. Again the visibility of the decay into jets is suppressed by the selection requirement. As before additional jets can be radiated off the two incoming quarks. This process has been generated with Alpgen[58] and split into a number of subsamples, separated by the number of additional jets and their transverse momenta. The LO cross section of each sample has been scaled by a factor $k = 1.24$, such that the total cross section equals the FEWZ NNLO prediction of 3.05 nb[61]. As for W-boson production, the uncertainty is 5%.

At LO the electromagnetic component of the calculation causes divergences if the mass of the resonance approaches zero, thus a lower mass cut of 50 GeV has been applied to this sample. However, MUSiC can analyse two-lepton masses below this cut, hence a separate MadGraph sample with dilepton masses between 10 and 50 GeV has been used. The same k-faktor has been applied, but the uncertainty is taken to be 10%, because the

aforementioned NNLO calculation is also limited to higher masses. Just for the muon channel there is another PYTHIA[56] sample with a mass between 2 and 10 GeV, with again the same k-factor but an even higher uncertainty of 20%.

Top quark pair production

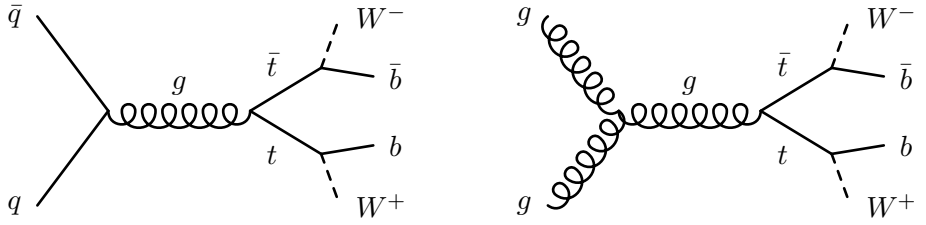

(4.3)

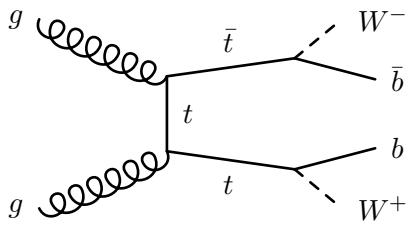

(4.4)

At leading order top quark pairs are dominantly produced with a gluon in the s-channel (Figure 4.3) or the top itself in the t-channel (Figure 4.4). While this is by far not the most probable strongly mediated process, it is very interesting as the top quark decays before it hadronizes. With a branching fraction of almost 100% it will decay into a bottom quark and a W-boson. The resulting two b-quarks on the other hand are stable enough to leave the range of asymptotic freedom and form b-hadrons, which can be detected as b-jets. Both W-bosons will decay either into a charged lepton and a neutrino, or into two quarks. While the latter happens more often, the resulting one or two jets can not easily be distinguished from other jets, which makes it hard to find this process in the background of other jet dominated events. Also, in case both Ws decay hadronically, the events do not pass the selection requirements. Hence for MUSiC two other outcomes are interesting: In the semi-leptonic channel one of the W decays into a charged lepton plus neutrino and the other into jets. In the fully leptonic channel both W-bosons decay into leptons. Both kinds of events show up in distinct signatures with one or more charged leptons, missing transverse energy and a number of hard jets. There are other productions channels than shown above, but they have lower cross sections and are thus not important here.

The sample used in this analysis has been generated with MadGraph, and it is scaled to a cross section of 165 pb[61]. The cross section is based on a NNLL[4] calculation[63]. Because of large higher order corrections, an uncertainty of 10% is used.

[4]Next-to-next-to-leading-logarithm

Boson pair production

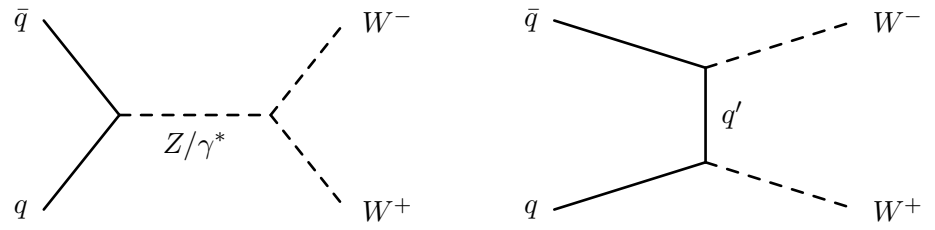

(4.5)

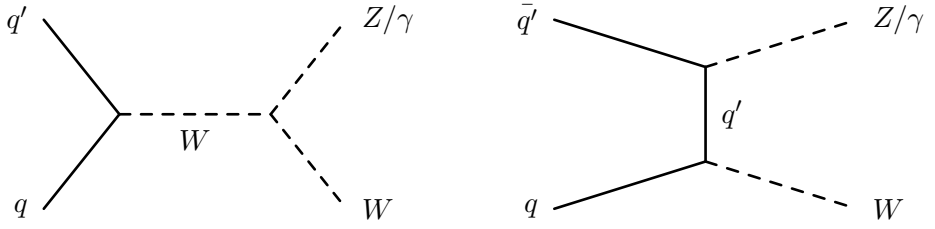

(4.6)

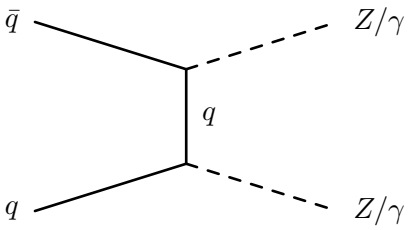

(4.7)

Vector bosons can also be produced in pairs, in all possible combinations of W, Z and photon, as shown to LO in Figures 4.5, 4.6 and 4.7. Except for the photons, the bosons will promptly decay, either leptonically or hadronically. Given the selection requirements of this analysis, at least one of the bosons must decay leptonically or a photon must be in the final state. The combinations without photons (WW, WZ and ZZ) are visible if at least one boson decays leptonically. However, if the other one decays hadronically, they are difficult to distinguish from single boson production with associated jets. The cross section of these processes, relative to the single boson production, is very low and thus both bosons decaying leptonically is the most interesting channel. This will show up as either four charged leptons (ZZ) or two or three charged leptons and missing energy (WZ, WW, and ZZ with one Z decaying into neutrinos). If the final state contains one photon, the other boson must decay leptonically, otherwise it will be indistinguishable from photon production with jets.

While the $W\gamma$ and $Z\gamma$ processes are grouped into one sample, generated by MadGraph, there are individual samples for WW, WZ and ZZ, all of them generated by Pythia. For the Pythia samples NLO calculations using MCFM[64] exist and thus an uncertainty of 10% has been applied. On the other hand no higher order calculations are available for the MadGraph samples and thus the uncertainty has been estimated to 50%.

Upsilon meson production

A number of hadrons with masses below 10 GeV are produced with significant cross sections and branching fractions to leptons. However, in this analysis the lowest cut on the

lepton p_T is 18 GeV, thus the hadron needs to be strongly boosted for the resulting leptons to pass this requirement. The lower the mass is the higher the boost needs to be and hence the lower the probability of this to happen. Eventually only the highest mass hadrons show a significant contribution, which are $\Upsilon(1S)$, $\Upsilon(2S)$ and $\Upsilon(3S)$.

The MC samples have been generated with Pythia separately for the decays into electrons and muons. According to [65] the cross sections calculated by Pythia are widely overestimated. Thus we use the measured cross sections for the muon channel. No measurements are available for the electron channel, but we assume lepton universality. Though the electron and muon samples are generated in a slightly different fashion and thus the muon cross section can not be used. Hence we use the same factor that is used to scale the generated muon cross section to the measured one to modify the generated electron cross section. This analysis uses a different kinematic selection than [65] and thus an uncertainty on the cross section of 30% is applied.

Multi-jet production

This is a notoriously difficult background. Firstly, its Feynman graphs contain a large number of strong interaction vertices and thus the process is very sensitive to higher order effects. Secondly, its cross section is very high and thus the number of simulated events is often insufficient. Given the selection requirements of this analysis, the process is not expected to contribute, but there are two mechanisms that make it show up: On the one hand a jet can be wrongly identified as a lepton, which happens predominantly for electrons, or it can be wrongly identified as a photon. On the other hand some hadrons of the jet can decay into leptons or photons, which are usually expected not to be isolated and thus should not be selected. However, in some cases they can be sufficiently separated from other jet constituents to appear isolated, or the jet actually consists of a single or very few hadrons that then decays into leptons or photons. This leads to another uncertainty in the prediction: A large cross section is paired with a small probability to pass the cuts, which is hard to measure without very large samples and a very detailed understanding of the fragmentation and detector response.

For most analyses, including this one, high energy jets are much more important, but they are also much rarer. Thus the sample is split into a number of subsamples with different p_T of the leading jets. This allows to increase the number of simulated events with high energy jets and mitigate the problem of too small samples at high p_T. Additionally a number of *enriched* samples has been used. During the simulation of the hadronisation events are selected when electromagnetic activity or muons are part of the decay products. This greatly increases the chance that the event in question subsequently passes the selection criteria. These kinds of event are, though in a low fraction, also part of the normal samples, thus the filters must be applied in reverse on the normal samples to avoid having the same kind of physics twice in the SM prediction. Both the samples as well the total cross sections come from Pythia and are thus only known at LO. To cover the effects of the strong dependency on α_S and the higher order corrections, an uncertainty of 50% is used.

Photons with associated jets

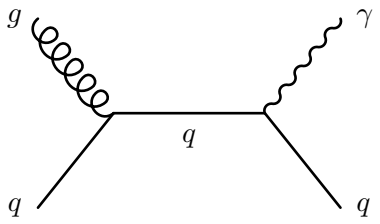

(4.8)

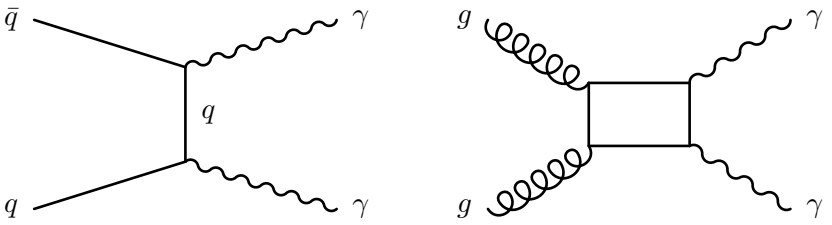

(4.9)

Single hard photons can be produced in association with jets or with more photons, as shown in Figure 4.8 and 4.9. Similarly to the previous process, the single photon sample is split in subsamples according to the p_T of the photon and the jet, in case of only one photon is generated. Additional samples are used for two photons. Again only LO cross section predictions are available and thus the uncertainty is taken as 50%.

5. Event and object selection

In conventional analyses the selection strategy is usually geared towards maximising the sensitivity to a certain signal, but this is not possible for a model independent analysis. Thus the selection employed in MUSiC is aimed at excluding regions where the experimental and theoretical uncertainties are large or not well known. A total of $8.7 \cdot 10^5$ measured events passes the selection criteria described in the following section and is used in the analysis.

5.1. Event selection

First and foremost any measured event needs to fire at least one trigger to be recorded and analysed. The triggers used in this analysis are shown in table 5.1. Due to the large variety of triggers applied in response to the rapidly changing instantaneous luminosity, additional criteria are required for a consistent treatment of all data and the simulation. Thus events are accepted if there is at least one muon with $p_T > 25$ GeV, one electron with $p_T > 30$ GeV, or one photon with $p_T > 90$ GeV, which also fulfils the object selection criteria. Figure 5.1 shows the efficiencies of the electron and muon triggers with respect to the p_T of reconstructed and selected objects. The electron and muon triggers reach an efficiency of about 95% and 90%, respectively, while the photon triggers are close to 100%[66] due to their much simpler requirements.

To select only events from colliding proton bunches, at least one properly reconstructed primary vertex is required. It must be reconstructed from at least five tracks and needs to be inside an envelope of 2 cm perpendicular to the beam and 24 cm in each direction from the nominal interaction region. The efficiency of this criterion exceeds 99.5 %[68].

Events with more than ten tracks are excluded, if the fraction of low quality tracks exceeds 25%, to reject events that are not from collisions, e.g. from beam-gas interactions[68].

Run range	Muon	Electron	Photon
135808-140070	Mu9	Ele20_LW	Photon30_8E29
140071-140362	Mu9	Ele20_LW	Photon20_Cleaned
140363-140387	Mu9	Ele20_LW	Photon30_8E29
140388-141949	Mu9	Ele20_LW	Photon20_Cleaned
141950-144114	Mu9	Ele20_SW	Photon30_Cleaned
144115-147116	Mu9	Ele17_SW_EleId	Photon30_Cleaned
147117-148818	Mu11	Ele17_SW_TightEleId	Photon50_Cleaned_v1
148819-149063	Mu15_v1	Ele22_SW_TighterEleId_v2	Photon70_Cleaned_v1
149064-149442	Mu15_v1	Ele22_SW_TighterEleId_v3	Photon70_Cleaned_v1
Simulation	Mu9	Ele17_SW_EleId	Photon20_Cleaned

Table 5.1.: *High level trigger used for MUSiC in 2010 CMS data and simulation. The number after the object name indicates the HLT p_T threshold in GeV.*

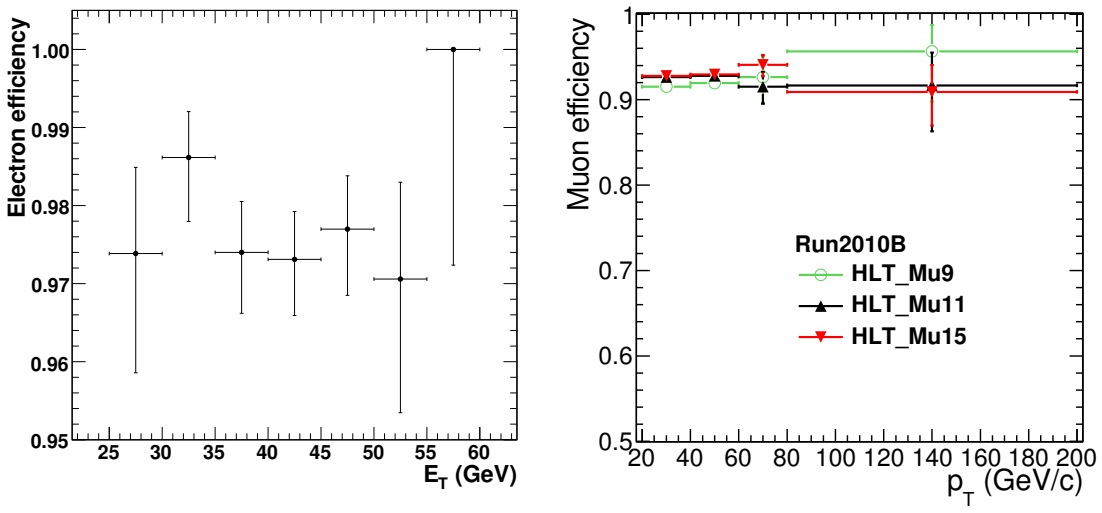

Figure 5.1.: *Efficiencies of the electron[66] and muon[67] triggers with respect to the E_T or p_T of reconstructed and selected objects.*

Both the light detectors of the HCAL as well as the electronic boxes may cause noise in the HCAL, which is excluded using a special filter[69].

If there is an electron pointing within $|\Delta\phi| < 0.1$ in the same direction as the $\not{E}_T$ [1], then the event is not considered, to exclude events where significant amounts of energy e.g. vanished in not instrumented or dead parts of the detector.

5.2. Object selection

5.2.1. Muons

A global fit including hits in the silicon tracker and the muon system is accepted as a good muon if it fulfils the following criteria, based on[70]:

- Reconstructed transverse momentum of the global track: $p_T > 18$ GeV
- Pseudorapidity of the global track must be in the reach of the trigger: $|\eta| < 2.1$
- Quality of the global fit: $\frac{\chi^2}{N_{DOF}} < 10$
- Global track fitted with at least 11 hits in the silicon tracker including the pixel detector, of which at least one must be in the pixel detector, and at least one hit in the muon system must be part of the successful fit. This excludes objects that did not pass through the whole detector, as muons usually do.
- The global track must be associated to a successful track fit using only the silicon tracker hits, and at least two muon stations with track segments matched to this track. This reinforces the selection of objects passing through the whole detector, similar to the criterion above.

[1] The $\not{E}_T$ must be larger than 30 GeV to be considered here.

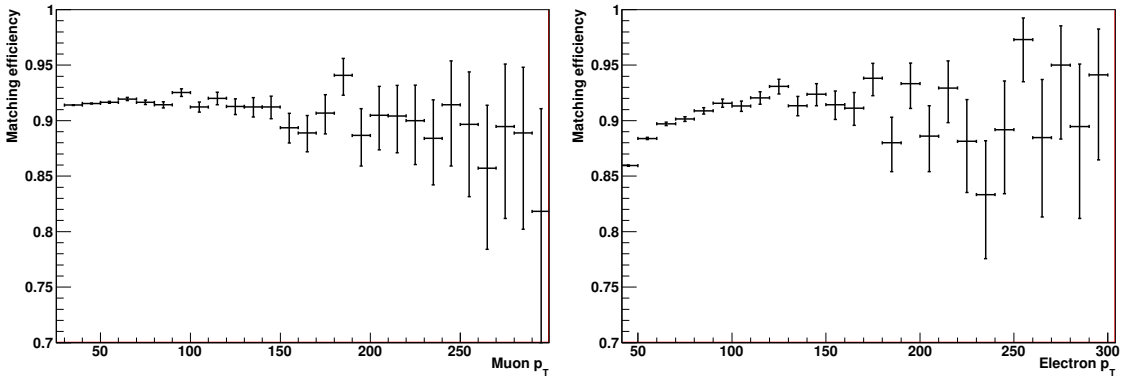

Figure 5.2.: *Reconstruction efficiency of muons and electrons in a W boson sample, as a function of the generated lepton's p_T after application of all selection criteria. The generator particle is isolated and with the same η selection applied as the reconstructed object.*

- The extrapolated trajectory must pass the nominal beam line at a maximum distance of 2 mm, to exclude muons from cosmic rays.
- The muon must be isolation with the sum of track $p_T < 3$ GeV within a cone of $\Delta R = \sqrt{\Delta\phi^2 + \Delta\eta^2} < 0.3$, excluding the track associated to the muon. This vetoes muons originating from hadron decay in jets, which are not isolated, in contrast to prompt muons.

Figure 5.2 shows the reconstruction efficiency after application of the above criteria including event selection and triggers. The efficiency is thus the combined probability for a generated particle to be part of an event that has been triggered and selected, and to be reconstructed and selected. The efficiency is determined in W boson samples for generator particles with the indicated p_T, selected to be isolated and within $|\eta| < 2.1$ for muons. A particle is considered to be reconstructed if a corresponding object has been reconstructed and selected within a distance of $\Delta R < 0.2$.

5.2.2. Electrons

Similar to muons, electrons leave hits in the tracking detectors. However, an electron does not traverse the whole detector, but it is instead stopped in the ECAL, thus it is identified by a track with a matching cluster in the ECAL. To be considered, an electron must pass the following selection criteria, based on[71]:

- Reconstructed transverse energy of the ECAL cluster: E_T >25 GeV
- The pseudorapidity $|\eta|$ of the track must be less than 1.442 in the ECAL barrel and $1.56 < |\eta| < 2.5$ in the ECAL endcap, in order to avoid the transition region between barrel and endcap.
- The GSF tracking algorithm (see Section 3.4.3) is based on track seeds matched to ECAL clusters.
- The extrapolated impact point of the track in the ECAL does not deviate from the cluster position by more than 0.09 in ϕ and more than 0.005 or 0.007 in η in the barrel and the endcap, respectively. This reduces the probability of a wrong combination of a track and a cluster.

- A strip of 1×5 crystals in $\eta \times \phi$ including the seed crystal must contain at least 83% of the cluster's energy, a strip of 2×5 must contain at least 94%. ECAL clusters of electrons can be quite wide in ϕ due to radiation of Bremsstrahlung photons in the magnetic field, they are however not expected to extend far in η direction.

- The spread of the energy $\sigma_{i\eta i\eta}$ in units of crystals in η direction must be less than 0.03 in the endcaps. Details about this criterion can be found in Appendix A.2.

- The reconstructed energy in the HCAL behind the ECAL cluster must be less then 5% of the cluster's energy. This reduces the number of charged hadrons reconstructed as electrons.

- Isolation:
  - Sum of the p_T of tracks in a cone of $\Delta R < 0.3$ must be less than 7.5 GeV in the barrel and less than 15 GeV in the endcap.
  - Isolation: In the barrel the transverse component of the energy in the HCAL in a cone of $\Delta R < 0.3$ must be smaller than $2\ \text{GeV} + 0.03 \cdot E_T$ with E_T being the transverse component of the supercluster's energy. Similarly the HCAL energy must be smaller than $2.5\ \text{GeV} + 0.03 \cdot E_T$ in the endcaps, but here the energy is measured only in the first layer of the HCAL.
  - Isolation: The energy measured in the second layer of the HCAL in the endcaps behind the supercluster must be less than 0.5 GeV.

Sometimes the APDs[2] of the ECAL are triggered by direct impact of particles and not by the scintillation light of the crystals. This effect is called an ECAL spike. In this case a very large discharge is measured which looks like a very large energy entry in one single crystal, or occasionally in two neighbouring crystals. Electromagnetic showers in the crystals however are expected to extend over multiple crystals. Also in the case of direct firing the delay caused by the scintillation decay is missing, and thus the discharge is detected earlier than expected. To exclude those spikes, the following criteria must be fulfilled by electrons:

- The timing of the seed crystal, that is the crystal with the highest energy, must be close to what is expected from electrons moving at relativistic speed and the properties of the scintillator.

- *Swiss cross* variable $1 - \frac{E_4}{E_{\text{seed}}}$ must be less than 0.95, with E_4 being the energy in the four crystals sharing a surface with the seed crystal. This is roughly equivalent to the seed crystal containing a maximum of 95% of the total cluster energy.

- Ratio $R_{29} = \frac{E_{\text{seed}} + E_{2\text{nd}}}{E_9}$ of the seed energy plus the second highest energy entry $E_{2\text{nd}}$ in the adjacent crystals to the energy E_9 of all nine crystals surrounding and including the seed crystal must be less than 0.9. Similar to the criteria above this requires the energy concentrated on two adjacent crystals to be less than 90% of the total energy.

The reconstruction efficiency using this selection as a function of p_T is shown in Figure 5.2, which has been determined by comparing generator information to reconstructed objects in W boson samples.

[2] Avalanche Photo-Diode

5.2.3. Photons

A photon, in contrast to electrons, is not associated to a track and thus only reconstructed from calorimeter measurements. Hence the selection criteria needs to be tighter to reliably distinguish it from other objects causing hits in the ECAL. Photons are accepted, if they pass the following selection criteria[72]:

- Reconstructed transverse energy of the ECAL cluster: $E_T > 25$ GeV
- Weighted average of the pseudorapidity $|\eta|$ of the cluster must be less than 1.442 in order to use only photons in the barrel region, because the higher activity of jets in the forward region causes a higher fake rate which needs to be studied in a future analysis.
- There must be no track seed in the pixel detector along the extrapolated photon trajectory, in order to reject electrons.
- The reconstructed energy in the HCAL behind the ECAL cluster must be less then 5% of the cluster's energy to reduce the number of neutral hadrons reconstructed as photons
- When calculating the energy of a photon, correction factors are applied to the energy of the individual ECAL crystals to account for response variations. In some cases these correction factors can be very large, negatively affecting both the resolution as well as the spike removal. Thus photons with a reconstructed energy more then twice as large as the raw energy are rejected.
- The spread of the energy in η direction in units of crystals must be $\sigma_{i\eta i\eta} < 0.013$. Details about this criterion can be found in Appendix A.2.
- The same spike cleaning criteria as described for the electrons (Section 5.2.2) is applied.
- Isolation:
  - Sum of the p_T of all tracks in a cone of $\Delta R < 0.4$ around the cluster, excluding an inner cone of $\Delta R < 0.04$: $\sum p_T^{\text{tracks}} < 2 \text{ GeV} + 0.001 \cdot p_T^{\gamma}$
  - Sum of the E_T of all ECAL hits in a cone of $\Delta R < 0.4$ around the cluster, excluding all hits of the cluster itself: $\sum E_T^{\text{ECAL}} < 4.2 \text{ GeV} + 0.006 \cdot p_T^{\gamma}$
  - Sum of the E_T of all HCAL towers in a cone of $\Delta R < 0.4$ around the cluster, excluding an inner cone of $\Delta R < 0.15$: $\sum E_T^{\text{HCAL}} < 2.2 \text{ GeV} + 0.0025 \cdot p_T^{\gamma}$

Figure 5.3 shows the reconstruction efficiency when this selection criteria are applied.

5.2.4. Jets

To select jets that come from hadronised coloured partons the following criteria are applied[73]:

- Reconstructed transverse energy $E_T >$50 GeV
- Reconstructed pseudorapidity $|\eta| < 2.5$
- Made from more than one Particle Flow object in order to select jets that are not just one single particle.

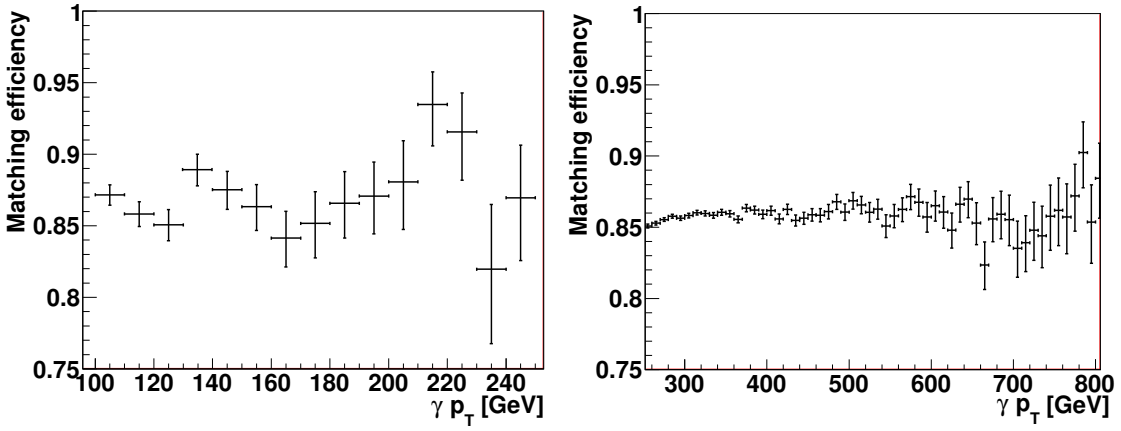

Figure 5.3.: *Reconstruction efficiency of photons as a function of the generated p_T after application of all selection criteria. The generator particle is isolated and with the same η selection applied as the reconstructed object. Di-photon samples have been used, with* 25 GeV $< p_T^\gamma <$ 250 GeV *and* $p_T^\gamma >$ 250 GeV, *respectively.*

- The jet must not by reconstructed only from neutral hadronic or electromagnetic objects, to exclude jets that are only reconstructed in either the HCAL or the ECAL.
- For jets close to the edges of the tracker and the endcap calorimeters ($|\eta| > 2.4$):
  - At least one charged object in the jet, to make sure tracker information has been part of the reconstruction.
  - The jet must not be reconstructed only from charged electromagnetic objects, to ensure the HCAL has been part of the reconstruction.

Reconstruction efficiency studies similar to those shown for leptons and photons cannot be performed in this analysis, because no jet triggers are used. However, the efficiency in selected and triggered events has been measured to exceed 99.5 %[74].

5.2.5. MET

The $\not\!\!E_T$ is reconstructed from all Particle Flow objects. It must exceed 30 GeV to be considered as part of the event.

5.3. Overlap cleaning

Particles passing the detector can be counted multiple times in a single event, if they are reconstructed in different parts of the detector. Also the same entry in the detector can be used for the reconstruction of multiple objects. Using the same energy entry more than once must be avoided, and thus a cleaning of objects too close to each other is applied:

- Jets are removed if electrons or photons are closer than $\Delta R < 0.2$
- Photons are removed if any selected electron shares its cluster
- Muons are removed if there is another muon close by ($\Delta R < 0.2$) with a better χ^2

6. Analysis

6.1. The search algorithm

The goal of MUSiC is to look at large fraction of all events taken by CMS, though focused on high energy processes. Nevertheless models of new physics rarely predict a general excess in all kinds of events, but usually in just a couple of final states. Thus the first step of the algorithm, after applying event and object selection, is to sort the events into classes depending on their object content. Each class can now be treated as a single counting experiment or a more detailed analysis can be performed by looking at a number of histograms of kinematic variables, which are expected to be sensitive to new physics. To identify possible signs of new physics the next step is to scan these distributions for deviating regions. Both for the treatment as counting experiments as well as after identifying deviating regions the last step is to determine the significance of any deviation.

6.1.1. First step: Classification

Each event includes a list of considered objects, that is at least one from the following list:

- Muons
- Electrons
- Photons
- Jets

Additionally each event may or may not contain a significant amount of missing energy. More types of objects, particularly jets coming from τ leptons or b hadrons, are currently under study, but are not part of this analysis at the time of writing. This list of objects is well defined for each event and thus each event can be put into precisely one *exclusive class*. Exclusive event classes ease the statistical treatment, because each event is in exactly one class, which reduces correlations between classes. However, the signature of some sorts of new physics is defined in one kind of objects, e.g. some heavy resonances show up in at least two leptons of same flavor and opposite charge, but less well defined in other objects, e.g. the number of additional jets is not fixed. Thus is can be beneficial to also analyse *inclusive classes*, which are more sensitive to certain models of new physics. These inclusive classes define just a minimal number of certain objects and take all events that fulfil this requirement. But now one has to keep in mind that in this case events are usually sorted into a number of classes and thus a single event can cause a number of deviations in different classes. The gain in significance hence comes with increased difficulties in the statistical interpretation. Figure 6.1 shows in which classes an exemplary event with one electron, one muon and two jets is being sorted.

For very obvious deviations it might be enough to simply look at the total number of events in each class, but in many cases new physics will only show up in certain kinematic configurations. Dedicated analyses can look at very specific kinematic variables to

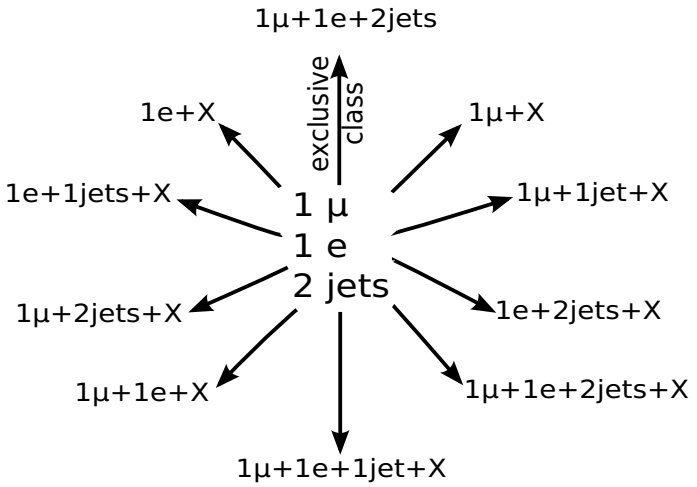

Figure 6.1.: *Scheme of the exclusive and inclusive classes an event with one electron, one muon and two jets is being sorted into*

maximise their sensitivity, but this is not feasible for MUSiC. Nevertheless there are some kinematic variables that are expected to be sensitive to a lot of new physics signals, of which three are used (see Section 6.2.2). Moreover, dedicated analyses can focus on small parts of the distributions of these kinematic variables by selecting just certain events, again to maximise sensitivity. MUSiC on the other hand tries look at the whole distribution and then scans for deviations, similar to the approach used at H1[4].

Lepton charges

The classification process of MUSiC can be run in two modes, ignoring or considering the lepton charges. The first mode, which is the default, ignores the lepton charge and the leptons are simply counted. For example, events containing two muons and one electron are sorted into the 2μ+$1e$ class. In the second mode the absolute total charge $Q = |\sum_l q_l|$ of all leptons is calculated and used as part of the class definition. The aforementioned events with two muons and one electron are then sorted into one of two classes, $2\mu + 1e[1Q]$ or $2\mu+1e[3Q]$, depending on whether all leptons carry the same charge or one of them carries a different charge than the other two. The second mode provides additional information, separating e.g. same-sign and opposite-sign events, but is also affected by an additional uncertainty, see Section 6.3.7.

: The lepton charge can be misassigned, reconstruction a positive charge from a negatively charged lepton and vice versa. For both muons and electrons this can happen at very high p_T with a nearly straight trajectory. Statistical fluctuations or

6.1.2. Second step: Scanning for deviations

To gain a broad overview each class can be considered as a single counting experiment with three values:

- Number of measured events N.
- Number of expected events B.
- Systematic uncertainty on the number of expected events σ.

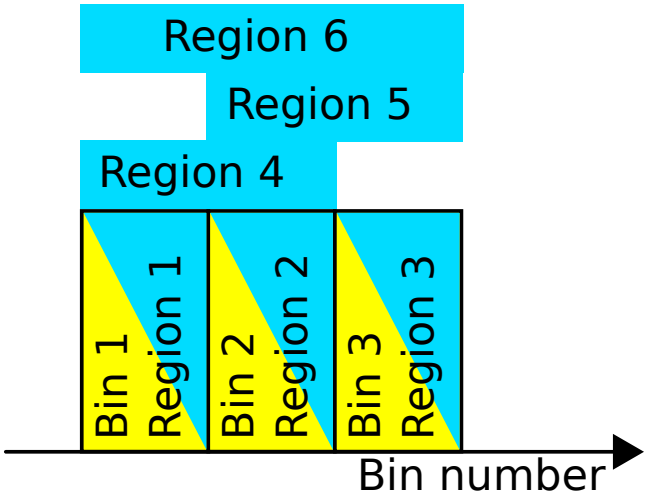

Figure 6.2.: *From three bins (yellow) a total of six regions can be formed: Three containing the individual bins (blue triangles). Two containing two bins and one containing all three bins (all shown as blue boxes). There is no region formed from the first and the last bin, because they are not adjacent.*

With these three values it is now possible to calculate a probability, or *p-value*, which shows how likely the statistical fluctuations of the Standard Model will generate deviations that are even more extreme than the measured data. Additionally the statistical uncertainty is taken into account, but it is calculated from B and thus not part of the input to the p-value. Details about the used p-value can be found in Section 6.2.1.

New physics can show up as a deviation in anything between a single bin, e.g. a narrow resonance in a mass spectrum, and the whole distribution, e.g. Supersymmetry in the $\not{E}_T$ distribution. Thus the MUSiC algorithm can also take a closer look into the classes by scanning the kinematic distributions of each class for deviations. This is done by defining *regions*, that is all possible combinations of adjacent bins. Figure 6.2 shows an example with all regions that can be formed from three bins. Given a distribution with n bins, this leads to a total number of $\frac{N}{2}(N-1)$ regions that can be formed.

For each of these regions again the three values N, B and σ are calculated: The regions with the smallest p-value, that is the region with the most improbable deviation, is called the *Region of Interest*.

When treating each class as a simple counting experiment the p-value can be interpreted as a probability, but by selecting the region with the smallest p-value a bias is introduced and different a question needs to be answered: What is the probability of a deviation like the one selected to show up anywhere in the distribution. The higher the number of considered regions, the higher the probability to encounter a certain deviation just by chance. This is called the *Look-Elsewhere Effect* and needs to be taken into account.

6.1.3. Look-Elsewhere Effect

To take into account the Look-Elsewhere Effect introduced by testing all regions, a new probability $\tilde{p}$ needs to be defined and calculated. In the case of n independent regions, this probability can easily be calculated (Equation 6.1).

$$\tilde{p} = 1 - (1-p)^n \tag{6.1}$$

However, in MUSiC regions are not independent for two reasons:

- Bins can and usually will be part of multiple regions. Thus a single deviating bin will cause the p-values of various regions to change.
- Some systematic uncertainties are correlated between bins. Deviations in these uncertainties will cause many, maybe even all bins to deviate.

To take this effects into account a Monte Carlo approach is used. The Standard Model expectation is taken as a template to draw pseudo-experiments that represent possible outcomes of a CMS measurement. For each bin a pseudo-truth value is randomised using the expectation value and all individual systematic uncertainties, taking into account correlations between bins as described in Section 6.3. This value is used as the expectation value of a Poisson distribution to draw a possible measurement for this bin. All bins together form one possible outcome of the kinematic distribution in question. Each pseudo-measurement is then fed through the scanning algorithm as the data, again determining the most significant region and its p-value p_{min}^{pseudo}. The selected region does not need to be, and usually is not, the same as the one selected on data. The new p-value including the Look-Elsewhere Effect $\tilde{p}$ is then simply the fraction of pseudo-measurements with $p_{min}^{pseudo} \leq p_{min}^{data}$, as such showing the probability of finding any region that deviates even more than the Region of Interest:

$$\tilde{p} = \frac{N_{pseudo}(p_{pseudo} < p_{data})}{N_{pseudo}} \tag{6.2}$$

While the Look-Elsewhere Effect in the described form does not need to be considered when treating each class as a counting experiment, pseudo-experiments are still useful to e.g. determine the expected distribution of p-values for all classes.

6.1.4. Presentation of results

No matter if each class is treated as a single counting experiment or if regions are selected and the Look-Elsewhere Effect is taken into account, there is a danger of introducing another bias by specifically looking at the class with the strongest deviation. Moreover a deviation from the Standard Model might not show up as a single very significant distribution, but instead in an increased number of classes with a slightly increased significance. To account for both effects a graphic way of presenting the result has been chosen: The distribution of the p or $\tilde{p}$ of all classes is plotted and can then be compared to the Standard Model expectation. The expectation is determined again by using the pseudo-experiments, this time to generate an ensemble of p-values of all classes. In the case of counting experiments enough of these ensembles can be used to determine the expected shape of the p distribution. When regions are selected, the p-values can be compared to more pseudo-experiments to determine the expected ensemble of $\tilde{p}$ values. A large number of these ensembles can then be used to determine the expected average shape of the $\tilde{p}$ distribution. The observed shape of the $\tilde{p}$ distribution can then be compared to the expected shape, see e.g. Figure 7.1.

It might be possible to compare in detail the ensemble of $\tilde{p}$ distributions to the measured distribution to determine a global significance. However, this would need a detailed study of possible *measures of agreement*, which can not be performed in this analysis. A very simple approach is to count the number of classes beyond a certain significance and compare it to the fraction of pseudo-experiments with a similar or larger number.

6.2. Detailed choices

6.2.1. p-value

The p-value is calculated as shown in Equation 6.3.

$$p = \begin{cases} A \cdot \sum_{i=0}^{N} \int_{0}^{\infty} \frac{e^{-\mu}\mu^i}{i!} \cdot e^{\frac{-(\mu-B)^2}{2\sigma^2}} d\mu & \text{if } N < B \\ A \cdot \sum_{i=N}^{\infty} \int_{0}^{\infty} \frac{e^{-\mu}\mu^i}{i!} \cdot e^{\frac{-(\mu-B)^2}{2\sigma^2}} d\mu & \text{if } N \geq B \end{cases} \tag{6.3}$$

The first term $\sum_{i=N}^{\infty} \frac{e^{-\mu}\mu^i}{i!}$ (or $\sum_{i=0}^{N} \frac{e^{-\mu}\mu^i}{i!}$) defines the probability of measuring N or more (respectively N or less) events, if the expected number of events is μ. The second term $e^{\frac{-(\mu-B)^2}{2\sigma^2}}$ then describes the credibility of a true expectation value μ in case the simulated expectation value is B with a total uncertainty of σ. Thus the total systematic uncertainty σ must contain all known systematic effects[1] that could cause the measured data to deviate from the prediction. The normalisation factor A is needed because the Normal distribution in Equation 6.3 is truncated at 0. It is calculated as shown in equation 6.4.

$$A^{-1} = \sum_{i=0}^{\infty} \int_{0}^{\infty} \frac{e^{-\mu}\mu^i}{i!} \cdot e^{\frac{-(\mu-B)^2}{2\sigma^2}} d\mu = \int_{0}^{\infty} e^{\frac{-(\mu-B)^2}{2\sigma^2}} d\mu \tag{6.4}$$

It has been shown[75] that this p-value has reasonable statistical properties[2], though it still has a number of drawbacks:

(a) There is no precise analytic solution, thus the integration must be approximated numerically. A partial integration approach could also be implemented, but would require a large number of evaluations of the error function[3], which is again a numerical approximation.

(b) All uncertainties are summarised in one single value σ assuming a Normal distribution. The total uncertainty is formed by summing the individual uncertainties in quadrature, hence they are assumed to follow a Normal distribution as well. This is valid for uncertainties that are known as absolute numbers, but it is not precise for relative uncertainties. A Normal distribution is also not correct for the uncertainty introduced by limited number of simulated events.

(c) The Normal distribution is truncated at zero, which leads to overcoverage[75] in case of deficits and if the uncertainty is of the same order as the expectation itself.

However, up to now no alternative approach has been found to be feasible, because there are some requirements:

1. Regions made from multiple bins are formed by summing up the observed events as well as the prediction and uncertainties. Any feasible p-value must use distributions with a well defined, but still simple behaviour in this case.

[1] Including those introduced by the limited MC sample size.

[2] The p-value, which is calculated from an experimental sample drawn from a truth distribution, is usually close to or larger than the underlying true probability.

[3] The error function can be used to calculate $\int_{x}^{\infty} e^{\frac{-(\mu-B)^2}{2\sigma^2}} d\mu$

2. During a full scan the p-value needs to be calculated very often, in the order of 10^{10} times. Thus the calculation needs to be fast.

3. Given the large number of calculations, it must be numerically stable, as no human supervision is possible.

The drawbacks b and c can be partially solved by using different distributions, e.g. a Lognormal, but it turned out this breaks requirement 1[76]. Using a different approach to take into account the uncertainty due to limited simulated sample size partially solves drawback b while still fulfilling requirement 1, but is not numerically stable and too slow (requirements 3 and 2)[77].

Skipping regions of interest

A region should be ignored, i.e. considered not significant, in three cases:

1. Zero observed events and an expectation that is close to zero relative to its uncertainty, i.e. closer than three standard deviations. As stated above, the used p-value overcovers in this situation. But even without overcoverage a region like this can never be of interest, because the measured value is too close to the expectation if one includes the systematic uncertainties.

2. Similarly a region can be ignored in case the observed value is less than three standard deviations away from the expectation. This requirement is applied, though it is optional, as its sole purpose is to avoid the time consuming p-value calculation as often as possible.

3. Zero observed events in case of an expectation below one. Besides a small performance increase, this requirement mitigates the artificial increase of the number of classes and regions by adding unimportant Standard Model processes with very low cross sections.

These requirements are applied to all considered regions and can thus lead to a class with all regions skipped. In case this happens the whole class is ignored and does not show up in the resulting $\tilde{p}$ distribution. The class is nevertheless considered in the simplified case of treating the classes as counting experiments.

6.2.2. Kinematic variables

The following variables are filled into histograms:

Sum of scalar transverse momenta

Many models of new physics predict deviations from the Standard Model in the regime of high energy or high mass. The Standard Model on the other hand predominantly covers regions with comparatively low energy. The sum of scalar transverse momenta ($\sum p_T$) is strongly correlated to the total amount of energy that took part in the interaction and is hence sensitive to new physics of this kind. This variable is sometimes called *effective mass*.

This sum is calculated from all objects including $\not{E}_T$ in exclusive classes. In inclusive classes the sum is calculated from the objects defining the class, but not including the additional objects. For instance in the inclusive class containing at least one electron and

two jets, the sum is calculated from the electron with the highest transverse momentum and similarly the two jets with the highest transverse momentum. Softer electrons and jets as well as all other particles are ignored.

Combined mass

New particles can be produced as resonances and then show up as very clear signals in the combined mass of their decay products. Thus the invariant mass (M) of a number of objects is a sensitive kinematic variable, too. The choice of objects to form the mass is the same as described for the sum of transverse momenta, though it can only be calculated in classes containing at least two objects. In case the $\not{E}_T$ passes the selection threshold (see Section 5.2.5), not the normal invariant mass is calculated, but the transverse mass, where the z-component is ignored.

Missing transverse energy

In the Standard Model only neutrinos are able to leave the detector unseen. New physics on the other hand might contain new invisible particles of higher mass or neutrinos with unexpectedly high momentum. Both will show up as large amounts of missing transverse energy ($\not{E}_T$), which is thus also a sensitive variable. It is however only analysed if it exceeds the selection threshold (see Section 5.2.5), because the low energy region is dominated by the Standard Model and the detector resolution.

6.2.3. Resolution and bin width

New physics signals, particularly resonances, can be very narrow, though the measured width can never be narrower than the resolution of the detector. Thus choosing a bin width much larger than the resolution could mean to lose a small and narrow signal in the background. It can be shown, for simple assumptions, that the ideal size of a region in terms of significance is around half the width of the resonance (see Section A.3). There is no gain in choosing a bin width significantly smaller than the resolution, because the MUSiC algorithm will anyway merge smaller bins into a larger region to minimise the p-value. Small bins actually implicate a large number of bins and thus an even larger number of regions[4]. Increasing the number of regions however increases the Look-Elsewhere Effect, thus reducing the resulting significance of the deviation. Even worse, a higher number of regions increases the chance of a random fluctuation somewhere else in the distribution beating the true signal as the most significant deviation. In summary, a bin size as large as possible, but not larger than the resolution, should be chosen to maximise sensitivity to new physics signals. Also in terms of p-value evaluations, hence computing time, it is beneficial to reduce the number of regions. Thus a bin width close to the expected resolution is chosen, see Appendix A.3.

As mentioned above resonances can be very narrow, but they are only expected to occur in the combined mass distribution. Deviations in the $\sum p_T$ and $\not{E}_T$ distributions on the other hand are expected to be wider, in case they are caused by new physics. To account for this, any considered region in the $\sum p_T$ and $\not{E}_T$ distributions needs to be at least three bins wide, while a single bin is enough in the combined mass distribution.

To ensure a consistent appearance of distributions with a constant bin width and those with a variable bin width, the number of events per bin needs to be normalised to the

[4]The number of regions is proportional to the square of the number of bins

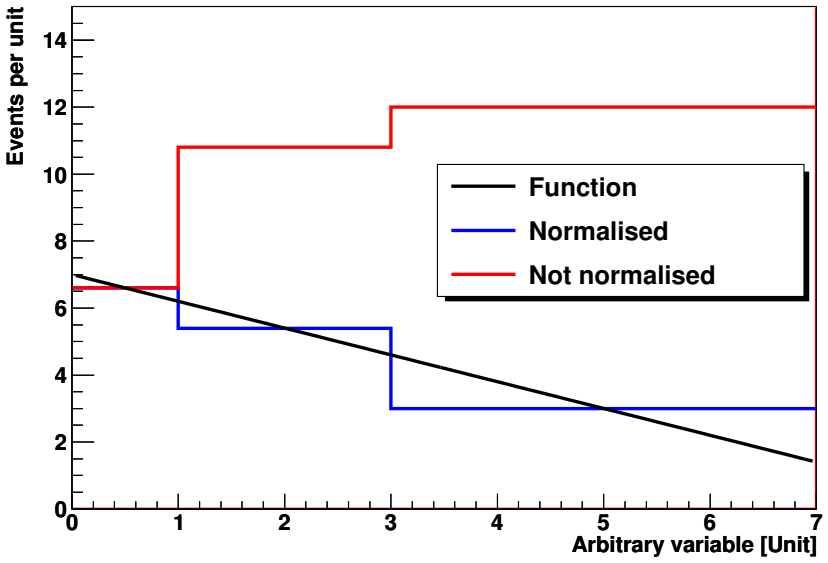

Figure 6.3.: *Histograms of a probability density function (black), normalised (blue) and not normalised (red) to the bin width. The height of the red bins equals the number of counts in this bin, while the area of the blue bins equals the area of the function.*

bin width. Then a smooth function will stay smooth even at places where the bin width changes dramatically. While this provides an intuitive grasp of the shape of the distribution, the resulting fractional number of events per bin can be confusing when trying to visually count events. To mitigate this effect it is advantageous to choose a bin width that is an integer multiple of some value; 10 GeV has been chosen in this analysis. Figure 6.3 shows two histograms obtained from a probability function (shown in black), which is falling linearly. The red histogram, not normalised to the bin width, shows the actual number of counts in this bin. The bin width is growing exponentially and thus the counts per bin increases in spite of the falling function. The blue histograms is normalised to the bin width and thus the area in each bin is proportional to the number of counts in this bin and thus proportional to the integral of the function in the range of this bin. In this case the shape of the histogram provides a more intuitive view of the shape of the function.

For the different kinematic variables different resolution functions need to be chosen. Even if the resulting kinematic variables are similar in different events, the resolution can be different, depending on the number and configuration of objects in the events. However, this information is lost when one looks at the kinematic distributions, thus the resolution functions need to be simple functions of one parameter, that is the kinematic variable, returning the resolution at this position. The influence of the event configuration can be partly taken into account by taking different resolution functions for different event classes. However, even in this case the event topology is not unambiguously defined, e.g. the $\sum p_T$ resolution of an event containing one muon and one jet depends on the individual energies of the two particles. Hence some simplifications need to be made to gain a reasonable estimate of the resolution. These simplifications are used to estimated the resolution, but when the histograms are filled the correct calculations are used.

Sum of scalar transverse momenta

It is a reasonable assumption that on average each participating object will carry an equal fraction of the total $\sum p_T$, i.e. $p'_T \approx \frac{\sum p_T}{N}$ with N being the total number of objects in the event class. Then the resolution can be estimated with:

$$\sigma_{\sum p_T}\left(\sum p_T\right) \approx \sqrt{\sum_i N_i \cdot \sigma_i^2\left(p'_T\right)} \tag{6.5}$$

Here N_i is the number of objects of one type, e.g. muons, and σ_i the resolution of these objects. The resolutions of the various objects can be found in Appendix A.4.

Combined mass

The resolution of the combined mass of all participating objects depends even more on the event topology, thus a bold but helpful assumption needs to be made: All objects are assumed to be at $\eta = 0$ and equally spaced around ϕ. In this simplified case the combined mass equals the $\sum p_T$, with the same resolution.

Missing transverse energy

As shown in Appendix A.4, the resolution of $\not{E}_T$ depends on the total $\sum p_T$ of the event. Obviously the $\sum p_T$ can be quite different even for events with similar $\not{E}_T$ and thus the resolutions can vary. For events with significant amounts of $\not{E}_T$ it can however be assumed that the $\sum p_T$ will be of the same order of magnitude as the $\not{E}_T$ itself. Then the resolution of the $\not{E}_T$ can be approximated with its resolution for $\not{E}_T = \sum p_T$.

6.2.4. Low statistics treatment

There will always be some regions of the phase space where the number of simulated events is insufficient. This can either be because of the high cross sections of certain SM processes or because the process in question is so rare it has not been simulated separately due to time and computing power constrains. The effect is an incomplete or non-existent SM prediction for some classes or kinematic regions. Without a prediction it is not possible to calculate a p-value and thus to judge the significance of measured events at this region. While a dedicated production of simulated events to cover these regions would be the optimal solution, it is not always possible. Thus the MUSiC algorithm needs to be able to deal with this situation, calculating at least an estimate for the p-value. To accomplish this a procedure called *uncertainty filling* is employed. This procedure (see Figure 6.4)consists of the following steps, which are performed for any SM process being part of the considered class:

1. Determine the lowest bin B_{min} that can be filled in a distribution. In the $\sum p_T$ distribution this is defined by the sum of the p_T thresholds of the participating objects. The lower limit on the combined mass can always be estimated to be zero. The $\not{E}_T$ threshold defines the lowest $\not{E}_T$ that can be filled in a class.

2. Determine the highest filled bin B_{max} of the considered process, and it centre value K_{max} of the considered kinematic variable. In almost all cases the SM prediction in a class is expected to drop steeply with the increase of the kinematic variables. It is assumed that the considered process will not contribute anymore at e.g. twice the reach of the highest filled bin. Thus the bin containing the value $2 \cdot K_{max}$ of the kinematic variable is taken as the highest bin to be filled.

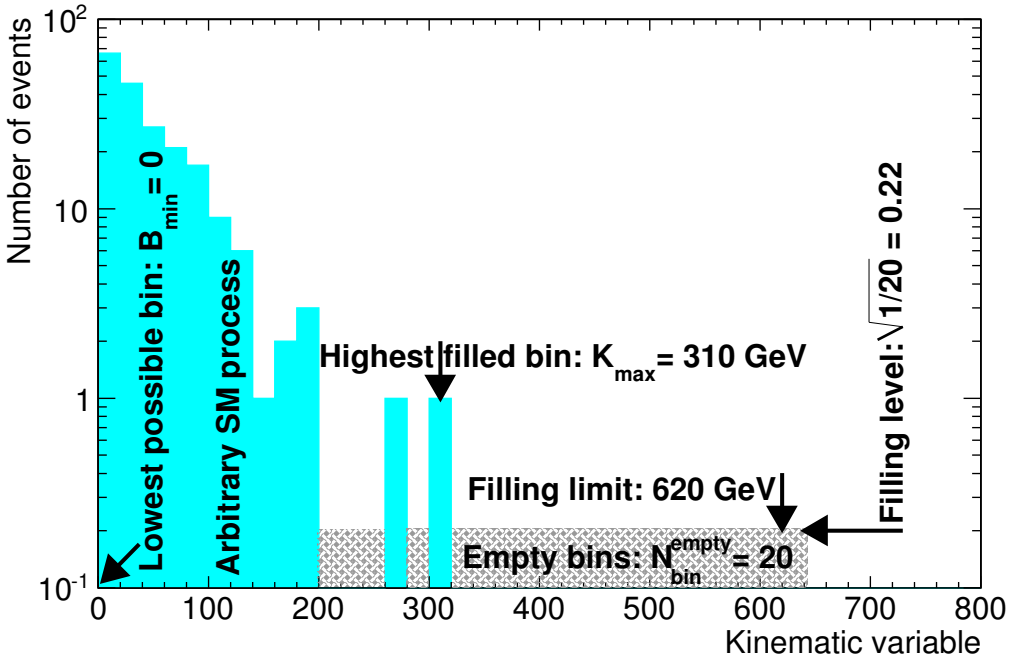

Figure 6.4.: *Example of the uncertainty added to an arbitrary SM process by the algorithm. The lowest filled bin in this example is the first bin, the highest filled bin at* 310 GeV *and the number of empty bins to be filled is 20.*

3. Count all bins (N_{bin}^{empty}) without MC events for the considered process between the lower and the upper limit.

4. Increase the uncertainty of those bins by $\sqrt{1/N_{bins}^{empty}}$. This is based on the assumption that each empty bin provides additional information: No event has been in this bis. Thus more empty bins provide more information, causing the fill-up per bin to decrease. This choice also means that changing the bin size does not change the fill-up.

In case a SM process does not contribute to a class at all, it is not treated at all and considered to be non-existent. Figure 6.4 shows the effect of the algorithm on an arbitrary SM process. This is just an example without a specific physical meaning. The upper edge of the highest filled bin is 320 GeV, thus the algorithm fills up to 640 GeV. Below the upper filling limit 20 bins are empty, thus the uncertainty of the empty bins is increased by $\sqrt{\frac{1}{20}}$.

This procedure yields useful results (see e.g. Figures 7.5, 7.10 and 7.14) as long as the number of simulated events is not much lower than the number of expected events. If this is not the case and the number of simulated events is lacking severely, no reliable prediction can be made.

6.3. Systematic uncertainties

The Standard Model simulation is not expected to perfectly describe the data. This is because parts of the simulation itself depend on measurements with limited precision,

while at other places the theoretical knowledge is imperfect. All of these effects can lead to discrepancies between simulation and data, but these deviations are not a sign for new physics. The precise effects of this imperfect knowledge are not known, but it is usually possible to estimate the size of a deviation that could still be explained by such effects. These uncertainties of the Standard Model predictions are described mathematically as probability density functions, called priors, which encode the credibility of predicted values deviating from the mean prediction. Depending on the cause of the uncertainty, the determination of those priors can be straightforward or highly non-trivial. For example the uncertainty of the predicted number of events follows a Poisson distribution around the simulated number of events under simple assumptions[5]. On the other hand there can only be estimates for the uncertainty caused by limited order perturbative cross section calculations. Due to mathematical limitations described in Section 6.2.1, the MUSiC algorithm can only use normal distributions as priors.

The individual uncertainties described below are calculated for each region of interest and then added in quadrature to determine the total systematic uncertainty. This total uncertainty, the predicted value and the measured number of events can then be used to calculate the significance of the currently considered region as shown in Section 6.2.1.

6.3.1. Integrated luminosity

To normalise the Standard Model prediction the integrated luminosity delivered by the LHC must be known, which has been measured to a relative precision of 4 %[78] in 2010. The total uncertainty on the number of predicted events introduced by this effect is thus calculated by taking the mentioned fraction of the total number of predicted events after summing up all bins in a region. The effect of this uncertainty is correlated over all bins in all event classes, that is for each pseudo-experiment the luminosity is set to one value for all classes.

6.3.2. Cross sections

The other component of the normalisation is the cross section prediction. The total cross section includes inputs from the Parton Distribution Functions, discussed in Section 6.3.3, and the partonic cross section. The uncertainty on the partonic cross section is mainly due to the limited order in α_S of the calculations. A detailed study of the effects of missing higher orders cannot be performed in this analysis, thus the following estimations are used:

- For electroweak process known to NNLO an uncertainty of 5 % is used.
- An uncertainty of 10 % is used for electroweak processes known to NLO and QCD processes known to NNLO or NNLL.
- For processes known to LO an uncertainty of 50 % is used.

Some exceptions to this rules are detailed in the next paragraph. This estimates are conservatively chosen and can be refined in future incarnations of this analysis.

Leptonic Drell-Yan processes $M(ll) > 50$ GeV and W-boson production have been calculated to NNLO[79] and are assigned an uncertainty on the cross section of 5 %. The same LO-to-NNLO factor is used for DY masses below 50 GeV, but higher uncertainties of 10 % and 20 % are used for masses between 10 and 50 GeV and below 10 GeV, respectively. To processes with two W or Z bosons an uncertainty of 10 % has been assigned,

[5] Assuming a uniform prior for the true number of events.

because they are only known to NLO[61]. While $t\bar{t}$ has also been calculated to NNLO[63], it is more sensitive to higher orders of α_S and thus an uncertainty of 10 % is used. For Υ resonances the measured cross section[65] value is used, but to account for different kinematics in the measurement, an uncertainty of 30 % is assigned. An uncertainty of 50 % is applied to processes for which only LO calculations are available (e.g. multi-jets and photon+jets).

The cross section uncertainty is assumed to be uncorrelated for different processes, but it is taken as correlated over all bins in all classes for each process. Hence the uncertainty is calculated from the mentioned fractions after summing up all bins of a region for each individual process. The individual uncertainties are then added in quadrature to obtain the total uncertainty. When generating pseudo-experiments a cross section value is drawn for each process which is then used in all classes.

6.3.3. Parton distribution functions

The PDFs are determined by fitting to experimental data, see Section 2.1.6. The fits itself introduce an uncertainty on the final results, as does the uncertainty of the measurements. Additionally not all measurements are compatible and additional uncertainties need to be introduced to cover this. The CTEQ and MSTW groups employ the Hessian method[80] to generate PDFs that represent these uncertainties additionally to the best fit PDFs. To determine the effect of those uncertainties on the final variables one can run the full event generation and simulation for all PDFs. However, it is much more effective in terms of computing power to reuse the existing events and apply weights for different PDFs, known as reweighting[23]. The result are N predictions X_i of the analysed variable, e.g. the number of expected events, that represent the possible uncertainty band around the central prediction X_0. The predictions can be combined into a single uncertainty on the analysed variable by using the equation[23] shown in Equation 6.6:

$$\begin{aligned} \sigma^{+}_{\text{Fit}} &= \sqrt{\sum_{i=1}^{N} \left(\max\left(X_i^{+} - X_0, X_i^{-} - X_0, 0\right)\right)^2} \\ \sigma^{-}_{\text{Fit}} &= \sqrt{\sum_{i=1}^{N} \left(\max\left(X_0 - X_i^{+}, X_0 - X_i^{-}, 0\right)\right)^2} \end{aligned} \tag{6.6}$$

Another uncertainty is introduced by the limited precision of the α_S measurements. Both CTEQ and MSTW thus provide two additional PDFs[81, 82] each which represent the best fit results using values for α_S varied by the measured uncertainty. Again using the reweighting method, two more uncertainties $\sigma^{\pm}_{\alpha_S}$ on the analysed variable can be calculated. The uncertainties introduced by the fit and by α_S can be added in quadrature[83], as shown in Equation 6.7.

$$\sigma^{\pm}_{\text{Fit}+\alpha_S} = \sqrt{{\sigma^{\pm}_{\text{Fit}}}^2 + {\sigma^{\pm}_{\alpha_S}}^2} \tag{6.7}$$

The NNPDF group on the other hand employs a special Monte Carlo approach[84] to generate additional PDFs that follow the uncertainty distributions of the data. The best fit then simply corresponds to the mean of those PDFs, while the uncertainty on the analysed variable is equal to the standard deviation. Similar sets of PDFs have been generated for α_S values around the measured value. A total uncertainty on the analysed variable can now be calculated by taking all PDFs, including those with deviating α_S values, but with a lower weight the further α_S is away from the measured value. Another way of giving the

$\alpha_S(M_Z)$	0.116	0.117	0.118	0.119	0.120	0.121	0.122
N_i	1	4	12	16	12	4	1

Table 6.1.: *Number of NNPDF replicas per PDFs set for different values of α_S*

various sets of PDFs a different weight is by using a corresponding number of PDFs from each set[83]. The number of PDFs used for the different α_S sets in shown in Table 6.1. Then the combined uncertainty on the analysed variable for NNPDF can be calculated using Equation 6.8.

$$\sigma_{\mathrm{NNPDF}} = \sqrt{\frac{1}{\sum N_i - 1} \sum_{i=1}^{N_{\alpha_S}} \sum_{j=1}^{N_i} (X_{i,j} - X_0)^2} \tag{6.8}$$

There are prescriptions how to calculate the uncertainties on the PDFs of each CTEQ, MSTW and NNPDF individually. All groups are trying to describe the same underlying physics, thus their results are not expected to deviate beyond the uncertainties. However, in some cases they do differ by larger amounts, and hence there is no statistically motivated method of combining the different results. Conservatively, the maximum deviations of the analysed variable in both directions are used, as shown in Equation 6.9.

$$\begin{aligned} 2 \cdot \sigma_{\mathrm{PDF}} = &\max(X_{\mathrm{CTEQ}} + \sigma^{+}_{\mathrm{CTEQ}}, X_{\mathrm{MSTW}} + \sigma^{+}_{\mathrm{MSTW}}, X_{\mathrm{NNPDF}} + \sigma_{\mathrm{NNPDF}}) \\ &- \min(X_{\mathrm{CTEQ}} - \sigma^{-}_{\mathrm{CTEQ}}, X_{\mathrm{MSTW}} - \sigma^{-}_{\mathrm{MSTW}}, X_{\mathrm{NNPDF}} - \sigma_{\mathrm{NNPDF}}) \end{aligned} \tag{6.9}$$

A practical prescription including details of the implementation can be found in[85], which is based on [86, 87].

In the MUSiC algorithm, the analysed variable is the number of events per class or per bin, thus the described recipe is applied to each one, resulting in one uncertainty on the number of events per bin. Possible deviations caused by uncertain PDF predictions are not expected to vary strongly for neighbouring bins, but it is not possible to gauge this effect for all possible bin combinations. Thus is it assumed that the PDF uncertainty is fully correlated for all bins in all classes. When forming regions the PDF uncertainties on the number of events are summed up linearly for all bins and then added in quadrature to the total uncertainty. In each pseudo-experiment one value is drawn, which is interpreted as the number of standard deviations, and is used in all bins to vary the prediction, e.g. if the drawn value is 1.2σ, each bin is varied by 120 % of the calculated PDF uncertainty.

6.3.4. Jet energy scale

The measured energy of reconstructed jets does not exactly match the energy of the underlying parton that caused the jet. There are fluctuations that vary in each measurement, affecting the jet energy resolution, but the energy is also reduced systematically due to e.g. undetected particles. These and other effects are taken into account by applying corrections, which depend on the type of the jet algorithm and the position of the jet in the detector. In 2010 these corrections are determined using simulated events exploiting the known underlying physics of those events, then they are verified using methods based on measured data. Nevertheless they are still not expected to provide a perfect match, and the limited knowledge has been encoded in p_T and η dependent uncertainty functions for the jet energy scale with values between 3 and 5 %[52]. Again there is no physical reason

for the miscalibration to be similar across the whole detector, but it is still expected to be similar for jets that are close to each other. In the MUSiC algorithm uncertainties must either be fully correlated or not at all, thus jet energies are assumed to deviate in the same direction across the whole detector.

Variations of the jet energy affect the analysed kinematic variables, but can also affect the class an event ends up in, if jets close to the cut threshold are pushed across it. Thus the analysis is performed three times: Once with the original jets, once with the energy of all jets increased by value given by the uncertainty functions and once with the energies lowered by the same value. The shifted energy will cause some jets to end up in different bins and some events to end up in different classes, when jets move across the selection threshold. The result are three different predictions of the number of events per bin, which are used to determine the jet energy scale uncertainty on the number of events in each bin. As the used normal uncertainty prior needs one single value, the two uncertainties of the up and down variations are averaged. Similarly to the PDF uncertainty, the deviation caused by the uncertain jet energy scale is not expected to vary strongly for neighbouring bins, thus the uncertainty is handled in the same way as the PDF uncertainty when drawing pseudo-data.

Some of the effects that affect the jet energy measurement also affect the $\not\!\!E_T$ measurement, and thus a correlated uncertainty must be applied. The objects used to calculate the $\not\!\!E_T$ can be split into clustered and unclustered energy, that is energy that is or is not part of a jet. The uncertainty on clustered energy on the other hand is closely related to the jet energy uncertainty. To estimate this effect, first the unclustered energy is calculated by subtracting the transverse components of the original jets from the $\not\!\!E_T$. Then the jets modified by the aforementioned procedure are added back on the unclustered energy, thus forming a new $\not\!\!E_T$ object with the effect of the jet energy scale uncertainty included. Both uncertainties on jets and $\not\!\!E_T$ are hence strongly correlated and are treated as one single uncertainty. The uncertainty on unclustered energy is currently not taken into account and could be studied in future analyses.

6.3.5. Reconstruction efficiencies

The probability that a certain physics object is actually measured, reconstructed and identified correctly by the detector, called efficiency, is usually close to, but rarely at 100%. Additionally it may be different for measured data and simulated events, due to effects in the detector that are not properly simulated. In simulated events the efficiency can easily be determined by comparing to the MC truth, but there are also methods to determine it in measured data[88, 89]. Due to the multitude of final states in MUSiC it is impossible to correct the simulation to the measured values, thus the differences between simulated and measured efficiencies are used as estimations for the uncertainties on the efficiencies. The total uncertainty on N_{MC} simulated events in a region in a class containing[6] N_i (e.g. N_e for electrons) objects of type i (e.g. electrons) with efficiency uncertainty σ_i (e.g. σ_e for the uncertainty on the electron efficiency) can be calculated as shown in Equation 6.10.

$$\sigma^2_{\mathrm{Eff}} = N^2_{\mathrm{MC}} \cdot \left(N^2_e \cdot \sigma^2_e + N^2_\mu \cdot \sigma^2_\mu + N^2_\gamma \cdot \sigma^2_\gamma + N^2_{Jet} \cdot \sigma^2_{Jet}\right) \tag{6.10}$$

Dedicated studies found uncertainties of 4 % for muons[88], and 3 % for electrons[89, 88] and photons[89]. The jet efficiency exceeds 99.5 %[74], and thus a small uncertainty of 1 % is assumed conservatively. The given fractions are relative to the efficiencies, e.g. an

[6] Here the number of reconstructed objects is used, thus it includes the effects of the inefficiency. However, the efficiency is expected to be close to 1 and thus the effect on the uncertainty is negligible.

uncertainty of 5 % on an efficiency of 90 % corresponds to a variation between 85.5 % and 94.5 %.

Imagine a bin in the $1\mu + 2e$ class containing 100 expected events. In this bin the effect of the reconstruction efficiency uncertainty amounts to:

$$\sigma_{\text{Eff}} = N_{\text{MC}} \sqrt{N_e^2 \cdot \sigma_e^2 + N_\mu^2 \cdot \sigma_\mu^2} = 100 \cdot \sqrt{(2 \cdot 0.03)^2 + (1 \cdot 0.04)^2} \approx 7.2 \tag{6.11}$$

Both the efficiency for one kind of object as well as the efficiency difference between data and simulation can vary depending on the presence of other objects, that is it can vary between event classes. A detailed study of those variations can be performed but is beyond the scope of this work, thus it is assumed that if the efficiency deviates by a certain fraction, it will do so for all classes. Thus the uncertainty is treated similarly to the aforementioned correlated uncertainties: One value is drawn for each object in each pseudo-experiment and is then used for all classes.

6.3.6. Misidentification fraction

A certain fraction of reconstructed objects does not originate from a corresponding physical object coming from the hard interaction, but is due to misidentified other objects or effects. This fraction is determined by looking for appropriate MC truth objects for each kind of reconstructed object in a cone of $\Delta R < 0.2$, e.g. isolated electrons in the MC truth for isolated reconstructed electrons. This definition works well for objects coming directly from the hard interaction, e.g. muons in a DY process, but it leads to high misidentification fractions in some processes, e.g. QCD. In this particular process a jet might e.g. consist of only one π^0 decaying into a pair of nearly collinear photons. The resulting photon object in the ECAL is nonetheless considered a fake, because the generated photons are part of a jet. The behaviour of these kinds of objects depends on theoretical assumptions that are hard to model, e.g. details of the jet showering, and thus a high uncertainty is unavoidable. In any way not the absolute fraction is of interest for detecting deviations, but the difference in misidentification fractions between simulation and data.

The effects of a deviating misidentification fraction are determined using a simple assumption: If e.g. the electron misidentification fraction is lower by 50% in data compared to simulation, then each simulated event containing one misidentified electron actually corresponds to 0.5 events in data. To determine the effect of this deviation, the analysis is run one more time[7], increasing the weight of each event containing one misidentified electron by the uncertainty on the misidentification fraction. To fully see the effects of all individual misidentification fractions and their combinations one would need to run the analysis a large number of times, which is unfeasible. Thus all misidentification uncertainties are treated in one additional run, where all fractions are increased at the same time by their individual uncertainty. The result is again two predictions for each bin, one corresponding to the expectation value and the other one to the 1σ deviation. The uncertainty per bin can now be calculated from both predictions. When forming regions or drawing pseudo-data, this uncertainty is treated in a similar fashion as the PDF uncertainties.

The uncertainties on the misidentification fractions have been estimated to be 30 % for photons[89], 50 % for muons[88] and 100 % for electrons[48]. Due to the abundance of jets comparted to other objects, their misidentification fraction is very low and thus the effect of the uncertainty can be neglected.

[7] Up and down variations are equal in the procedure.

6.3.7. Charge misassignment

In case the charge of muons and electrons is considered at all, the assigned charge may be wrong. For both muons and electrons this can happen at very high p_T with a nearly straight trajectory. Statistical fluctuations or systematic shifts in the tracking detectors can cause the curvature of the reconstructed track to flip. The radiation of bremsstrahlung of electrons in the tracker material can also cause the track to be reconstructed with a wrong curvature.

The probability of this effect is determined similarly to the misidentification fraction, using the MC truth. Also the uncertainty on this fraction is determined using the same approach as used for the misidentification fraction, that is running the analysis a second time using an increased weight for events containing leptons with the wrong charge. The relative uncertainty on the missassignment probability used for both muons and electrons is 50 %[90], i.e. the weight of an event containing one misassigned lepton is increased by 50 %.

6.3.8. Simulated number of events

The number n of simulated events passing the cuts does not represent the true expectation value μ, but is itself just a sample, which will follow a Poisson distribution around μ on repeated trials. Assuming a flat prior, the Bayesian posterior of μ based on a certain n is again a Poisson, this time with parameter n. This posterior can now be used as a prior for the uncertainty on n. The MUSiC p-value however can only deal with Gaussian priors, thus the standard deviation $\sigma_{MC} = \sqrt{n}$ is used as an uncertainty. These uncertainties are independent for each bin and each simulated sample, thus the uncertainties of both bins and samples in a region are simply added in quadrature to the total uncertainty of the region. When drawing pseudo-data, the prediction for each sample is randomised individually in each bin.

7. Results

The MUSiC analysis has been applied to the LHC collision data taken by CMS in 2010. In total $8.7 \cdot 10^5$ measured events have been selected and are used to fill the classes. First the classes are treated as counting experiments, that is the total number of measured events is compared to the expected number. Then up to three kinematic distributions per class are analysed in detail to look for deviations.

Previous results of a former version of this analysis have been published in [91].

7.1. Classes as counting experiments

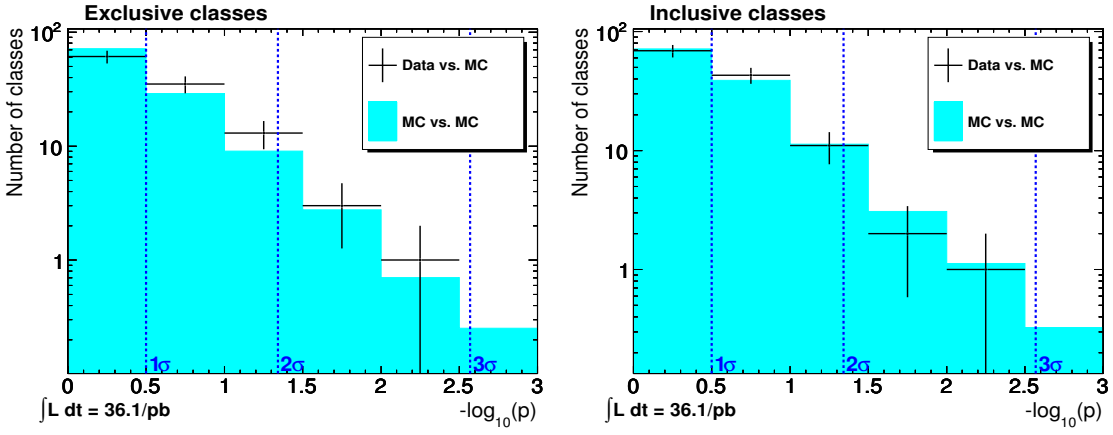

Figure 7.1.: *p-value distributions of data-vs-SM (black crosses) compared to SM-vs-SM (shaded area) for exclusive and inclusive event classes.*

A total of 113 exclusive and 126 inclusive event classes contain at least one measured event or a Standard Model expectation of more than one event. Those include final states with up to four leptons, up to two photons and up to eight jets. The charge of the leptons has not been taken into account, which means events containing same-sign leptons and events containing opposite-sign leptons end up in the same class, presuming the total number of leptons is the same. Standard Model predictions exist for all classes containing measured events. The p-values of all classes can be found in Figure 7.1. Figures 7.2 and 7.3 show the number of measured events, SM prediction and total systematic uncertainty of the 55 exclusive and inclusive classes with the smallest p-values, i.e. whose deviations are most significant, sorted by increasing p-value. Similar figures (C.1, C.2) for the remaining classes and tables detailing the results can be found in Appendix C.1. The p-value distributions of the measured data compared to the SM prediction agrees within statistical uncertainties with the p-value distribution determined from pseudo-experiments. Thus there is no class where the number of events deviates more from the prediction than what is expected from statistical and systematic uncertainties. The Standard Model prediction can be considered to be a valid description of the data within the sensitivity of MUSiC.

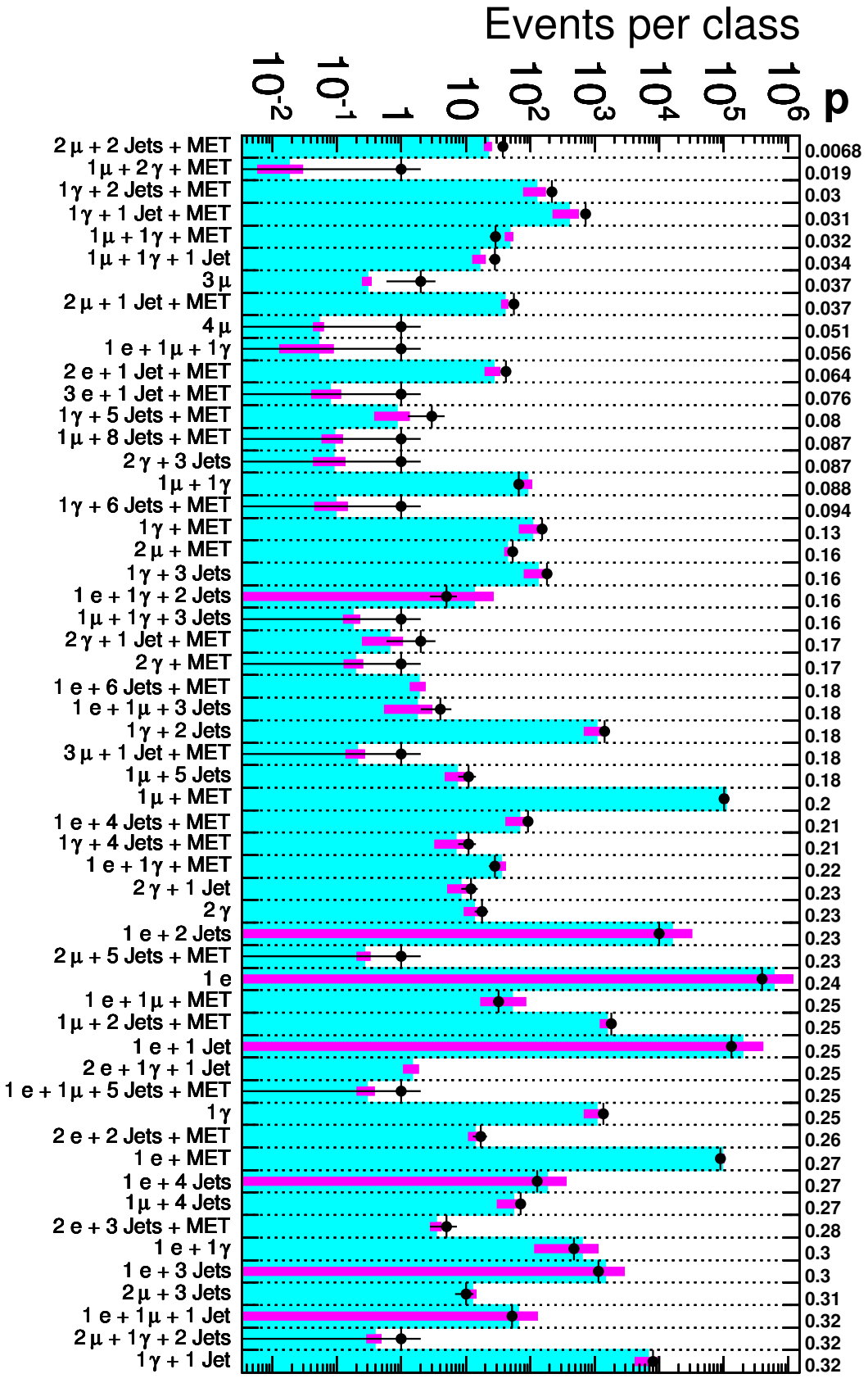

Figure 7.2.: *Number of events (black markers) measured by CMS, simulated number of SM events (light shaded area) and total systematic uncertainty (dark bars) of the 55 most significant exclusive classes, sorted by p-value, which is displayed on the right.*

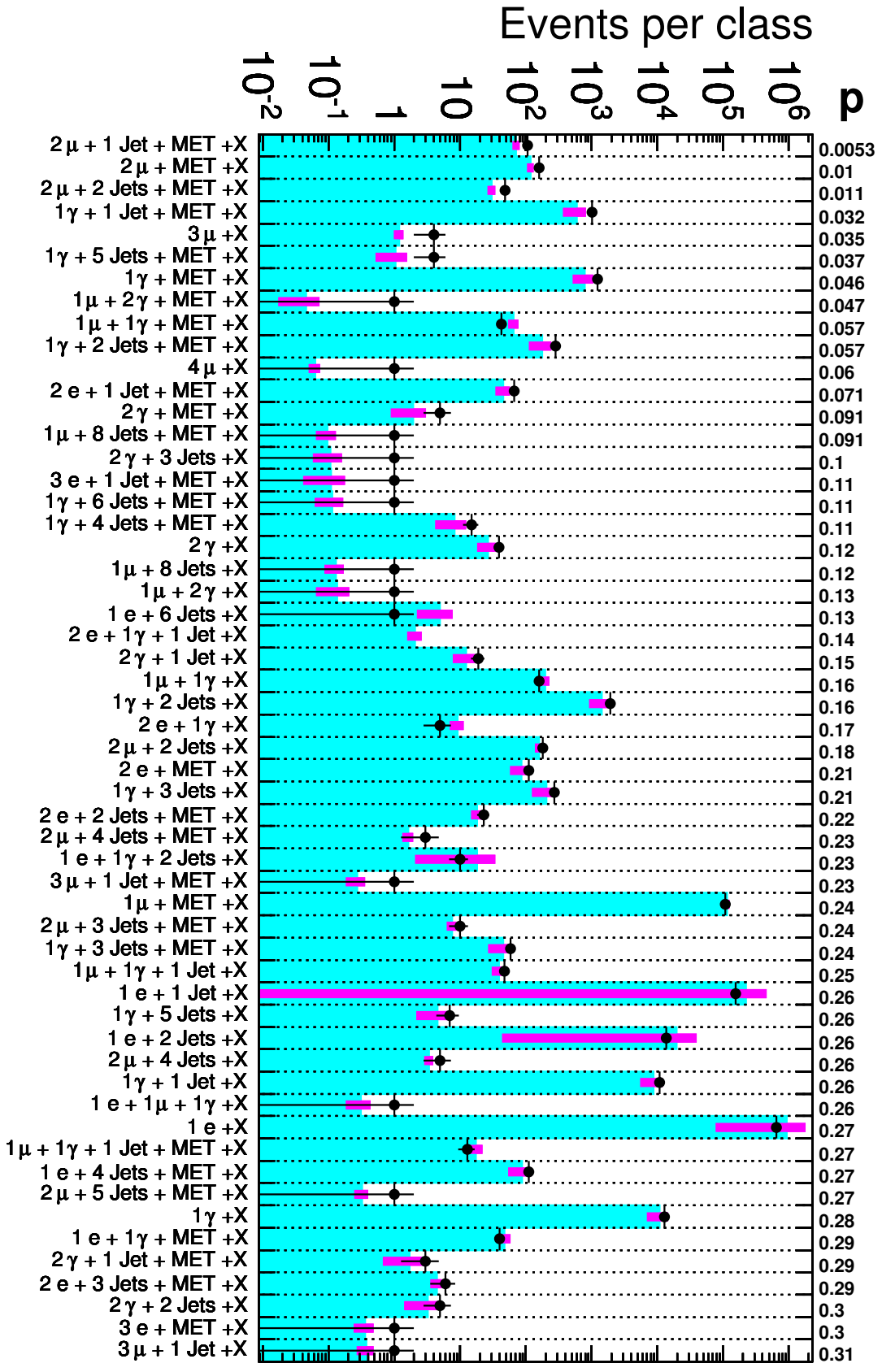

Figure 7.3.: *Number of events (black markers) measured by CMS, simulated number of SM events (light shaded area) and total systematic uncertainty (dark bars) of the 55 most significant inclusive classes, sorted by p-value, which is displayed on the right.*

7.2. Detailed scans of kinematic distributions

Even in classes where the total number of events agrees, the shape of the distribution of the kinematic variables might be in disagreement to the prediction. This can be the case because either the bulk of the distribution is correctly described, hiding deviations in areas with lower number of events, e.g. in the high energy regions. Or because events are moved with respect to the kinematic variables, without changing the overall number of events. Both effects can be detected using detailed scans of the kinematic distributions.

7.2.1. Sum of transverse momenta

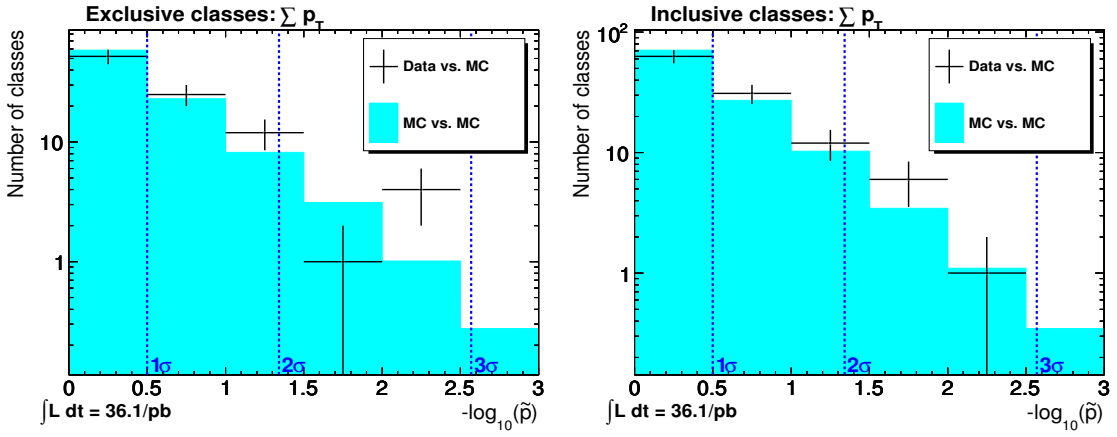

Figure 7.4.: *Distributions of $\tilde{p}$ of data-vs-SM (black crosses) compared to SM-vs-SM (shaded area) for the $\sum p_T$ variable of exclusive and inclusive classes.*

The sum of transverse momenta can be calculated for all classes, thus all distributions from the 113 and 126 classes of the previous section are analysed. However, in some distributions all considered regions are skipped due to the requirement of a deviation of at least three times the systematic uncertainty, and thus no p-value has been calculated. These classes do not show up in the $\tilde{p}$ distributions, but they are listed in the tables in Appendix C.2.1.

Figure 7.4 shows the $\tilde{p}$ distribution of all exclusive and all inclusive classes. The distribution of significance observed in data agrees within uncertainties with the SM expectation, expect for the bin $0.0032 < \tilde{p} < 0.01$ of the exclusive classes, where one class is expected, but four are observed. In about 3%[1] of all MC pseudo-experiments four or more classes with $\tilde{p} < 0.01$ can be observed, thus the deviating classes are worth a look, which is done later in this section. Thus not only the total number of events per class is consistent with the SM prediction, as shown in the previous section, but also the $\sum p_T$ distributions agree within statistical and systematic uncertainties.

Figures 7.5, 7.6 and 7.7 show some distributions that are dominated by W boson, γ+jets and $t\bar{t}$production and can hence be used to verify the SM predictions. These plots contain the following information:

- The name of the event class, the calculated p-value for the selected region and the $\tilde{p}$ of this region taking into account the Look-Elsewhere Effect at the top of the plot.

[1] (2.8 ± 1.2)% due to the limited number of completely diced pseudo-experiments

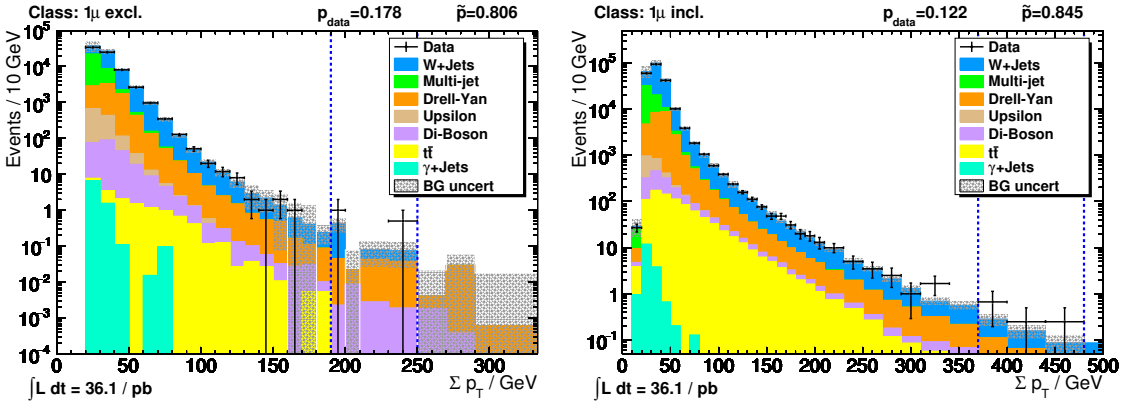

Figure 7.5.: *p_T distribution of the leading muon in exclusive and inclusive single muon classes.*

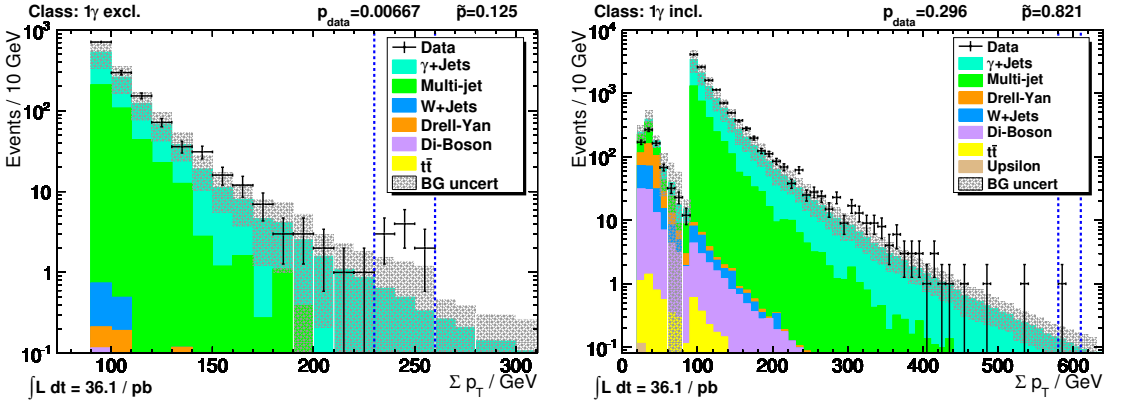

Figure 7.6.: *p_T distribution of the leading photon in exclusive and inclusive single photon classes.*

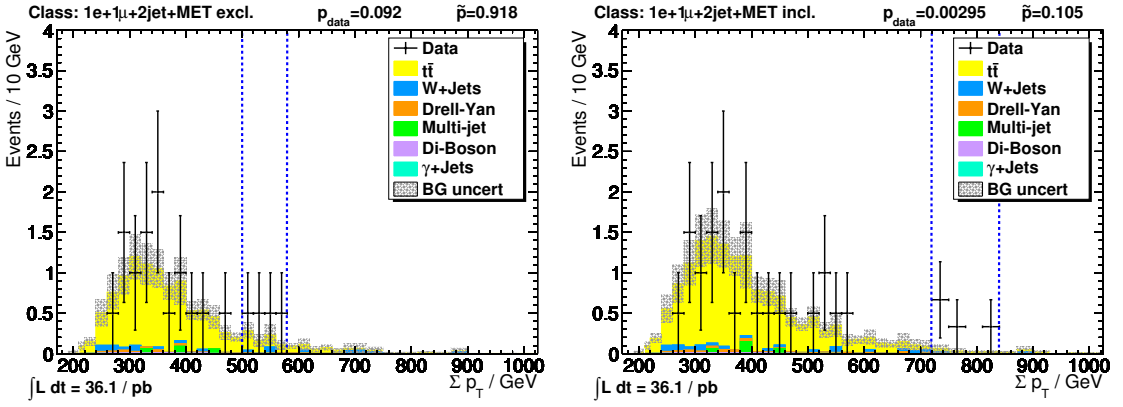

Figure 7.7.: *$\sum p_T$ distribution of $t\bar{t}$ dominated classes.*

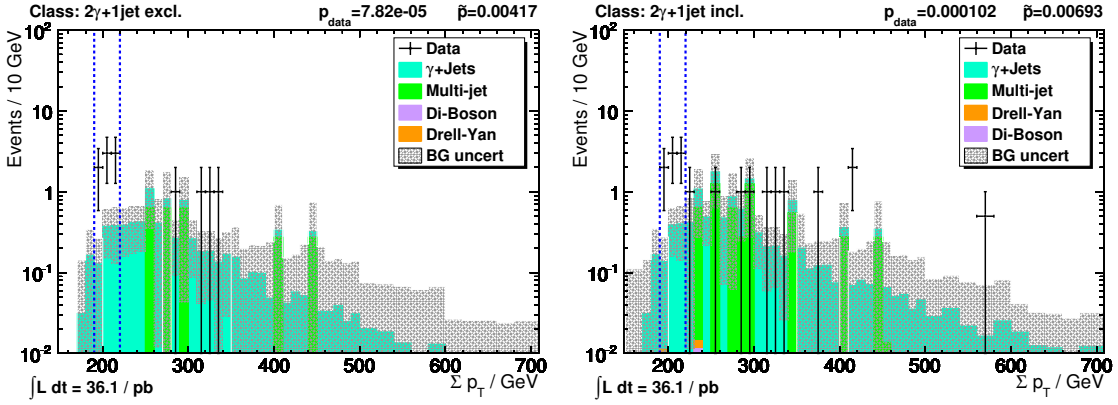

Figure 7.8.: *Second most significant exclusive and most significant inclusive class.*

- The integrated luminosity and the kinematic variable at the bottom of the plot.
- The Region of Interest indicated by the two dashed blue lines.
- The number of measured events per 10 GeV (black markers) and the SM prediction (stacked coloured bars).
- The total systematic uncertainty of the SM expectation (grey shaded area).

Figure 7.5 shows the p_T distribution of the exclusive and inclusive single muon class, which is equivalent to the p_T of the leading muon. These distributions are dominated by W-boson production, and the data are well described by the SM simulation, resulting in $\tilde{p}$ values close to 1.

In Figure 7.6 comparable distributions for photons are shown, which exhibit a particular feature of the current selection algorithm affecting inclusive classes: If no lepton passes the trigger thresholds, the photon needs at least 90 GeV for the event to be selected. But in case a lepton did pass the trigger threshold, a lower p_T of at least 25 GeV is enough for the photon to enter the inclusive distribution. This causes the step at 90 GeV in the inclusive distribution. In the exclusive distribution no other selected objects are allowed and thus no lepton can pass the trigger threshold, so there are no events below 90 GeV. Compared to the muons in Figure 7.5 the photon distribution deviates further from the mean SM expectation, but this can be explained by the inferior LO knowledge of the Photon+Jets prediction compared to the NNLO prediction of the W-boson production. However, this inferior knowledge has been taken into account in the systematic uncertainties, and the measured number of events agrees with the expectation within uncertainties.

In a class with two leptons of different flavor, two jets and missing energy the $t\bar{t}$ production process can easily be discerned from the other SM processes, as shown in Figure 7.7. The inclusive class contains about 30% more events than the exclusive class. In both the inclusive and exclusive class the measured data are well described by the SM prediction and no significant deviation is observed.

Figures 7.8 and 7.9 show the two most significant exclusive and inclusive distributions. The $2\gamma + 1$jet class shown in Figure 7.8 shows up with a similar significance both in the inclusive and exclusive case. A close look reveals that both regions of interest contain the same events, in other words the deviating events do not contain any additional selected objects. Just the higher number of expected events in the inclusive distribution leads to a slightly reduced significance. A similar, though less obvious effect can be observed in

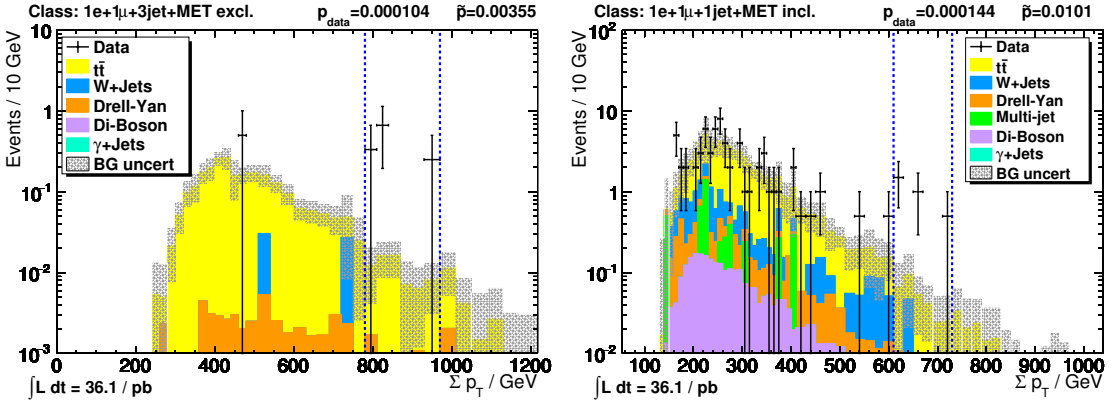

Figure 7.9.: *Most significant exclusive and second most significant inclusive class.*

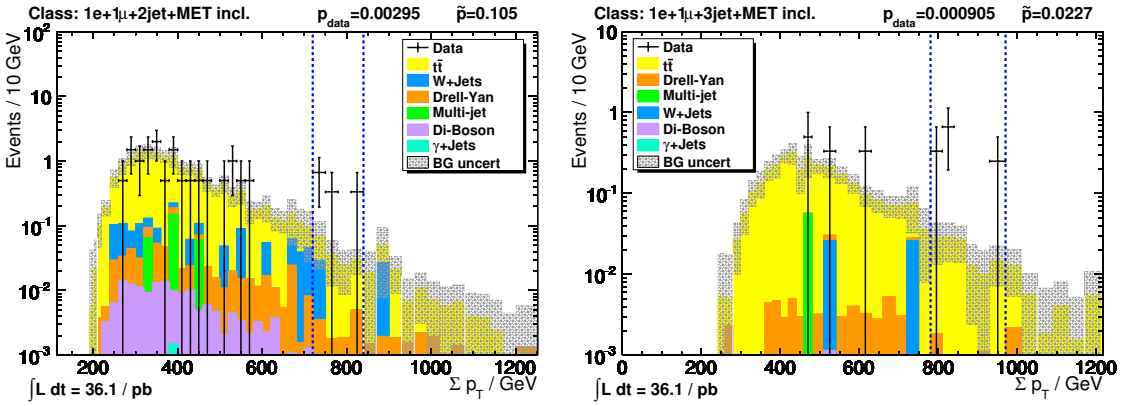

Figure 7.10.: *Inclusive classes containing events from the exclusive class in Figure 7.9*

Figure 7.9, where the region of interest of the inclusive $1e + 1\mu + 1\text{jet} + \not{E}_T$ class contains the same 4 events (plus two more) as the exclusive $1e + 1\mu + 3\text{jet} + \not{E}_T$ class. However, due to the two jets that are not part of the calculation in the inclusive class, the determined p_T sum is smaller. Figure 7.10 shows two other inclusive classes that contain the events from the exclusive class in question. Again the same four events are selected, in case of the inclusive $1e + 1\mu + 3\text{jet} + \not{E}_T$ even precisely the same region of interest. This is one example for why inclusive classes put up statistical difficulties, as four unexpected events cause deviations in at least three classes.

Figure 7.11 shows two more exclusive classes with a small p-value. The single event in the 4μ class might be a statistical fluctuation which needs to be checked when more data is available. The $1\mu + 2\gamma + \not{E}_T$ class on the other hand is a typical case of a class that lacks a decent SM prediction due to a limited number of simulated events. A p-value can be calculated using the uncertainty filling algorithm, but to make a statement about this deviation more data and more simulated events are needed in a future analysis.

7.2.2. Combined mass

The combined mass can only be calculated in classes containing at least two objects, thus the 1μ, $1e$ and 1γ classes are excluded, and the number of analysed exclusive and inclusive classes drops to 110 and 123, respectively. In events with $\not{E}_T$ above the selection threshold

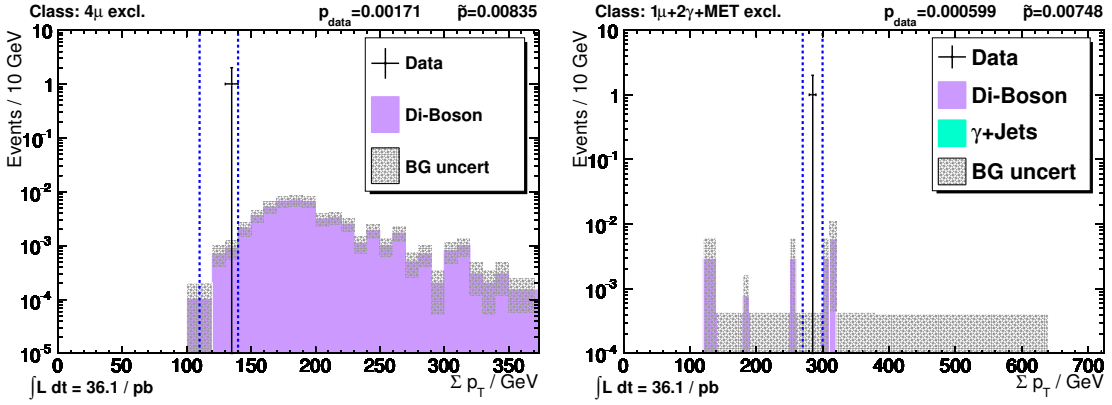

Figure 7.11.: *Two of the four most significant exclusive classes*

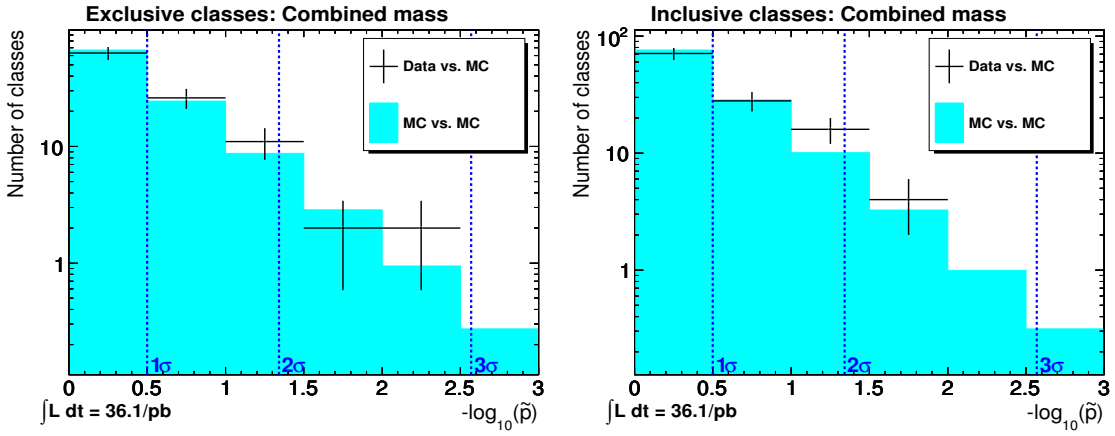

Figure 7.12.: *Distributions of $\tilde{p}$ of data-vs-SM (black crosses) compared to SM-vs-SM (shaded area) for the combined mass variable of exclusive and inclusive classes.*

the z components is ignored when the mass is calculated, which is then called *transverse mass*. As shown in Figure 7.12 the distribution of $\tilde{p}$ agrees with the SM prediction within uncertainties. Details can be found in Appendix C.2.2.

Again a number of distributions dominated by individual physics processes, here Drell-Yan, can be checked to verify the prediction. Figure 7.13 shows the combined mass of the two leading muons in the exclusive class without additional selected objects and in the inclusive class with potentially more selected objects. Due to the NNLO prediction and the low misidentification rate of muons the prediction has small uncertainties and describes the data very well. The small differences between the exclusive and inclusive distribution show that the inclusive class is dominated by exclusive events. This effect also explains the selection of very similar regions of interest in the $2e$ classes shown in Figure 7.14: A deviation in the exclusive events that is also visible in the inclusive distribution. The higher misidentification rate of electrons causes a higher fraction of multi-jet events in the class and thus higher uncertainties in the mass ranges away from the Z-peak.

Even if the $\tilde{p}$ distribution agrees with the expectations, it is still wise to have a look at the most significant classes to validate the method. Figure 7.15 shows the most significant exclusive and inclusive classes. The most significant exclusive class is the same as in the p_T sum distribution, and also looks very similar to this distribution, which shows the

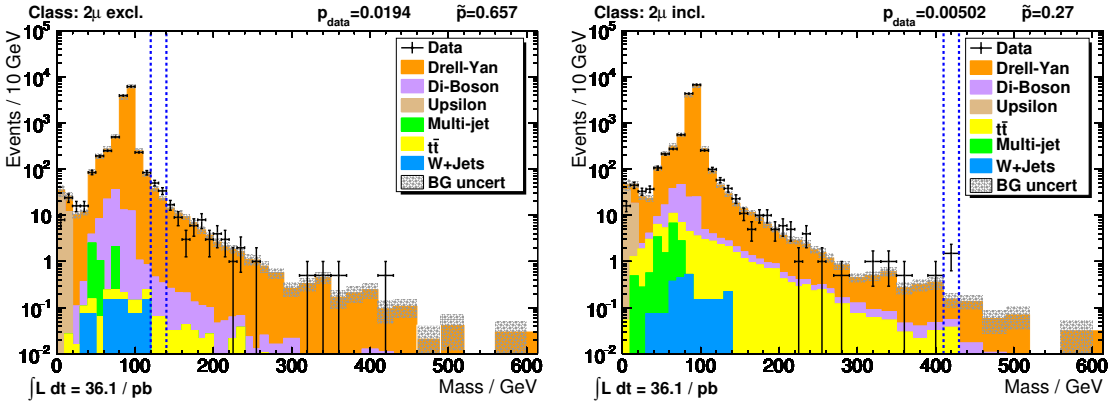

Figure 7.13.: *Two-muon mass of the DY dominated exclusive and inclusive 2μ classes.*

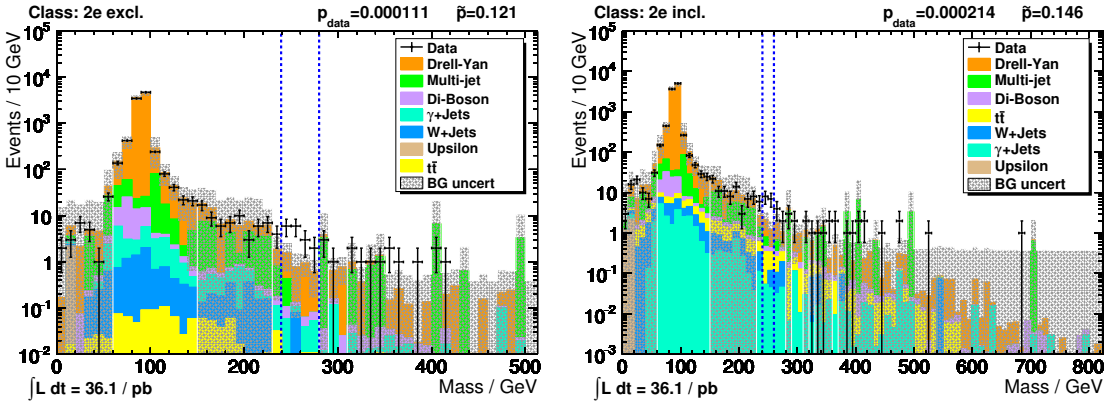

Figure 7.14.: *Two-electron mass of the DY dominated exclusive and inclusive 2e classes.*

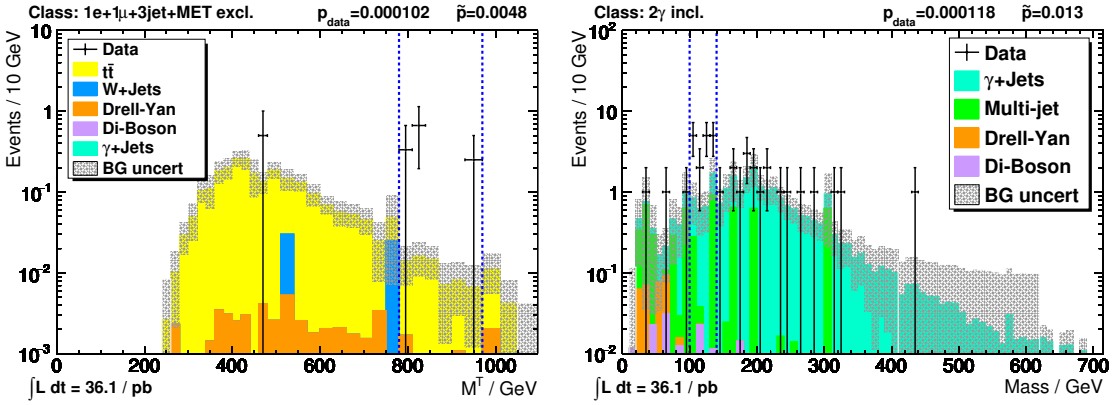

Figure 7.15.: *Most significant exclusive and inclusive class in the combined mass distribution.*

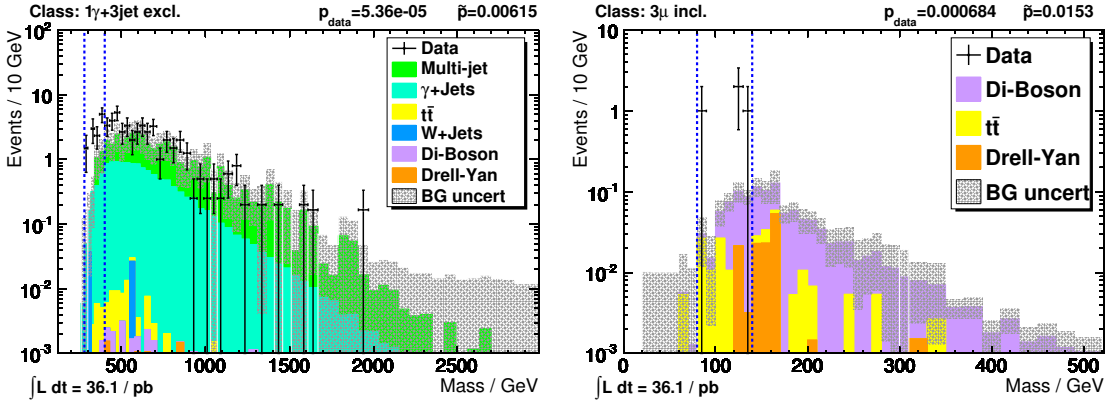

Figure 7.16.: *Second most significant exclusive and inclusive class in the combined mass distribution.*

strong correlation between p_T sum and mass if many objects are in the events. It also underlines the difficulties in the statistical interpretation of the relation of deviations in multiple distributions in one class. Here the fact that the deviation can be seen in both the p_T sum and in the mass is not a sign for increased significance, because the deviation is caused by the same four events. The second most significant exclusive class and the two most significant inclusive classes are compatible with statistical fluctuations, consistent with the agreement in the $\tilde{p}$ distribution.

7.2.3. Missing transverse energy

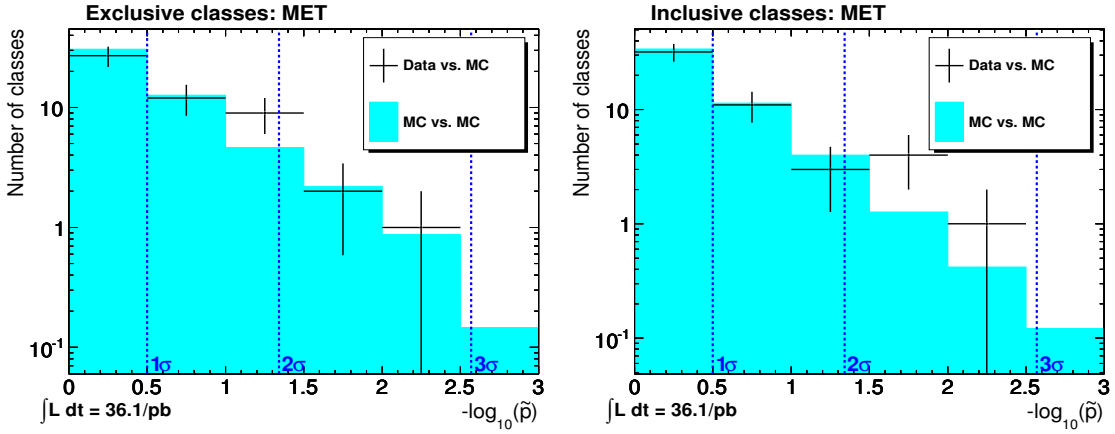

Figure 7.17.: *Distributions of $\tilde{p}$ of data-vs-SM (black crosses) compared to SM-vs-SM (shaded area) for the $\not{E}_T$ variable of exclusive and inclusive classes.*

Most classes exist with and without $\not{E}_T$, thus 51 classes containing $\not{E}_T$ have been analysed. The $\tilde{p}$ distributions in Figure 7.17 show some deviations slightly beyond the uncertainties, which are worth a closer look.

Some classes, which are expected to contain large $\not{E}_T$, can be checked to verify that the Standard Model is a good description in general. Figure 7.18 shows the $\not{E}_T$ distribution of the exclusive and inclusive $1\mu + \not{E}_T$ classes, which is dominated by W boson production. In contrast to all previously shown distributions the region of interest in the inclusive class

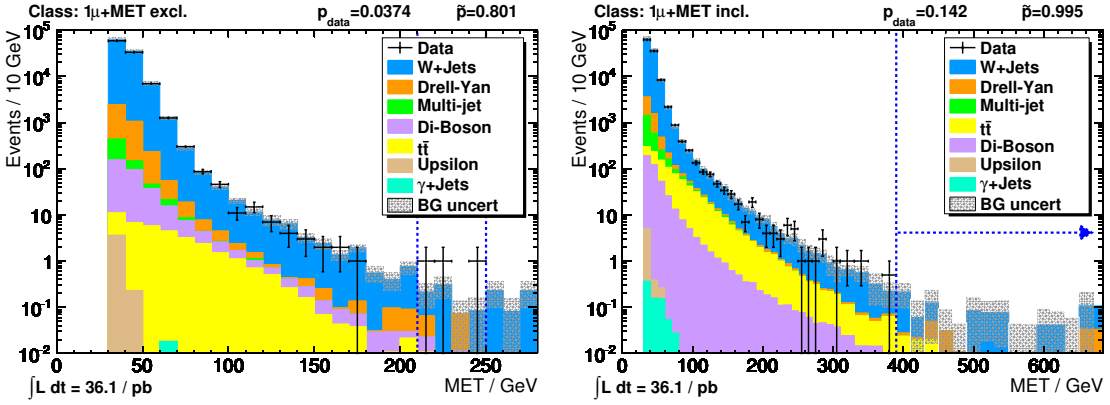

Figure 7.18.: *$\not\!\!E_T$ of $1\mu + \not\!\!E_T$ classes, which are dominated by W boson production. The region of interest of the inclusive class, which in this case selects a deficit, runs from the blue line to the end of the distribution.*

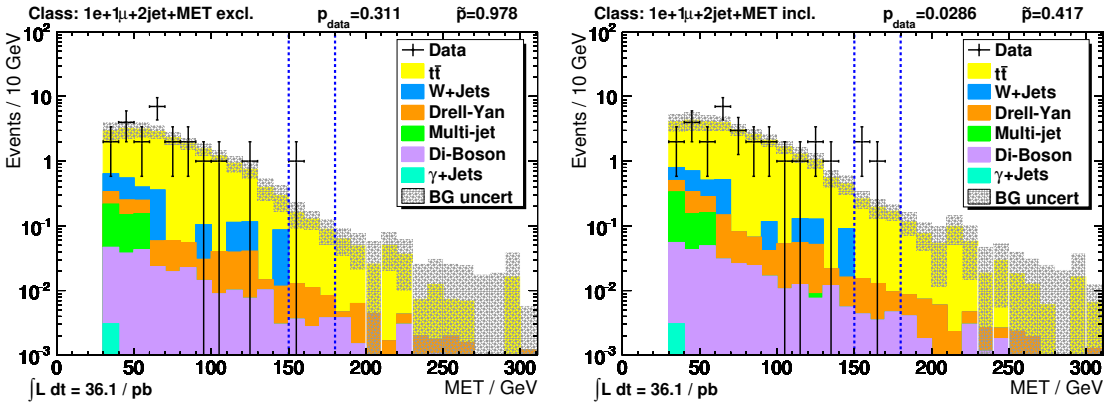

Figure 7.19.: *$\not\!\!E_T$ of the $t\bar{t}$ dominated $1e + 1\mu + 2jets + \not\!\!E_T$ classes.*

contains a deficit of events, which is the reason why it runs from the visible blue line to the end of the distribution. In this region 2.1 ± 0.5 events are expected but none has been seen. This deviation however is not significant and the data are well described by the SM prediction. The previously shown $1e + 1\mu + 2\text{jets} + \not\!\!E_T$ events are mostly from $t\bar{t}$ production with fully-leptonic decays. Thus a significant $\not\!\!E_T$ is expected, which can be seen in Figure 7.19. One can see that not only the p_T sum as shown before is well described, but also the $\not\!\!E_T$ distribution.

As one can see in Appendix C.2.3, the majority of the deviating classes in the $\not\!\!E_T$ variable are classes of the type $2\mu + N\text{jets} + \not\!\!E_T$. Figures 7.20 and 7.21 show some examples. It appears the significance of the deviation drops with increasing number of jets, which is equivalent to an increasing fraction of $t\bar{t}$ events. A similar, though less prominent effect can be seen in the comparable electron classes, e.g. Figure 7.22, but in the mixed-flavour, $t\bar{t}$ dominated classes (Figure 7.23) no deviation can be seen. This suggests that events containing real $\not\!\!E_T$ (that is $t\bar{t}$) are less affected than DY events, which are not supposed to contain physical $\not\!\!E_T$. Presumably the pile-up simulation (see Section 4.2.2) used by CMS is thus not perfect, causing less additional $\not\!\!E_T$ than measured. This can be studied in future analyses using more data.

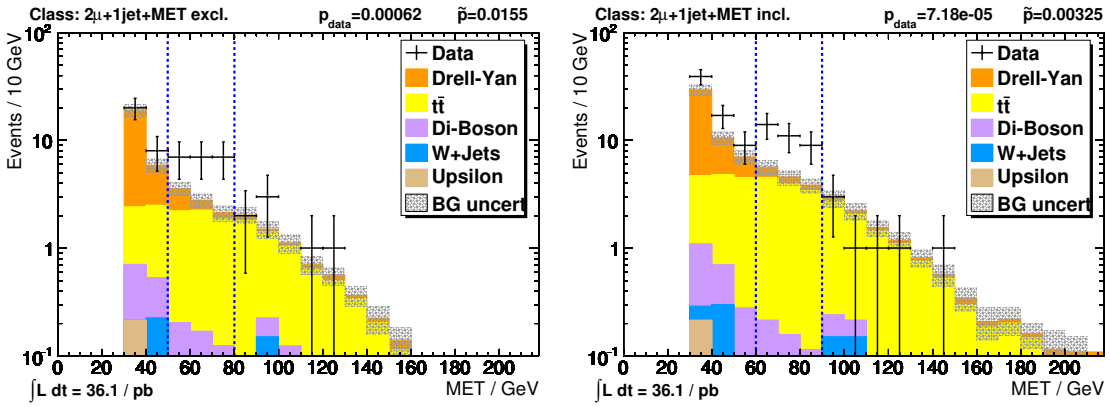

Figure 7.20.: *Deviating $\not{E}_T$ distribution in the $2\mu + 1jet + \not{E}_T$ classes*

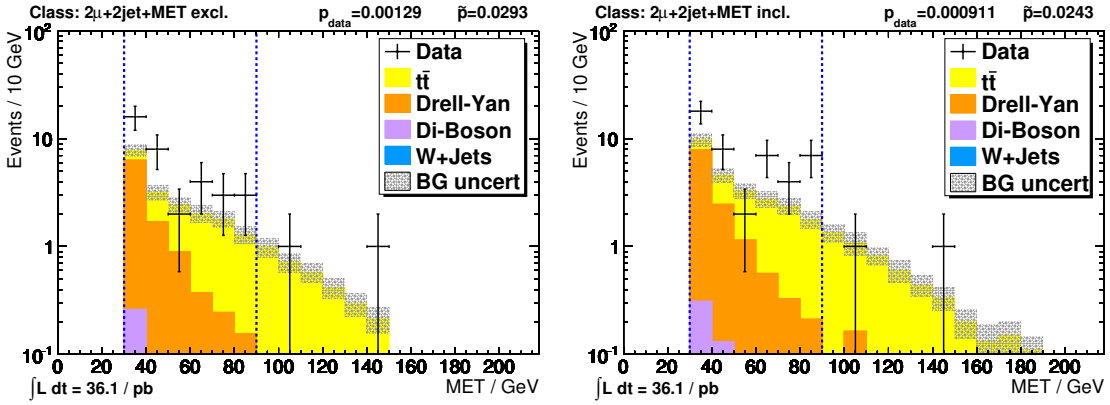

Figure 7.21.: *Deviating $\not{E}_T$ distribution in the $2\mu + 2jets + \not{E}_T$ classes*

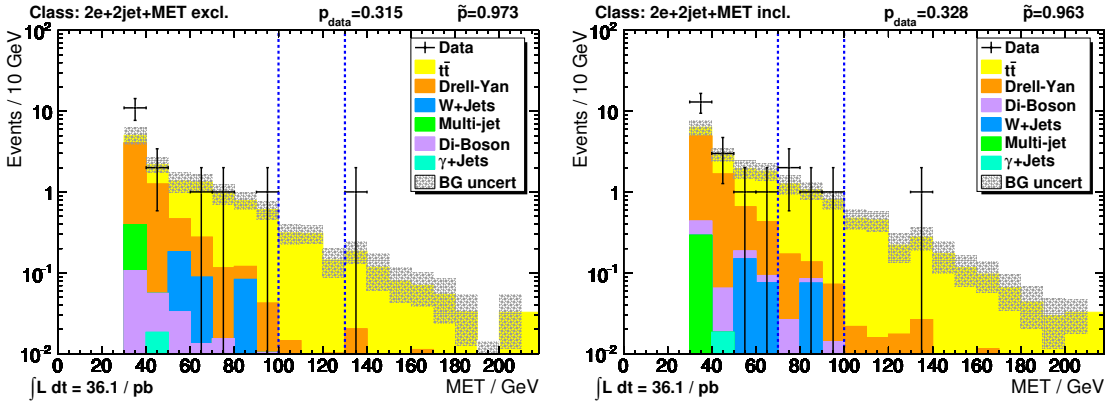

Figure 7.22.: *Electron distributions comparable to the deviating $2\mu + 2jets + \not{E}_T$ classes*

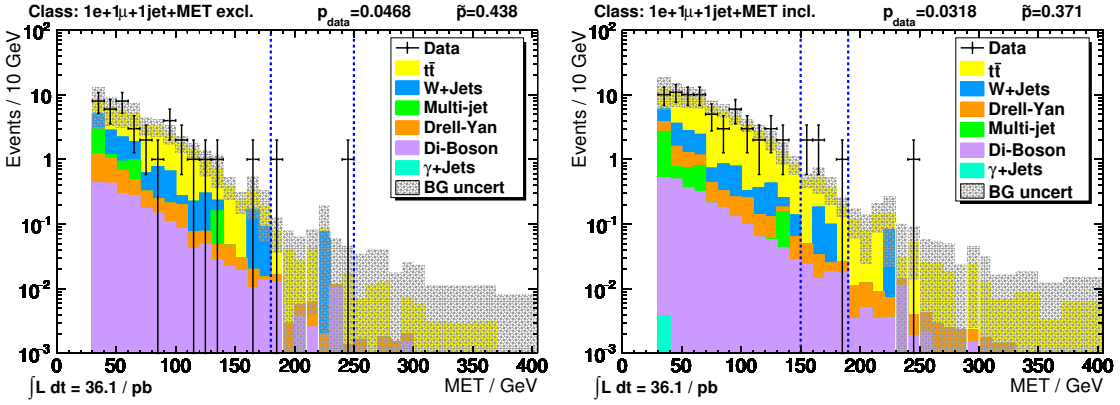

Figure 7.23.: *Mixed-flavour lepton classes comparable to the deviating $2\mu + 2jets + \not{E}_T$ classes*

7.2.4. Conclusions

In all three analysed kinematic distributions ($\sum p_T$, combined mass and $\not{E}_T$) the SM prediction agrees with the measured data within statistical and systematic uncertainties. The most significant deviations need to be studied in future incarnations of this analysis using more data and further insights in detector understanding and SM prediction.

7.3. Charge analysis

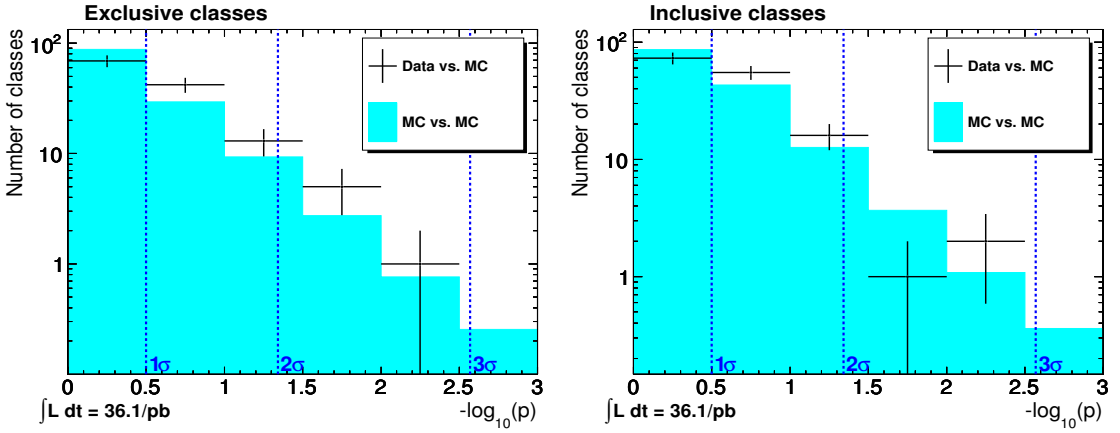

Figure 7.24.: *P-value distributions of data-vs-SM (black crosses) compared to SM-vs-SM (shaded area) for exclusive and inclusive event classes, taking into account the total charge of the leptons.*

In this section the lepton charge is considered when assigning events to classes. The absolute charge sum of all leptons is used as an additional parameter to define the class, e.g. same-sign di-muon events end up in the $2\mu[2Q]$ class, while opposite-sign di-muon events end up in the $2\mu[0Q]$ class. Figure 7.24 shows the $\tilde{p}$ distributions obtained taking the charge into account. The distributions agree within uncertainties with the distributions of Section 7.1. Similarly the $\tilde{p}$ distributions when analysing the kinematic variables in detail, Figures 7.25, 7.26 and 7.27, agree with the charge-agnostic analysis results shown

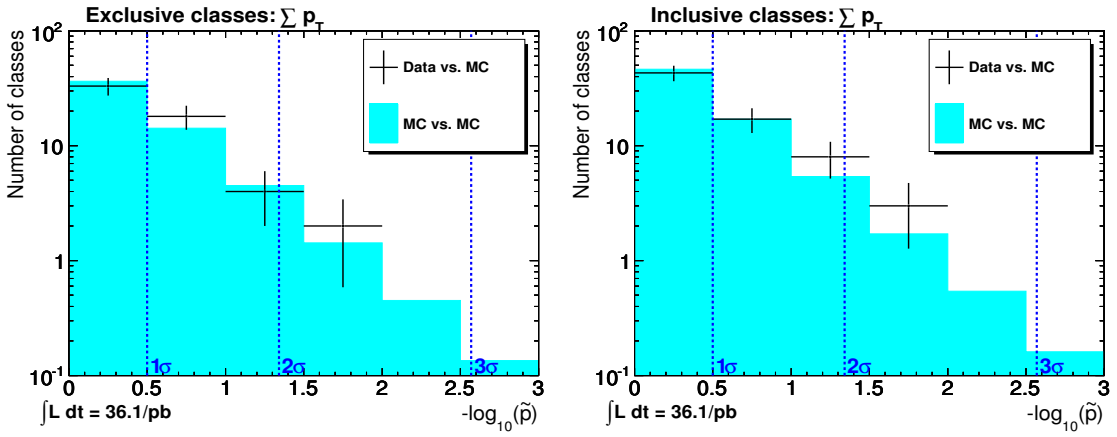

Figure 7.25.: *Distributions of $\tilde{p}$ of data-vs-SM (black crosses) compared to SM-vs-SM (shaded area) for the $\sum p_T$ variable of exclusive and inclusive classes, taking into account the total charge of the leptons.*

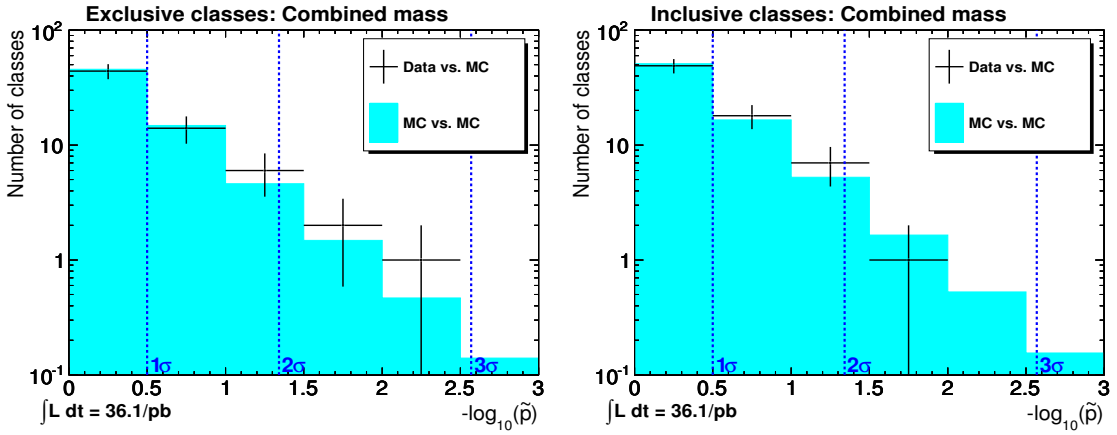

Figure 7.26.: *Distributions of $\tilde{p}$ of data-vs-SM (black crosses) compared to SM-vs-SM (shaded area) for the combined mass variable of exclusive and inclusive classes, taking into account the total charge of the leptons.*

in Figures 7.4, 7.12 and 7.17.

Figures 7.28 and 7.29 show some typical examples of classes where the SM simulation predicts mostly opposite-sign leptons. It is obvious that the charge misidentification rate is much higher for electrons than muons. Figure 7.30 on the other hand shows a class where the number of opposite-sign and same-sign lepton events is in the same order of magnitude. The opposite-sign events are mostly $t\bar{t}$, that is both leptons come directly from the hard interaction. The same-sign events on the other hand are mostly W-boson production, which means that one lepton comes from the W boson, but the other one comes from associated jets. Thus there is no charge correlation between the two leptons and same-sign events can occur.

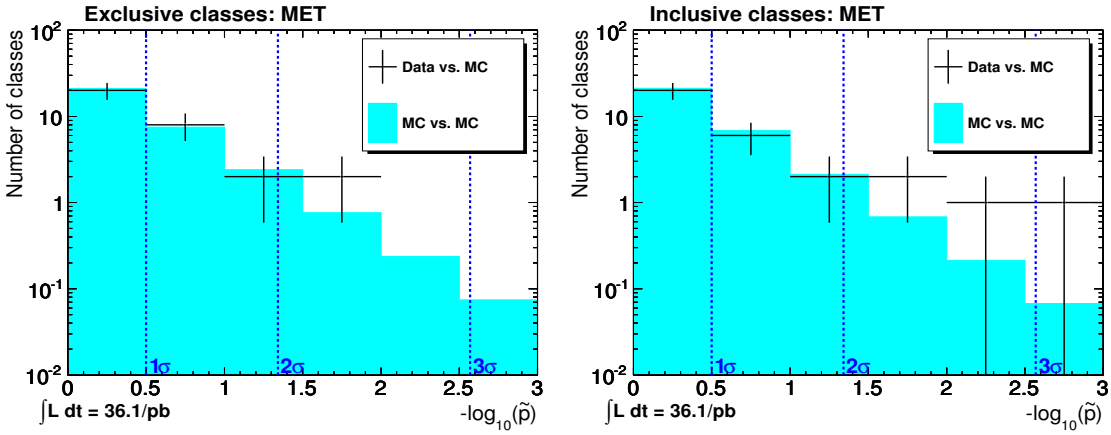

Figure 7.27.: *Distributions of $\tilde{p}$ of data-vs-SM (black crosses) compared to SM-vs-SM (shaded area) for the $\not{E}_T$ variable of exclusive and inclusive classes, taking into account the total charge of the leptons.*

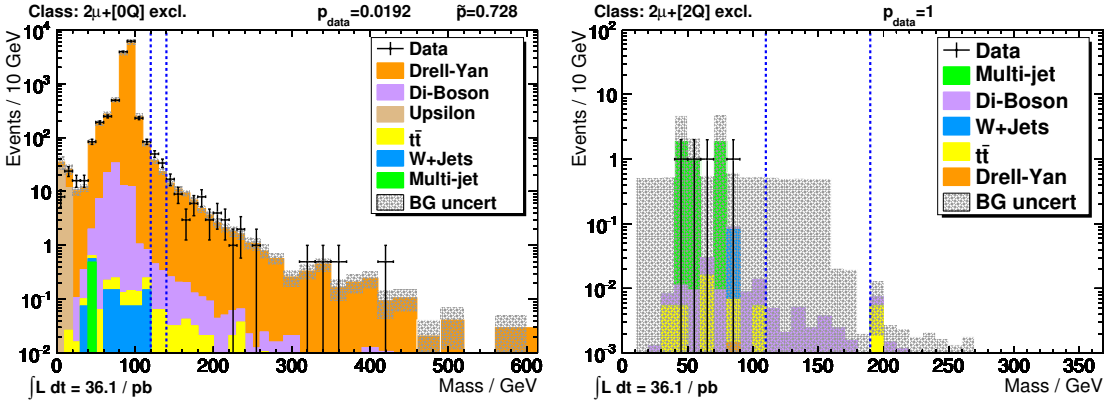

Figure 7.28.: *Combined mass of the 2μ class with opposite-sign and same-sign muons.*

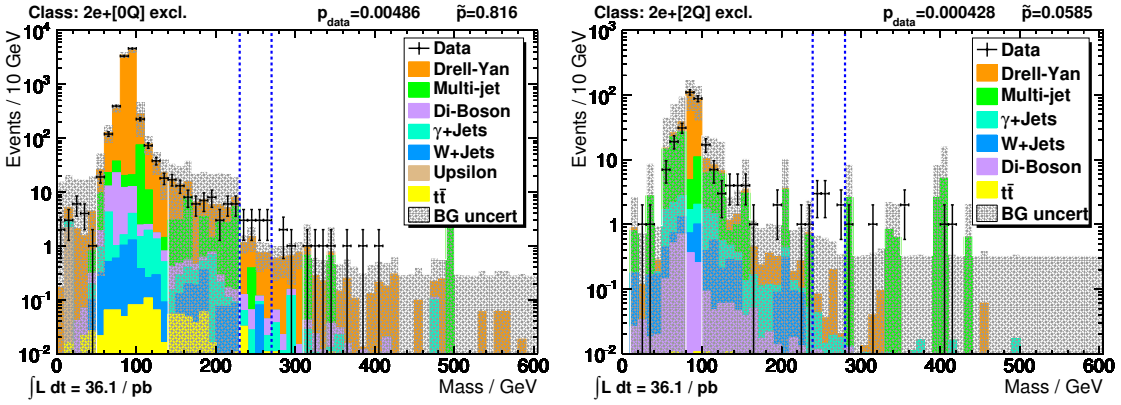

Figure 7.29.: *Combined mass of the $2e$ class with opposite-sign and same-sign electrons.*

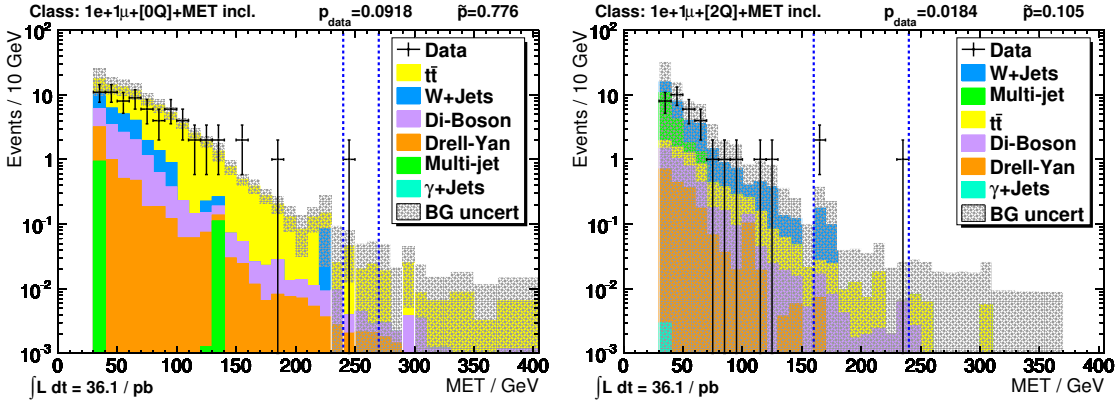

Figure 7.30.: *$\not{E}_T$ distribution of the $1e+1\mu+\not{E}_T$ class with opposite-sign and same-sign leptons.*

7.3.1. Conclusions

To look for deviations in the lepton charge behaviour, classes containing multiple leptons are split into multiple classes depending on the total charge of the observed leptons. The SM prediction agrees within statistical and systematic uncertainties with the measured data. The observed $\tilde{p}$ distributions are compatible with those obtained in the charge-unaware analysis.

8. Sensitivity examples

To claim the absence of a certain type of signal the analysis in question needs to be sensitive to this kind of signal. Proving this is straightforward for a conventional analysis: Use a MC generator capable of generating events containing this signal, put it through the same simulation as the SM prediction, apply the analysis, and verify that a significant deviation with respect to the SM prediction is visible. Given the generalised sensitivity of a model independent analysis it is not feasible to check the sensitivity for all possible deviations. However, a procedure similar to a dedicated analysis can be used to determine whether the analysis is sensitive to certain benchmark signals. The sensitivity studies presented here use only exclusive classes, in order to allow a more straightforward statistical interpretation of the results.

8.1. Incomplete Standard Model

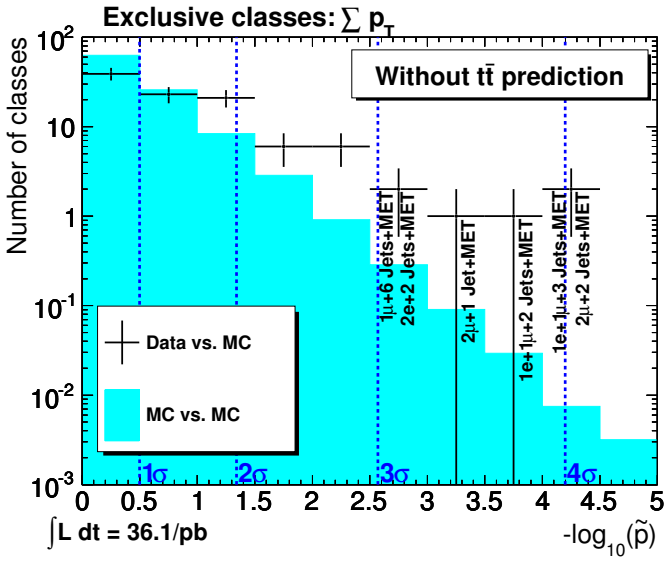

Figure 8.1.: *Distributions of $\tilde{p}$, without $t\bar{t}$ in the list of SM backgrounds.*

One way to check the sensitivity for deviations from the Standard Model is to purposely use a modified Standard Model known to be wrong, e.g. with missing processes that are known to exist. Figure 8.1 shows the $\tilde{p}$ distribution in case the $t\bar{t}$ process is not in the list of SM backgrounds. One can see a generalised tendency towards a higher-than-expected significance with some classes exceeding three or even four σ. As indicated, the classes deviating most are those including fully leptonic top decays, that is precisely the processes that should be visible to MUSiC given the selection that is used. The two most significant classes can be seen in Figure 8.2.

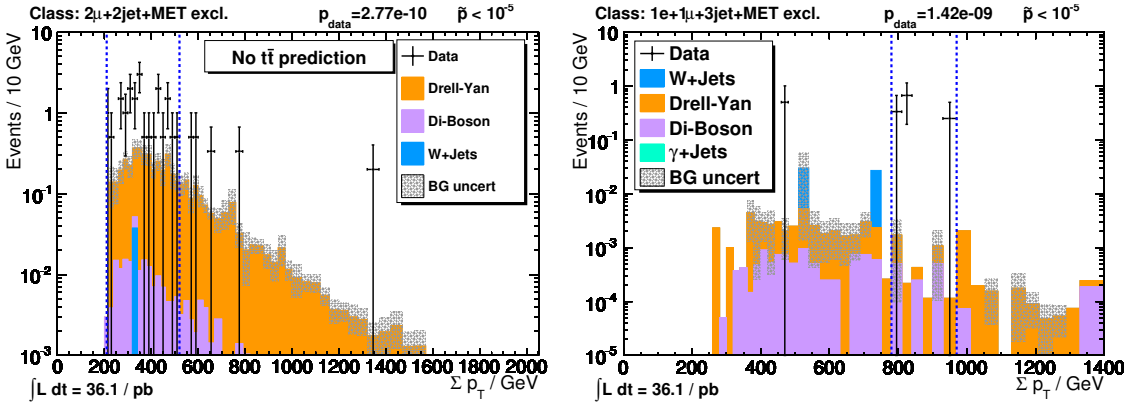

Figure 8.2.: *Distributions of $\sum p_T$ of the most and second most significant class, without $t\bar{t}$ in the list of SM backgrounds.*

8.2. Beyond the Standard Model

Simulated signals of physics processes beyond the Standard Model can be used in pure simulation studies to determine the sensitivity of MUSiC to certain deviations. There are no obvious reasons to pick one or the other BSM model, but some of them are often studied, of which a subset will be used here.

Obviously there are no measured data for BSM processes, thus the procedures in Section 6.1.2 must be modified to determine the expected significance. Similar to what is described in Section 6.1.3, pseudo-data are generated using the SM expectation, but this time including the BSM process of choice. These pseudo-data are compared to the SM prediction to determine the region of interest and its significance. A sufficiently high number, e.g. 100, of full sets of pseudo-data can then be used to find the median p-value for each class. This information is useful to determine the expected data distribution in a single class presuming the chosen BSM model is true. Thus a hypothetical real measurement is expected to yield either a higher or a lower significance with equal probability. To get the expected $\tilde{p}$ distribution the individual $\tilde{p}$ distributions containing all classes of one complete pseudo-experiment are averaged, similar to how the expected $\tilde{p}$ distribution of the background is determined in Section 6.1.4.

Given a certain BSM process, cross section, and integrated luminosity, it is now possible to judge whether MUSiC would have been able to detect this signal or not at this luminosity. With fixed model parameters and cross sections the minimal luminosity for a significant deviation can be determined. Similarly a fixed luminosity allows to determine the regions in parameter space that promise a significant deviation. In the following sections at least one class showing a median $\tilde{p}$ of around or less than 10^{-4} is considered a significant deviation.

The plots of the kinematic distributions are similar to those in Section 7.2, with some notable exceptions:

- The red line shows the expected distribution taking both SM background as well as the chosen signal.
- The printed p-value is the median value described before.
- The printed $\tilde{p}$ is associated to the median p-value.

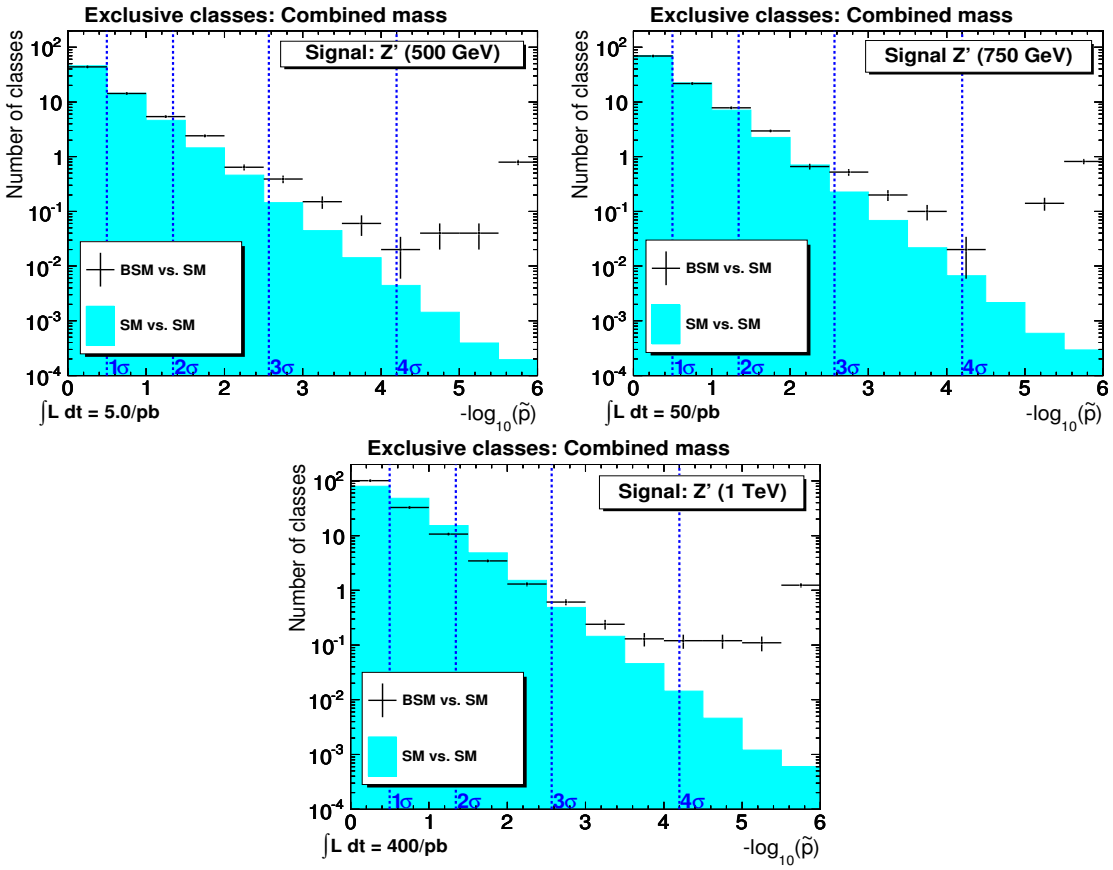

Figure 8.3.: *Expected $\tilde{p}$ distributions taking Z' as a possible BSM signal.*

- The black markers show one possible CMS measurement presuming the chosen signal describes nature. This outcome has been selected to be the one that yielded the median p-value.

8.2.1. Heavy vector bosons

Simulated samples involving hypothetical heavy neutral vector bosons, usually called Z', have been produced with various masses, of which 500 GeV, 750 GeV and 1000 GeV have been used here. The samples have been restricted such that the Z' can only decay into electrons and muons. For those samples the cross sections times branching ratios calculated by PYTHIA are 4.0 pb, 0.84 pb and 0.18 pb, respectively. The luminosities at which at least one class is expected to exceed a median significance of 10^{-4} has been estimated with MUSiC to be 5 pb^{-1} for a mass of 500 GeV, 50 pb^{-1} for a mass of 750 GeV, and 400 pb^{-1} for a mass of 1000 GeV. Thus with the luminosity of 2010 MUSiC is expected to be sensitive to Z' with a mass of 500 GeV, with a bit of luck to a mass of 750 GeV, but not to a mass of 1000 GeV, which is close to the limit[92] of dedicated analyses. Figure 8.3 shows the expected $\tilde{p}$ distributions of the various signal samples at their respective luminosities. An excess of classes with high significance can be observed. In this and all following $\tilde{p}$ distributions the last bin includes the overflow, e.g. for the 500 GeV Z' about one class is expected to show a $\tilde{p}$ of $3.2 \cdot 10^{-6}$ or less. Figure 8.4 shows the di-lepton mass in the exclusive di-muon and di-electron classes. The di-muon spectrum provides a clear signal,

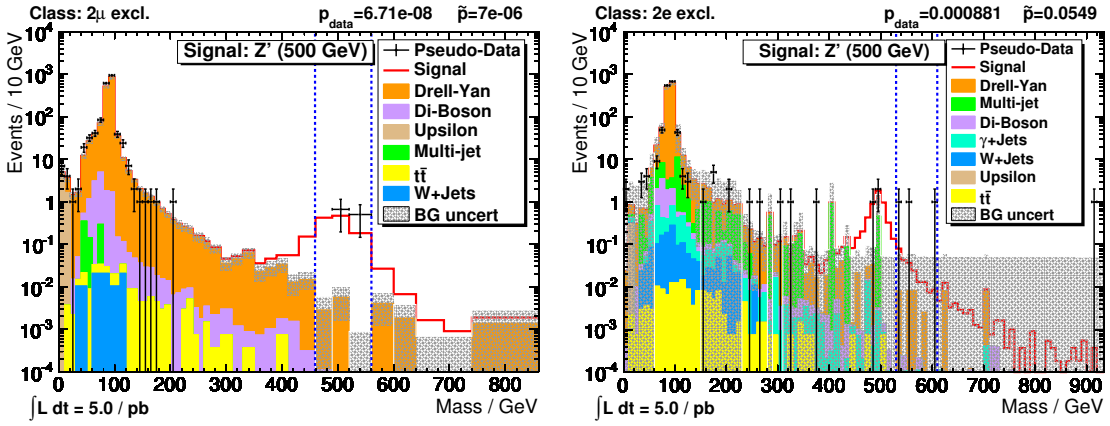

Figure 8.4.: *Mass distributions in the two-lepton classes with a* 500 GeV *Z' as possible BSM signal.*

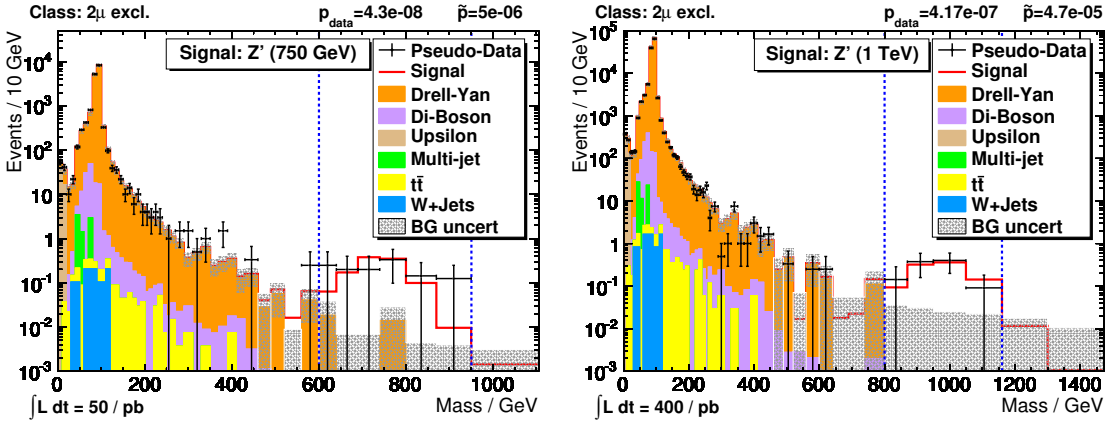

Figure 8.5.: *Mass distributions in the two-muon classes with a* 750 GeV *and* 1000 GeV *Z' as possible BSM signals.*

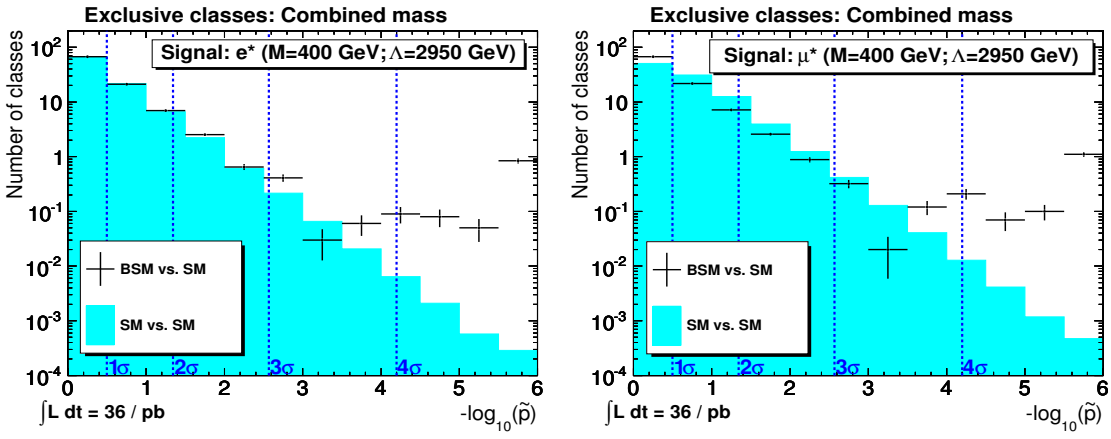

Figure 8.6.: *Expected $\tilde{p}$ distributions for excited electrons and muons as possible BSM signals.*

while the di-electron spectrum is negatively affected by the higher jet-to-electron fake rate, allowing some multijet background to pass the selection. In both cases it can be seen that the SM prediction for such high masses becomes spurious, which is even more obvious in Figure 8.5. The uncertainty filling algorithm (see Section 6.2.4) still allows to calculate a p-value, however the calculated values should be considered with care. It still means that such a deviation would have been seen by MUSiC, but in this case special SM samples would be needed to be generated to allow a detailed analysis.

8.2.2. Excited leptons

The heavy vector bosons served as an example for searching for the minimal integrated luminosity needed to be sensitive to a certain model. In contrast models with excited leptons have two free parameters: The mass M and a scale Λ which only affects the cross section. Thus it is possible to look for the range of Λ at a given integrated luminosity where the analysis is sensitive. While lepton universality has been assumed in the Z' models, equally treating decays into electrons and muons, it is assumed that the existence of a composite muon does not also mean that the electron is not fundamental and vice versa. Figure 8.6 shows the expected $\tilde{p}$ distributions for excited electrons and muons, respectively. Both excited electrons and excited muons can be detected at 36 pb^{-1} if the cross section exceeds 0.3 pb, which is equivalent to a scale $\Lambda < 2950$ GeV. Thus in contrast to the Z', electrons and muons are equally sensitive in the search for excited leptons. Dedicated analyses obtained limits[88] of 0.19 pb electrons and 0.16 pb for muons. Similar to the effect seen in the higher mass Z' analyses, the predicted significances need to be considered with care, because they are based on the results of the uncertainty filling algorithm (see Section 6.2.4), which can be seen in Figures 8.7 and 8.8. Surprisingly, the most significant class with the excited muon signal is not $2\mu + 1\gamma$ but $2\mu + 1\gamma + \not{E}_T$, though no real $\not{E}_T$ is expected in these events. This effect cannot be observed in the excited electron events. Thus it is probably caused by the decreasing resolution of the momentum measurement at increasing p_T, causing an imbalance between the two muons.

8.2.3. mSUGRA

Both Z' and excited lepton models are examples where the final state signature is clear and thus a single class or maybe a few classes are expected to deviate from the SM prediction.

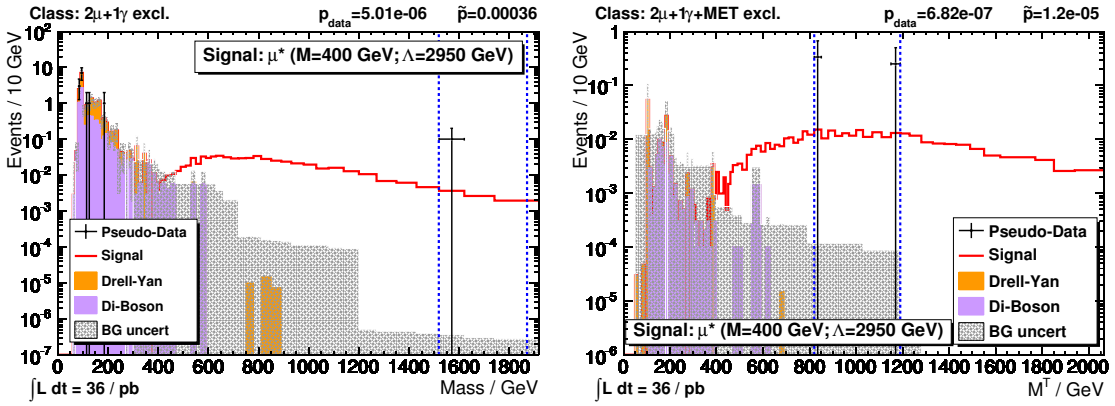

Figure 8.7.: *Two classes with the highest expected significance taking excited muons as a possible BSM signal.*

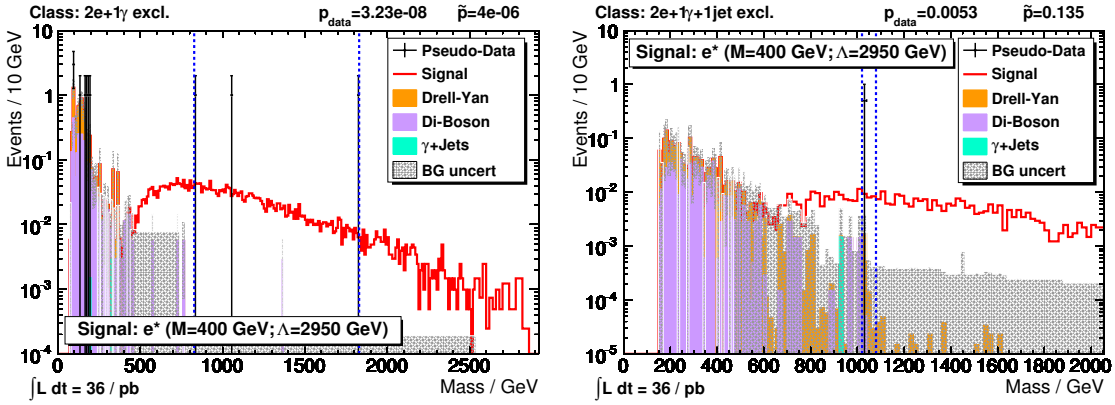

Figure 8.8.: *Two classes with the highest expected significance taking excited electrons as a possible BSM signal.*

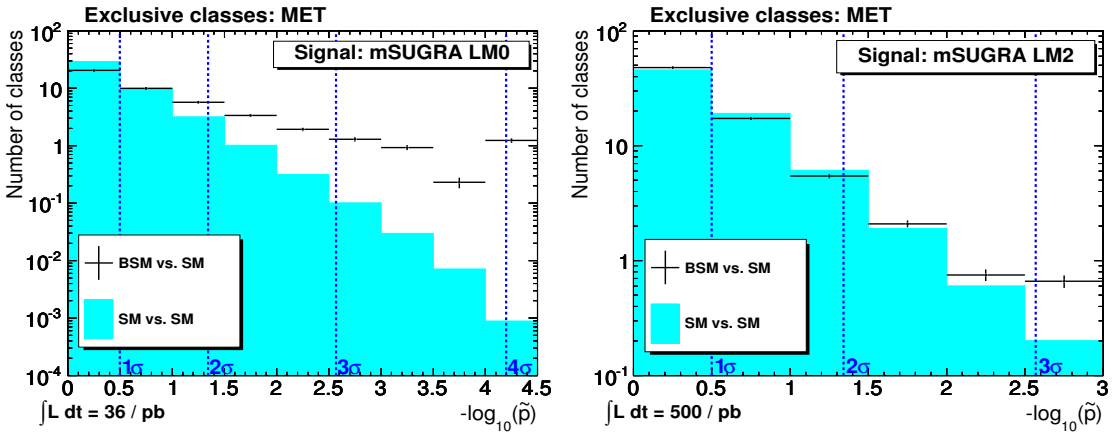

Figure 8.9.: *Expected $\tilde{p}$ distributions for mSUGRA LM0 and LM2 at 36 pb^{-1} and 500 pb^{-1}, respectively.*

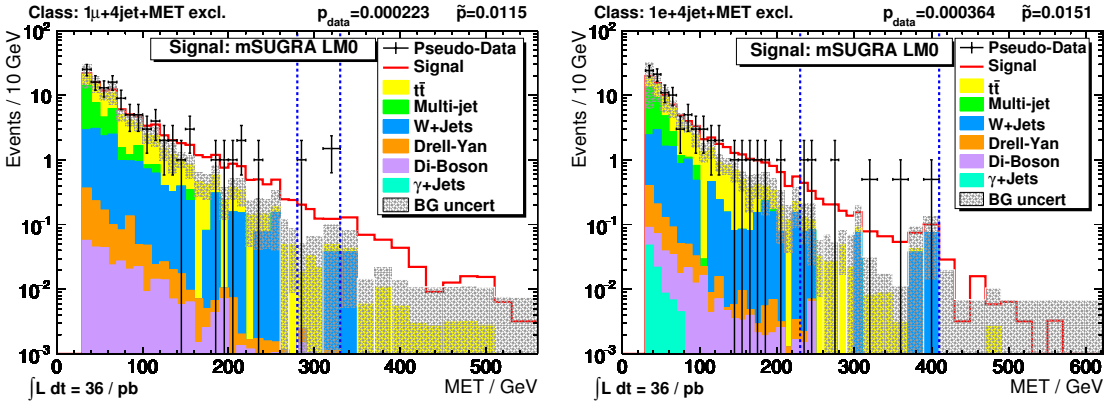

Figure 8.10.: *With the mSUGRA LM0 signal, classes with one lepton, four jets and $\not\!\!E_T$ show the highest median significance.*

In mSUGRA on the other hand the signatures are less constrained and deviations can be expected in a large number of final states, but these deviations are not necessarily very strong. Figure 8.9 shows the expected $\tilde{p}$ distributions taking the mSUGRA benchmark points LM0[1] and LM2[2] with integrated luminosities of 36 pb^{-1} and 500 pb^{-1}, respectively. Taking LM0, one can see not only one class expected to deviate strongly, but a generalised excess of classes with an increased, but not necessarily very high significance. In Figure 8.9 the two classes with the highest median significance expected when taking LM0 as signal are shown. Both classes are on average not expected to deviate strongly, which is true for all other lepton+jets+$\not\!\!E_T$ classes as well. But there are enough classes where LM0 can show up that the total number of classes expected to exceed three standard deviations is still about three. These classes are similar to the final states used by dedicated mSUGRA analyses.

The other $\tilde{p}$ distribution shown in Figure 8.9 is an example for a signal MUSiC is not able to detect even at an integrated luminosity of 500 pb^{-1}.

[1] $m_0 = 200$ GeV, $m_{1/2} = 160$ GeV, $\tan\beta = 10$, $\mathrm{sgn}(\mu) = +$, $A_0 = -400$
[2] $m_0 = 185$ GeV, $m_{1/2} = 350$ GeV, $\tan\beta = 35$, $\mathrm{sgn}(\mu) = +$, $A_0 = 0$

8.2.4. Sensitivity studies conclusions

It has been shown in this section that MUSiC is able to detect and successfully tag deviations e.g. caused by missing SM backgrounds. It is also sensitive to certain kinds of new physics signals, but it is usually not able to compete with dedicated searches. This underlines the conclusions of the scans of 2010 LHC data, showing no significant deviations.

9. Preview 2011

To the greatly increased integrated luminosity of 4.7 fb^{-1} of the 2011 LHC run made the analysis more challenging, e.g. due to higher pile-up or the introduction of SM process with small cross sections which have not been simulated properly. While most of these difficulties have been solved at end of 2011, some still affect a number of classes, causing deviations. Thus a full scan of the 2011 data is not yet feasible, however it is still possible to have a look at some classes, particularly those with large deviations in 2010 data. Besides the obvious differences between 2010 and 2011 caused by much more data, there are also differences e.g. caused by changed trigger thresholds, thus the results are not always comparable. Only the muon and electron triggers were used, hence only classes containing at least one muon or electron can be analysed. The muon and electron trigger thresholds has been raised to 32 GeV and 82 GeV, respectively.

Two of the deviating $\sum p_T$ distributions in 2010 are shown in comparison to 2011 in Figures 9.1 and 9.2. In contrast to the results obtained in 2010, the deviations are of very little significance, as visible in the $\tilde{p}$ values of 0.93 and 0.63, respectively. This means that deviations in 2010 were either just statistical fluctuations, or the underlying cause has been eliminated by improved detector understanding or other technical changes in the CMS software. Similarly, the deviation in the combined mass distribution of the exclusive $1e+1\mu+3\text{Jets}+\not{E}_T$ class, correlated to the $\sum p_T$ distribution in Figure 9.2, is not present in 2011 anymore, as shown in Figure 9.3. And finally Figures 9.4 and 9.5 show that the deviations in the $2\mu + N\text{jets} + \not{E}_T$ classes vanished as well.

In conclusion, some of the most significant deviations in the 2010 data cannot be observed in the 2011 data anymore. Other deviations and those which have been introduced by the increased integrated luminosity need to be studied in future analyses.

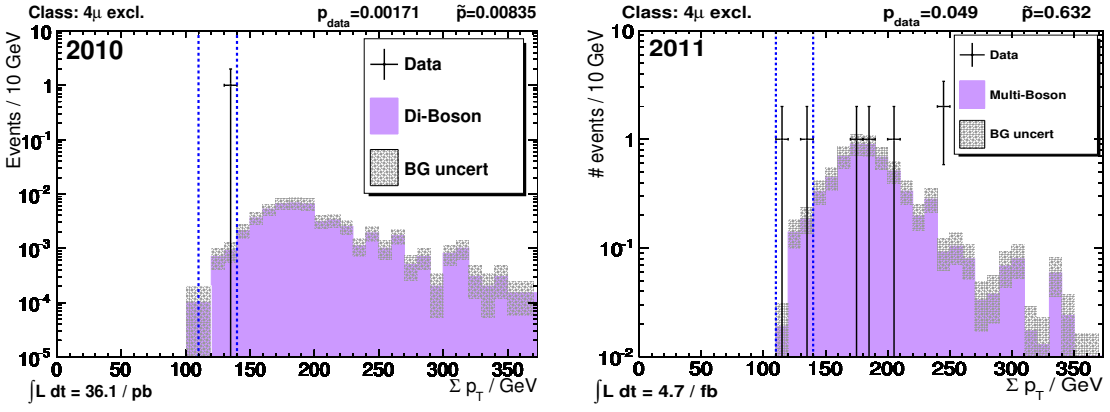

Figure 9.1.: *p_T distributions of the exclusive 4μ class containing 2010 and 2011 data. This class shows large deviations in 2010, but little deviations in 2011.*

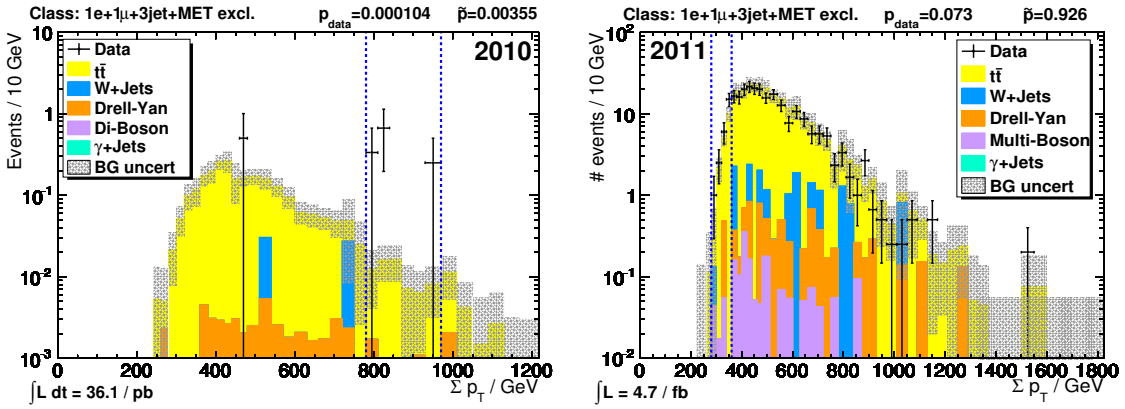

Figure 9.2.: *p_T distributions of the exclusive $1e+1\mu+3Jets+\not{E}_T$ class containing 2010 and 2011 data. This class shows large deviations in 2010, but little deviations in 2011.*

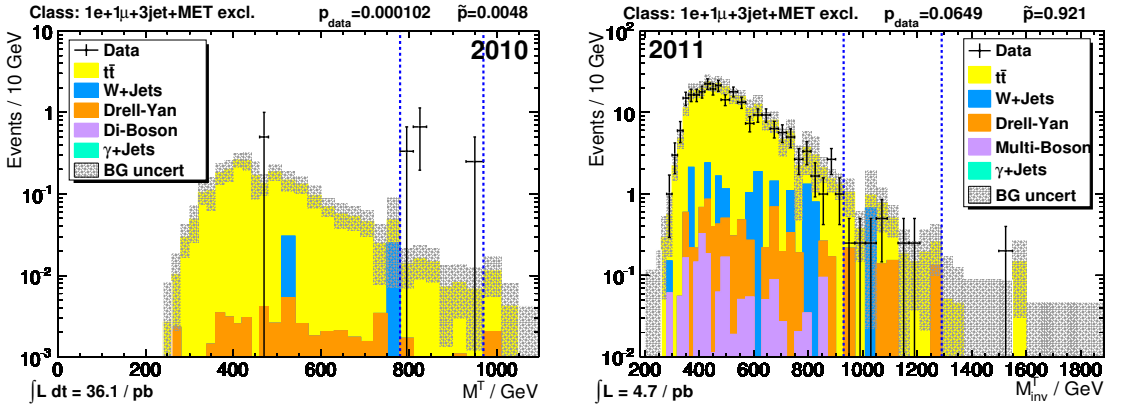

Figure 9.3.: *Combined mass distributions of the exclusive $1e+1\mu+3Jets+\not{E}_T$ class containing 2010 and 2011 data. This class shows large deviations in 2010, but little deviations in 2011.*

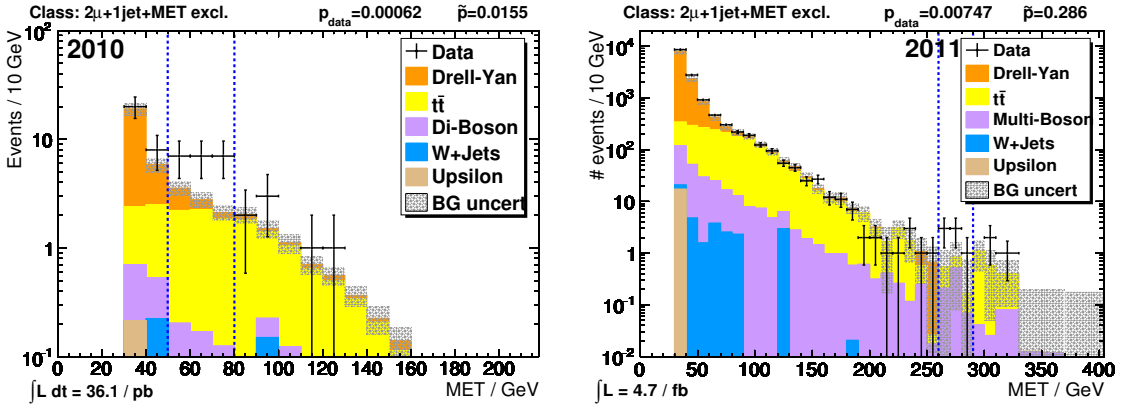

Figure 9.4.: *$\not{E}_T$ distributions of the $2\mu+1Jet+\not{E}_T$ class containing 2010 and 2011 data. This classes was one of the most significant classes in 2010 data.*

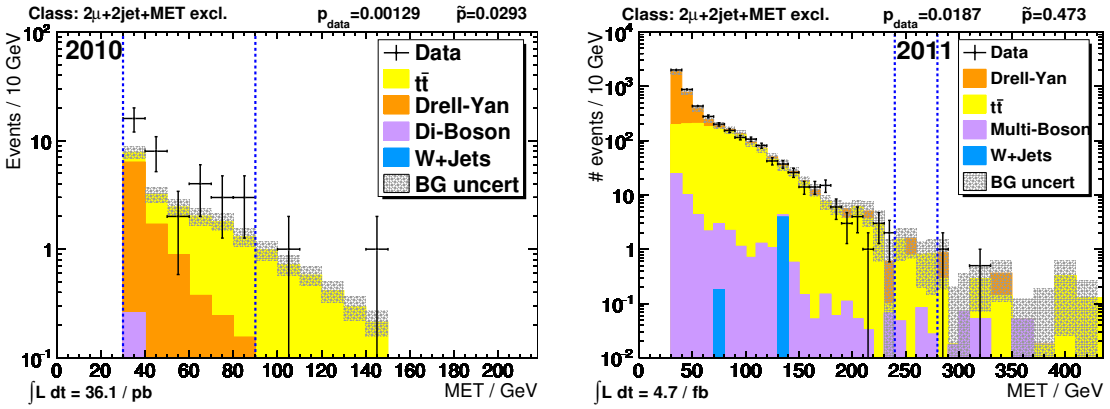

Figure 9.5.: *$\not{E}_T$ distributions of the $2\mu + 2Jets + \not{E}_T$ class containing 2010 and 2011 data. This classes was one of the most significant classes in 2010 data.*

10. Conclusion

The implementation and results of the Model Unspecific Search in CMS (MUSiC) using the 2010 CMS data have been presented. Taking into account systematic uncertainties, automatic scans of a large number of event classes have been performed to compare the measured data to the Standard Model predictions. An event class is defined by a number of objects (muons, electrons, photons, jets and $\not\!\!E_T$) and includes all events containing these object. Events and objects are selected using robust criteria. Besides considering the event classes as counting experiments, detailed scans of kinematic distributions have been performed as well, to reveal deviations in the shape of the kinematic distributions. To calculate the significance of the identified deviations, the systematic uncertainties and the Look-Elsewhere Effect have been considered. No deviations beyond expected statistical and systematic effects have been observed. To evaluate the sensitivity of the analysis to certain kinds of new physics or other types of deviations, simulation studies have been performed.

Appendix A.

Miscellaneous

A.1. Coordinate system

The coordinated system used by CMS is centred on the nominal interaction point. The x axis points inwards to the centre of LHC and the y axis vertically upwards. The z axis thus points in the direction of the counterclockwise rotating beam. The azimuthal angle ϕ starts at the x axis and the polar angle θ at the z axis. The pseudorapidity is defined as $\eta = -\ln(\tan(\theta/2))$.

A.2. Shower shape variable

The spread of energy in η in the cluster of ECAL crystals being part of an electron or photon object can be quantified with[93]:

$$\sigma^2_{i\eta i\eta} = \frac{\sum_i^{5\times5} w_i(\eta_i - \overline{\eta_{5\times5}})^2}{\sum_i^{5\times5} w_i} \tag{A.1}$$

with i running over all crystals in a 5x5 matrix around the seed crystal, η_i being the η position of the ith crystal, and $\overline{\eta_{5\times5}}$ the energy weighted mean of the η positions of all crystals in the matrix. The weights are defined as $w_i = 4.2 + \ln\left(\frac{E_i}{E_{5\times5}}\right)$.

However, this variable turned out to be unstable near the cracks of the ECAL and needs different thresholds for different parts of the detector[94, 95]. Thus a slightly different variable $\sigma_{i\eta i\eta}$[93] is used, which does not employ the actual η position of the crystals, but instead just enumerates them starting from $\eta = 0$, which is equivalent to using an average crystal width.

A.3. Resolution and region width

A simple, but illustrative example for a possible deviation MUSiC should be able to detect is a normal distributed signal above a flat background, as shown in Figure A.1(a). Using the number of expected signal events S and background events B in the indicated region, one can calculate the estimated significance $Z = S/\sqrt{B}$. One can now calculate the expected significance depending on the region width in units of standard deviations of the signal distribution, as shown in Figure A.1(b). The absolute normalisation of signal and background changes the scale of the vertical axis, but does not change the general shape.

Ideally a single bin with a width of 3σ is centred on the deviation, as shown in Figure A.1(a). However, if the deviation is split between two bins, a total region width of 6σ results in a greatly reduced significance. The difference in significance between the

centred and the split case decreases with decreasing bin size. A reasonable compromise is a bin width equal to the standard deviation, which is used in MUSiC. In the centred case the significance is still maximal, while in the split case a region of either 2 or 4 standard deviations can be chosen by the algorithm, both avoiding too large drops in significance.

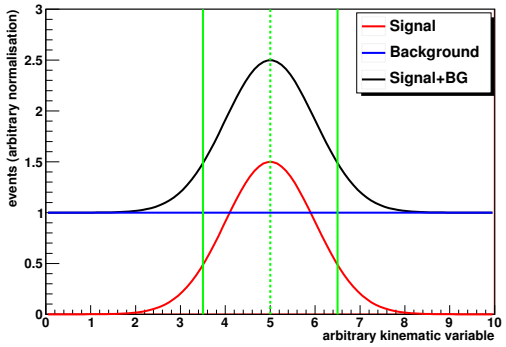

(a) Signal and background

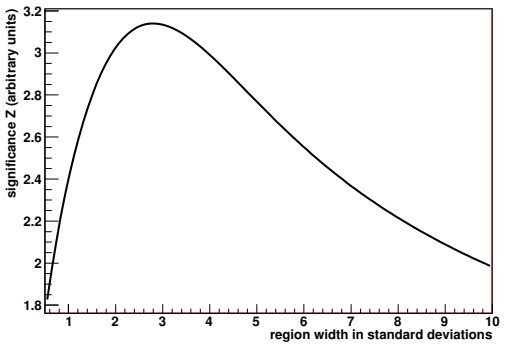

(b) Signal and background

Figure A.1.: *A normally distributed signal (red) in front of a flat background (blue). The expected measurement, signal and background combined, is shown in black. The green lines indicate a Region of Interest centred on the signal. Figure (b) shows the expected significance depending on the region width in units of standard deviations of the signal distribution.*

A.4. Object resolutions

The estimated resolutions of the considered physics objects have been collected from various sources. Those resolutions are not critical for this analysis, as they are only used to determine the bin width. Also they are only used as the input for rough estimations, thus they do not need to be very precise.

Muons

A detailed study of the expected muon resolution based on simulations can be found in [96]. Based on the top left plot in Figure 2 of [96], the following function is used:

$$\frac{\sigma_{p_T}}{p_T} = \left(1.6 + 0.015 \cdot \frac{p_T}{\mathrm{GeV}}\right) \% \tag{A.2}$$

Electrons and photons

In this analysis only the ECAL measurement is used to determine the electron energy and thus the resolution is similar to those of photons, which are based solely on the ECAL. For both objects the equation and numbers of page 16 of [97] are used, which are compatible to test-beam measurements:

$$\sigma_E^2 = 3.88 \cdot 10^{-2}\,\mathrm{GeV}^2 + 6.25 \cdot 10^{-4}\,\mathrm{GeV} \cdot E + 2.704 \cdot 10^{-5} \cdot E^2 \tag{A.3}$$

Jets

The resolution of jets depends not only on the energy, but also on the rapidity. Conservatively, the worst case ($2 < \eta < 2.5$) of Table 4 in [98] in conjunction with Equation 7 of [98] is used:

$$\left(\frac{\sigma_{p_T}}{p_T}\right)^2 = \left(\frac{1.05\,\text{GeV}}{p_T}\right)^2 + 0.218 \cdot \left(\frac{p_T}{\text{GeV}}\right)^{-0.81} \tag{A.4}$$

Missing transverse energy

The $\not{E}_T$ resolution is expected to be proportional to the square-root of the total $\sum p_T$ of the events. The following function has been fitted approximately to the values in Figure 11 of [99]:

$$\sigma_{\not{E}_T} = 0.567 \cdot \sqrt{\frac{\sum p_T}{\text{GeV}}} \cdot \text{GeV} \tag{A.5}$$

Appendix B.

Standard Model samples

Process	Events	Cross section
$W \to l\nu + \text{Jets}$	15 M	31 nb

Table B.1.: *Details of the simulated W sample. Cross section is NNLO. Generator is MadGraph.*

Process	Generator	$M(ll)$	$p_T(ll)$	Events	Cross section
$DY \to \mu\mu$	PYTHIA	2 – 10	–	1 M	94 nb
$DY \to ll + \text{Jets}$	MadGraph	10 – 50	–	178 k	413 pb
$DY \to ll + 0\text{Jets}$	Alpgen	> 50	–	1.4 M	2.4 nb
$DY \to ll + 1\text{Jet}$	Alpgen	> 50	0 – 100	300 k	471 pb
$DY \to ll + 1\text{Jet}$	Alpgen	> 50	100 – 300	265 k	11 pb
$DY \to ll + 1\text{Jet}$	Alpgen	> 50	300 – 800	110 k	91 fb
$DY \to ll + 1\text{Jet}$	Alpgen	> 50	800 – 1600	33 k	170 ab
$DY \to ll + 2\text{Jets}$	Alpgen	> 50	0 – 100	118 k	128 pb
$DY \to ll + 2\text{Jets}$	Alpgen	> 50	100 – 300	129 k	11 pb
$DY \to ll + 2\text{Jets}$	Alpgen	> 50	300 – 800	109 k	142 fb
$DY \to ll + 2\text{Jets}$	Alpgen	> 50	800 – 1600	11 k	374 ab
$DY \to ll + 3\text{Jets}$	Alpgen	> 50	0 – 100	55 k	28 pb
$DY \to ll + 3\text{Jets}$	Alpgen	> 50	100 – 300	55 k	4.9 pb
$DY \to ll + 3\text{Jets}$	Alpgen	> 50	300 – 800	54 k	103 fb
$DY \to ll + 3\text{Jets}$	Alpgen	> 50	800 – 1600	11 k	306 ab
$DY \to ll + 4\text{Jets}$	Alpgen	> 50	0 – 100	44 k	5.7 pb
$DY \to ll + 4\text{Jets}$	Alpgen	> 50	100 – 300	44 k	1.6 pb
$DY \to ll + 4\text{Jets}$	Alpgen	> 50	300 – 800	11 k	49 fb
$DY \to ll + 4\text{Jets}$	Alpgen	> 50	800 – 1600	11 k	172 ab
$DY \to ll + 5\text{Jets}$	Alpgen	> 50	0 – 100	11 k	1.4 pb
$DY \to ll + 5\text{Jets}$	Alpgen	> 50	100 – 300	11 k	588 fb
$DY \to ll + 5\text{Jets}$	Alpgen	> 50	300 – 800	11 k	24 fb
$DY \to ll + 5\text{Jets}$	Alpgen	> 50	800 – 1600	11 k	89 ab

Table B.2.: *Details of the simulated DY samples. Cross sections are NNLO for $M > 50$ GeV, otherwise LO with k-factor of 1.24.*

Process	Events	Cross section
$t\bar{t} + \text{Jets}$	1.1 M	165 pb

Table B.3.: *Details of the simulated $t\bar{t}$samples. Cross section is NNLL. Generator is MadGraph.*

Process	Generator	Events	Cross section
$W + W$	PYTHIA	2 M	43 pb (NLO)
$W + Z$	PYTHIA	2.2 M	18 pb (NLO)
$Z + Z$	PYTHIA	2.1 M	5.9 pb (NLO)
$W/Z + \gamma + Jets$	MadGraph	2.2 M	173 pb (LO)

Table B.4.: *Details of the simulated di-boson samples.*

Process	Events	Cross section
$\Upsilon(1S) \to ee$	183 k	6 nb
$\Upsilon(1S) \to \mu\mu$	2.3 M	7.4 nb
$\Upsilon(2S) \to ee$	220 k	4.3 nb
$\Upsilon(2S) \to \mu\mu$	1.1 M	1.9 nb
$\Upsilon(3S) \to ee$	112 k	1.2 nb
$\Upsilon(3S) \to \mu\mu$	938 k	1 nb

Table B.5.: *Details of the simulated Υ samples. Cross sections are measured ($\mu\mu$) or LO with k-factor (ee). Generator is PYTHIA.*

Process	$p_T(partons)$	Events	Cross section
standard QCD	0 – 5	550 k	47 mb
standard QCD	5 – 15	1.6 M	37 mb
standard QCD	15 – 30	5 M	810 μb
standard QCD	30 – 50	3 M	50 μb
standard QCD	50 – 80	2.7 M	5.5 μb
standard QCD	80 – 120	2.6 M	642 nb
standard QCD	120 – 170	2.4 M	93 nb
standard QCD	170 – 300	3.1 M	23 nb
standard QCD	300 – 470	3 M	1.1 nb
standard QCD	470 – 600	1.9 M	67 pb
standard QCD	600 – 800	1.8 M	15 pb
standard QCD	800 – 1000	2 M	1.8 pb
standard QCD	1000 – 1400	1 M	319 fb
standard QCD	1400 – 1800	980 k	10 fb
standard QCD	> 1800	508 k	346 ab
BC→EM enriched QCD	20 – 30	2.2 M	130 nb
BC→EM enriched QCD	30 – 80	1.9 M	131 nb
BC→EM enriched QCD	80 – 170	957 k	8.6 nb
EM enriched QCD	20 – 30	37 M	2.4 μb
EM enriched QCD	30 – 80	42 M	3.8 μb
EM enriched QCD	80 – 170	7.9 M	137 nb
μ enriched QCD	15 – 20	2.7 M	1.5 μb
μ enriched QCD	20 – 30	11 M	1.2 μb
μ enriched QCD	30 – 50	11 M	578 nb
μ enriched QCD	50 – 80	11 M	144 nb
μ enriched QCD	80 – 120	833 k	29 nb
μ enriched QCD	120 – 150	949 k	4.4 nb
μ enriched QCD	> 150	923 k	2.8 nb

Table B.6.: *Details of the simulated QCD samples. Cross sections are LO. Generator is PYTHIA.*

Process	$p_T(\gamma)$	Events	Cross section
γ+Jets	0 – 15	1 M	84 μb
γ+Jets	15 – 30	1 M	172 nb
γ+Jets	30 – 50	1 M	17 nb
γ+Jets	50 – 80	1 M	2.7 nb
γ+Jets	80 – 120	1 M	447 pb
γ+Jets	120 – 170	1 M	84 pb
γ+Jets	170 – 300	1 M	23 pb
γ+Jets	300 – 470	1 M	1.5 pb
γ+Jets	470 – 800	1 M	132 fb
γ+Jets	800 – 1400	1 M	3.5 fb
γ+Jets	1400 – 1800	1 M	13 ab
γ+Jets	> 1800	1 M	0.3 ab
$\gamma + \gamma$ (Born)	10 – 25	479 k	236 pb
$\gamma + \gamma$ (Born)	25 – 250	534 k	22 pb
$\gamma + \gamma$ (Born)	> 250	496 k	8.1 fb
$\gamma + \gamma$ (Box)	10 – 25	793 k	358 pb
$\gamma + \gamma$ (Box)	25 – 250	778 k	12 pb
$\gamma + \gamma$ (Box)	> 250	736 k	208 ab

Table B.7.: *Details of the simulated γ samples. Cross sections are LO. Generator is PYTHIA.*

Process	$M(Z')$	Events	Cross section
$Z' \to ee$	500	55 k	2 pb
$Z' \to ee$	750	55 k	357 fb
$Z' \to ee$	1000	50 k	91 fb
$Z' \to \mu\mu$	500	55 k	2 pb
$Z' \to \mu\mu$	750	55 k	357 fb
$Z' \to \mu\mu$	1000	55 k	91 fb

Table B.8.: *Details of the simulated Z' samples. Cross sections are LO. Generator is PYTHIA.*

Process	$M(l^*)$	Events	Cross section
$ee^* \to ee\gamma$	400	22 k	depends on Λ; $\mathcal{O}$(pb)
$\mu\mu^* \to \mu\mu\gamma$	400	22 k	depends on Λ; $\mathcal{O}$(pb)

Table B.9.: *Details of the simulated excited lepton samples. Cross sections are LO. Generator is PYTHIA.*

Process	Events	Cross section
mSUGRA LM0	220 k	39 pb
mSUGRA LM2	220 k	600 fb

Table B.10.: *Details of the simulated mSUGRA samples. Cross sections are LO. Generator is PYTHIA.*

Appendix C.

Additional results

C.1. Classes as counting experiments

C.1.1. Figures

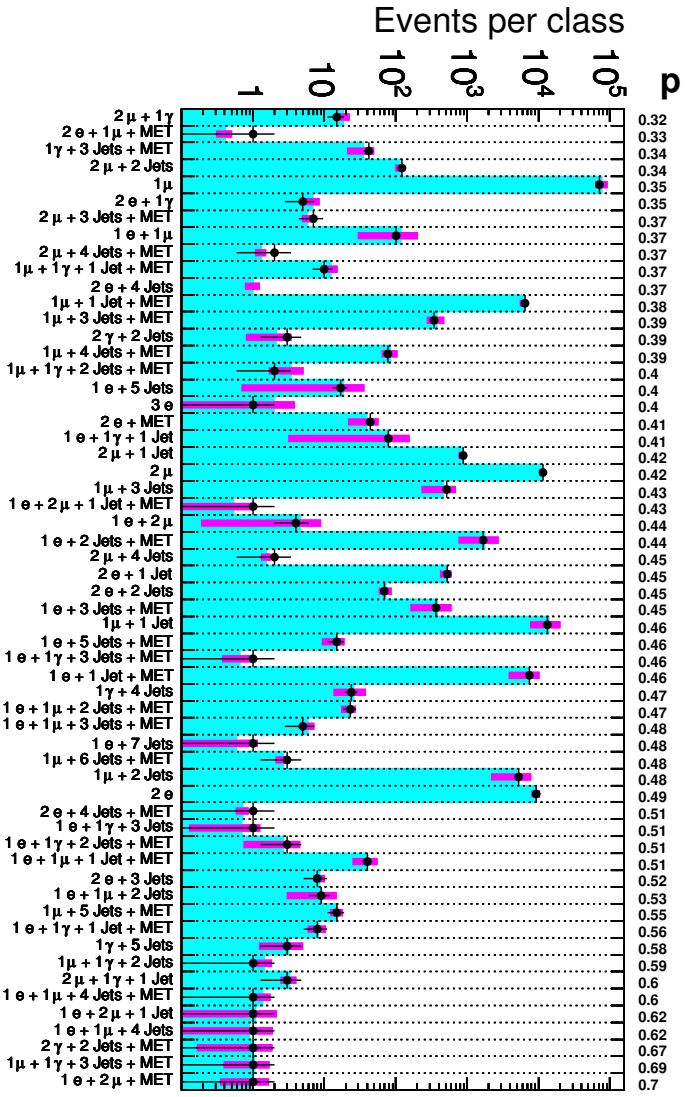

Figure C.1.: *Number of events (black markers) by CMS, simulated number of SM events (light shaded area) and total systematic uncertainty (dark bars) of the remaining exclusive classes, sorted by p-value, which is displayed on the right.*

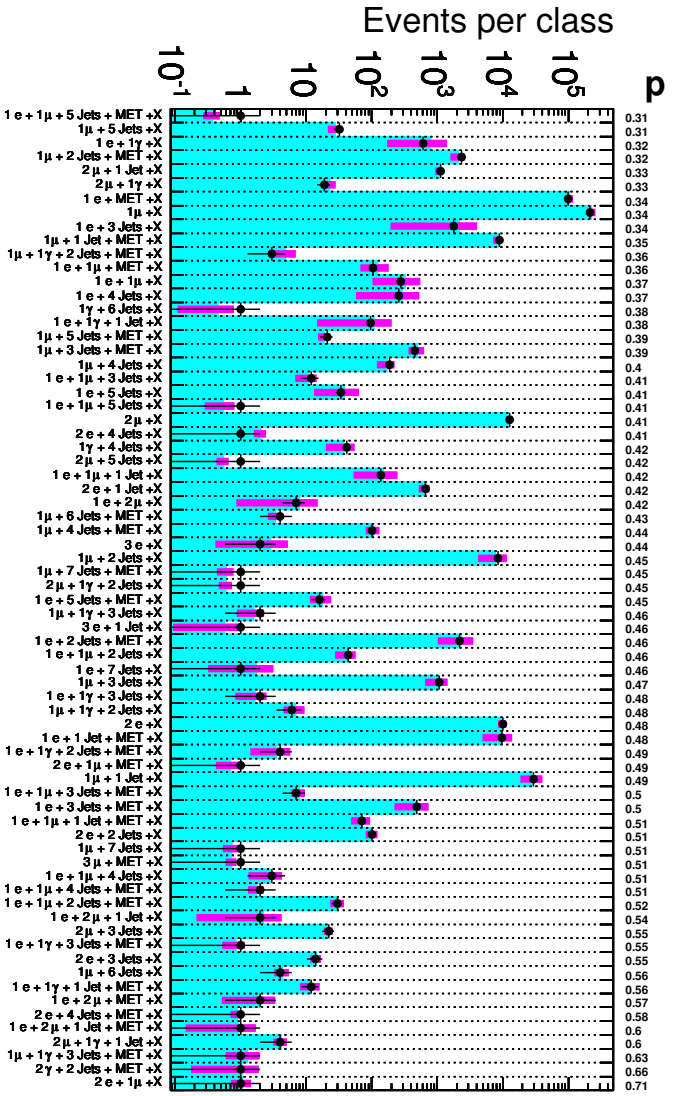

Figure C.2.: *Number of events (black markers) by CMS, simulated number of SM events (light shaded area) and total systematic uncertainty (dark bars) of the remaining inclusive classes, sorted by p-value, which is displayed on the right.*

C.1.2. Table of exclusive classes

Event class	p-value	Data	SM $\pm \sigma_{sys}$
2μ + 2 Jets + $\not\!\!E_T$	0.0068	38	22.3 ± 3.1
$1\mu + 2\gamma + \not\!\!E_T$	0.019	1	0.018 ± 0.012
1γ + 2 Jets + $\not\!\!E_T$	0.03	218	125 ± 47
1γ + 1 Jet + $\not\!\!E_T$	0.031	724	397 ± 1.7e+02
$1\mu + 1\gamma + \not\!\!E_T$	0.032	29	47.4 ± 7.5
$1\mu + 1\gamma$ + 1 Jet	0.034	28	16.4 ± 4.0
3μ	0.037	2	0.30 ± 0.05
2μ + 1 Jet + $\not\!\!E_T$	0.037	56	40.3 ± 5.1
Continued on next page...			

Event class	p-value	Data	SM $\pm \sigma_{sys}$
4μ	0.051	1	0.052 ± 0.011
1 e + 1μ + 1γ	0.056	1	0.052 ± 0.039
2 e + 1 Jet + $\not\!\!E_T$	0.064	42	27.0 ± 7.6
3 e + 1 Jet + $\not\!\!E_T$	0.076	1	0.078 ± 0.039
1γ + 5 Jets + $\not\!\!E_T$	0.08	3	0.86 ± 0.48
1μ + 8 Jets + $\not\!\!E_T$	0.087	1	0.091 ± 0.033
2γ + 3 Jets	0.087	1	0.090 ± 0.046
1μ + 1γ	0.088	66	91 ± 16
1γ + 6 Jets + $\not\!\!E_T$	0.094	1	0.096 ± 0.051
1γ + $\not\!\!E_T$	0.13	154	107 ± 40
2μ + $\not\!\!E_T$	0.16	53	44.1 ± 5.0
1γ + 3 Jets	0.16	183	130 ± 51
1 e + 1γ + 2 Jets	0.16	5	13 ± 14
1μ + 1γ + 3 Jets	0.16	1	0.178 ± 0.053
2γ + 1 Jet + $\not\!\!E_T$	0.17	2	0.65 ± 0.41
2γ + $\not\!\!E_T$	0.17	1	0.192 ± 0.066
1 e + 6 Jets + $\not\!\!E_T$	0.18	0	1.86 ± 0.51
1 e + 1μ + 3 Jets	0.18	4	1.8 ± 1.2
1γ + 2 Jets	0.18	1437	1.07e+03 ± 4e+02
3μ + 1 Jet + $\not\!\!E_T$	0.18	1	0.204 ± 0.069
1μ + 5 Jets	0.18	11	7.2 ± 2.5
1μ + $\not\!\!E_T$	0.2	100419	1.074e+05 ± 8.3e+03
1 e + 4 Jets + $\not\!\!E_T$	0.21	92	68 ± 27
1γ + 4 Jets + $\not\!\!E_T$	0.21	11	6.9 ± 3.7
1 e + 1γ + $\not\!\!E_T$	0.22	28	35.4 ± 6.6
2γ + 1 Jet	0.23	12	8.4 ± 3.3
2γ	0.23	18	13.6 ± 4.2
1 e + 2 Jets	0.23	10061	1.6e+04 ± 1.7e+04
2μ + 5 Jets + $\not\!\!E_T$	0.23	1	0.269 ± 0.066
1 e	0.24	393267	6.0e+05 ± 6.1e+05
1 e + 1μ + $\not\!\!E_T$	0.25	32	52 ± 35
1μ + 2 Jets + $\not\!\!E_T$	0.25	1815	1.56e+03 ± 3.7e+02
1 e + 1 Jet	0.25	132581	2.0e+05 ± 2.1e+05
2 e + 1γ + 1 Jet	0.25	0	1.47 ± 0.42
1 e + 1μ + 5 Jets + $\not\!\!E_T$	0.25	1	0.294 ± 0.091
1γ	0.25	1348	1.08e+03 ± 4e+02
2 e + 2 Jets + $\not\!\!E_T$	0.26	17	13.7 ± 2.8
1 e + $\not\!\!E_T$	0.27	89283	9.49e+04 ± 9.1e+03
1 e + 4 Jets	0.27	129	1.8e+02 ± 1.8e+02
1μ + 4 Jets	0.27	71	55 ± 25
2 e + 3 Jets + $\not\!\!E_T$	0.28	5	3.49 ± 0.72
1 e + 1γ	0.3	474	633 ± 5.2e+02
1 e + 3 Jets	0.3	1139	1.4e+03 ± 1.5e+03
2μ + 3 Jets	0.31	10	12.7 ± 2.0
1 e + 1μ + 1 Jet	0.32	52	65 ± 67
2μ + 1γ + 2 Jets	0.32	1	0.39 ± 0.10
1γ + 1 Jet	0.32	7994	6.8e+03 ± 2.6e+03

Continued on next page...

Event class	p-value	Data	SM $\pm \sigma_{sys}$
$2\mu + 1\gamma$	0.32	15	18.5 ± 4.1
2 e + 1μ + $\not\!\!E_T$	0.33	1	0.41 ± 0.10
1γ + 3 Jets + $\not\!\!E_T$	0.34	42	35 ± 15
2μ + 2 Jets	0.34	122	114 ± 16
1μ	0.35	71362	7.8e+04 ± 1.6e+04
2 e + 1γ	0.35	5	6.9 ± 1.7
2μ + 3 Jets + $\not\!\!E_T$	0.37	7	5.81 ± 0.95
1 e + 1μ	0.37	101	118 ± 89
2μ + 4 Jets + $\not\!\!E_T$	0.37	2	1.30 ± 0.24
1μ + 1γ + 1 Jet + $\not\!\!E_T$	0.37	10	12.3 ± 3.1
2 e + 4 Jets	0.37	0	1.01 ± 0.24
1μ + 1 Jet + $\not\!\!E_T$	0.38	6476	6.23e+03 ± 7.9e+02
1μ + 3 Jets + $\not\!\!E_T$	0.39	344	376 ± 1.1e+02
2γ + 2 Jets	0.39	3	2.1 ± 1.3
1μ + 4 Jets + $\not\!\!E_T$	0.39	77	84 ± 22
1μ + 1γ + 2 Jets + $\not\!\!E_T$	0.4	2	3.4 ± 1.7
1 e + 5 Jets	0.4	17	19 ± 18
3 e	0.4	1	2.0 ± 1.9
2 e + $\not\!\!E_T$	0.41	44	39 ± 18
1 e + 1γ + 1 Jet	0.41	79	80 ± 77
2μ + 1 Jet	0.42	889	867 ± 1.1e+02
2μ	0.42	11595	1.14e+04 ± 1.2e+03
1μ + 3 Jets	0.43	514	465 ± 2.4e+02
1 e + 2μ + 1 Jet + $\not\!\!E_T$	0.43	1	0.54 ± 0.44
1 e + 2μ	0.44	4	4.6 ± 4.4
1 e + 2 Jets + $\not\!\!E_T$	0.44	1676	1.76e+03 ± 1.0e+03
2μ + 4 Jets	0.45	2	1.53 ± 0.24
2 e + 1 Jet	0.45	523	511 ± 96
2 e + 2 Jets	0.45	70	73 ± 15
1 e + 3 Jets + $\not\!\!E_T$	0.45	368	382 ± 2.2e+02
1μ + 1 Jet	0.46	13380	1.40e+04 ± 6.4e+03
1 e + 5 Jets + $\not\!\!E_T$	0.46	15	14.2 ± 5.1
1 e + 1γ + 3 Jets + $\not\!\!E_T$	0.46	1	0.65 ± 0.29
1 e + 1 Jet + $\not\!\!E_T$	0.46	7409	7.1e+03 ± 3.2e+03
1γ + 4 Jets	0.47	24	26 ± 12
1 e + 1μ + 2 Jets + $\not\!\!E_T$	0.47	23	22.3 ± 5.1
1 e + 1μ + 3 Jets + $\not\!\!E_T$	0.48	5	5.9 ± 1.3
1 e + 7 Jets	0.48	1	0.58 ± 0.58
1μ + 6 Jets + $\not\!\!E_T$	0.48	3	2.65 ± 0.59
1μ + 2 Jets	0.48	5310	5.1e+03 ± 2.9e+03
2 e	0.49	9239	9.2e+03 ± 1.3e+03
2 e + 4 Jets + $\not\!\!E_T$	0.51	1	0.72 ± 0.15
1 e + 1γ + 3 Jets	0.51	1	0.70 ± 0.57
1 e + 1γ + 2 Jets + $\not\!\!E_T$	0.51	3	2.7 ± 1.9
1 e + 1μ + 1 Jet + $\not\!\!E_T$	0.51	40	40 ± 16
2 e + 3 Jets	0.52	8	8.6 ± 1.6
1 e + 1μ + 2 Jets	0.53	9	8.9 ± 5.9

Continued on next page...

Event class	p-value	Data	SM $\pm \sigma_{sys}$
1μ + 5 Jets + $\not\!\!E_T$	0.55	15	15.2 ± 3.2
1 e + 1γ + 1 Jet + $\not\!\!E_T$	0.56	8	8.2 ± 2.4
1γ + 5 Jets	0.58	3	3.1 ± 1.9
1μ + 1γ + 2 Jets	0.59	1	1.43 ± 0.42
2μ + 1γ + 1 Jet	0.6	3	3.24 ± 0.84
1 e + 1μ + 4 Jets + $\not\!\!E_T$	0.6	1	1.38 ± 0.37
1 e + 2μ + 1 Jet	0.62	1	1.1 ± 1.1
1 e + 1μ + 4 Jets	0.62	1	0.9 ± 1.0
2γ + 2 Jets + $\not\!\!E_T$	0.67	1	1.02 ± 0.86
1μ + 1γ + 3 Jets + $\not\!\!E_T$	0.69	1	1.05 ± 0.67
1 e + 2μ + $\not\!\!E_T$	0.7	1	1.01 ± 0.66

C.1.3. Table of inclusive classes

Event class	p-value	Data	SM $\pm \sigma_{sys}$
2μ + 1 Jet + $\not\!\!E_T$ +X	0.0053	106	71.7 ± 9.2
2μ + $\not\!\!E_T$ +X	0.01	160	117 ± 14
2μ + 2 Jets + $\not\!\!E_T$ +X	0.011	48	30.3 ± 4.3
1γ + 1 Jet + $\not\!\!E_T$ +X	0.032	1027	595 ± 2.3e+02
3μ +X	0.035	4	1.18 ± 0.20
1γ + 5 Jets + $\not\!\!E_T$ +X	0.037	4	1.04 ± 0.52
1γ + $\not\!\!E_T$ +X	0.046	1240	786 ± 2.7e+02
1μ + 2γ + $\not\!\!E_T$ +X	0.047	1	0.045 ± 0.028
1μ + 1γ + $\not\!\!E_T$ +X	0.057	43	65 ± 12
1γ + 2 Jets + $\not\!\!E_T$ +X	0.057	283	177 ± 65
4μ +X	0.06	1	0.062 ± 0.012
2 e + 1 Jet + $\not\!\!E_T$ +X	0.071	66	46 ± 11
2γ + $\not\!\!E_T$ +X	0.091	5	1.9 ± 1.1
1μ + 8 Jets + $\not\!\!E_T$ +X	0.091	1	0.096 ± 0.033
2γ + 3 Jets +X	0.1	1	0.108 ± 0.051
3 e + 1 Jet + $\not\!\!E_T$ +X	0.11	1	0.109 ± 0.068
1γ + 6 Jets + $\not\!\!E_T$ +X	0.11	1	0.115 ± 0.053
1γ + 4 Jets + $\not\!\!E_T$ +X	0.11	15	8.2 ± 4.0
2γ +X	0.12	39	26.7 ± 8.4
1μ + 8 Jets +X	0.12	1	0.128 ± 0.041
1μ + 2γ +X	0.13	1	0.136 ± 0.072
1 e + 6 Jets +X	0.13	1	5.0 ± 2.8
2 e + 1γ + 1 Jet +X	0.14	0	2.08 ± 0.52
2γ + 1 Jet +X	0.15	19	12.4 ± 4.7
1μ + 1γ +X	0.16	159	197 ± 34
1γ + 2 Jets +X	0.16	1943	1.43e+03 ± 5.2e+02
2 e + 1γ +X	0.17	5	9.1 ± 2.2
2μ + 2 Jets +X	0.18	183	160 ± 21
2 e + $\not\!\!E_T$ +X	0.21	111	86 ± 29
1γ + 3 Jets +X	0.21	272	205 ± 82
2 e + 2 Jets + $\not\!\!E_T$ +X	0.22	23	18.3 ± 3.7
2μ + 4 Jets + $\not\!\!E_T$ +X	0.23	3	1.63 ± 0.30

Continued on next page...

Event class	p-value	Data	SM $\pm \sigma_{sys}$
1 e + 1γ + 2 Jets +X	0.23	10	18 ± 16
3μ + 1 Jet + $\not\!\!E_T$ +X	0.23	1	0.27 ± 0.09
1μ + $\not\!\!E_T$ +X	0.24	109456	1.159e+05 ± 9.1e+03
2μ + 3 Jets + $\not\!\!E_T$ +X	0.24	10	7.5 ± 1.2
1γ + 3 Jets + $\not\!\!E_T$ +X	0.24	59	45 ± 18
1μ + 1γ + 1 Jet +X	0.25	47	39.3 ± 9.2
1 e + 1 Jet +X	0.26	154390	2.3e+05 ± 2.4e+05
1γ + 5 Jets +X	0.26	7	4.6 ± 2.4
1 e + 2 Jets +X	0.26	13653	2.0e+04 ± 2.0e+04
2μ + 4 Jets +X	0.26	5	3.40 ± 0.55
1γ + 1 Jet +X	0.26	10803	8.7e+03 ± 3.3e+03
1 e + 1μ + 1γ +X	0.26	1	0.31 ± 0.13
1 e +X	0.27	646871	9.3e+05 ± 8.5e+05
1μ + 1γ + 1 Jet + $\not\!\!E_T$ +X	0.27	13	17.5 ± 4.5
1 e + 4 Jets + $\not\!\!E_T$ +X	0.27	110	88 ± 34
2μ + 5 Jets + $\not\!\!E_T$ +X	0.27	1	0.322 ± 0.077
1γ +X	0.28	12943	1.07e+04 ± 3.8e+03
1 e + 1γ + $\not\!\!E_T$ +X	0.29	40	48 ± 10
2γ + 1 Jet + $\not\!\!E_T$ +X	0.29	3	1.7 ± 1.0
2 e + 3 Jets + $\not\!\!E_T$ +X	0.29	6	4.41 ± 0.90
2γ + 2 Jets +X	0.3	5	3.3 ± 1.9
3 e + $\not\!\!E_T$ +X	0.3	1	0.36 ± 0.12
3μ + 1 Jet +X	0.31	1	0.37 ± 0.11
1 e + 1μ + 5 Jets + $\not\!\!E_T$ +X	0.31	1	0.38 ± 0.10
1μ + 5 Jets +X	0.31	32	27.7 ± 6.4
1 e + 1γ +X	0.32	605	784 ± 6.1e+02
1μ + 2 Jets + $\not\!\!E_T$ +X	0.32	2336	2.10e+03 ± 5.1e+02
2μ + 1 Jet +X	0.33	1134	1.07e+03 ± 1.3e+02
2μ + 1γ +X	0.33	19	22.8 ± 5.1
1 e + $\not\!\!E_T$ +X	0.34	99098	1.04e+05 ± 1.3e+04
1μ +X	0.34	213013	2.26e+05 ± 3.1e+04
1 e + 3 Jets +X	0.34	1789	2.1e+03 ± 1.9e+03
1μ + 1 Jet + $\not\!\!E_T$ +X	0.35	8920	8.4e+03 ± 1.3e+03
1μ + 1γ + 2 Jets + $\not\!\!E_T$ +X	0.36	3	4.8 ± 2.1
1 e + 1μ + $\not\!\!E_T$ +X	0.36	105	125 ± 58
1 e + 1μ +X	0.37	278	326 ± 2.2e+02
1 e + 4 Jets +X	0.37	258	294 ± 2.4e+02
1γ + 6 Jets +X	0.38	1	0.45 ± 0.34
1 e + 1γ + 1 Jet +X	0.38	97	108 ± 94
1μ + 5 Jets + $\not\!\!E_T$ +X	0.39	21	19.1 ± 4.0
1μ + 3 Jets + $\not\!\!E_T$ +X	0.39	458	495 ± 1.3e+02
1μ + 4 Jets +X	0.4	186	172 ± 51
1 e + 1μ + 3 Jets +X	0.41	12	10.6 ± 3.8
1 e + 5 Jets +X	0.41	34	38 ± 25
1 e + 1μ + 5 Jets +X	0.41	1	0.54 ± 0.26
2μ +X	0.41	12805	1.25e+04 ± 1.3e+03
2 e + 4 Jets +X	0.41	1	2.01 ± 0.42

Continued on next page...

Event class	p-value	Data	SM $\pm \sigma_{sys}$
1γ + 4 Jets +X	0.42	42	38 ± 18
2μ + 5 Jets +X	0.42	1	0.54 ± 0.11
1 e + 1μ + 1 Jet +X	0.42	138	150 ± 97
2 e + 1 Jet +X	0.42	667	642 ± 1.2e+02
1 e + 2μ +X	0.42	7	8.0 ± 7.1
1μ + 6 Jets + $\not\!\!E_T$ +X	0.43	4	3.36 ± 0.75
1μ + 4 Jets + $\not\!\!E_T$ +X	0.44	101	106 ± 26
3 e +X	0.44	2	2.8 ± 2.4
1μ + 2 Jets +X	0.45	8393	7.8e+03 ± 3.7e+03
1μ + 7 Jets + $\not\!\!E_T$ +X	0.45	1	0.61 ± 0.17
2μ + 1γ + 2 Jets +X	0.45	1	0.60 ± 0.13
1 e + 5 Jets + $\not\!\!E_T$ +X	0.45	16	17.7 ± 6.3
1μ + 1γ + 3 Jets +X	0.46	2	1.59 ± 0.71
3 e + 1 Jet +X	0.46	1	0.58 ± 0.48
1 e + 2 Jets + $\not\!\!E_T$ +X	0.46	2208	2.3e+03 ± 1.3e+03
1 e + 1μ + 2 Jets +X	0.46	44	43 ± 15
1 e + 7 Jets +X	0.46	1	1.7 ± 1.4
1μ + 3 Jets +X	0.47	1072	1.04e+03 ± 3.9e+02
1 e + 1γ + 3 Jets +X	0.48	2	1.66 ± 0.83
1μ + 1γ + 2 Jets +X	0.48	6	7.0 ± 2.5
2 e +X	0.48	9957	9.9e+03 ± 1.4e+03
1 e + 1 Jet + $\not\!\!E_T$ +X	0.48	9709	9.4e+03 ± 4.5e+03
1 e + 1γ + 2 Jets + $\not\!\!E_T$ +X	0.49	4	3.6 ± 2.2
2 e + 1μ + $\not\!\!E_T$ +X	0.49	1	0.71 ± 0.28
1μ + 1 Jet +X	0.49	29330	2.9e+04 ± 1.1e+04
1 e + 1μ + 3 Jets + $\not\!\!E_T$ +X	0.5	7	7.8 ± 1.8
1 e + 3 Jets + $\not\!\!E_T$ +X	0.5	489	480 ± 2.6e+02
1 e + 1μ + 1 Jet + $\not\!\!E_T$ +X	0.51	71	72 ± 23
2 e + 2 Jets +X	0.51	101	101 ± 20
1μ + 7 Jets +X	0.51	1	0.74 ± 0.20
3μ + $\not\!\!E_T$ +X	0.51	1	0.73 ± 0.14
1 e + 1μ + 4 Jets +X	0.51	3	2.8 ± 1.5
1 e + 1μ + 4 Jets + $\not\!\!E_T$ +X	0.51	2	1.77 ± 0.46
1 e + 1μ + 2 Jets + $\not\!\!E_T$ +X	0.52	30	30.5 ± 7.1
1 e + 2μ + 1 Jet +X	0.54	2	2.2 ± 2.0
2μ + 3 Jets +X	0.55	22	22.1 ± 3.3
1 e + 1γ + 3 Jets + $\not\!\!E_T$ +X	0.55	1	0.84 ± 0.32
2 e + 3 Jets +X	0.55	14	14.2 ± 2.6
1μ + 6 Jets +X	0.56	4	4.4 ± 1.1
1 e + 1γ + 1 Jet + $\not\!\!E_T$ +X	0.56	12	12.0 ± 4.0
1 e + 2μ + $\not\!\!E_T$ +X	0.57	2	2.0 ± 1.4
2 e + 4 Jets + $\not\!\!E_T$ +X	0.58	1	0.89 ± 0.19
1 e + 2μ + 1 Jet + $\not\!\!E_T$ +X	0.6	1	0.93 ± 0.78
2μ + 1γ + 1 Jet +X	0.6	4	4.15 ± 0.98
1μ + 1γ + 3 Jets + $\not\!\!E_T$ +X	0.63	1	1.28 ± 0.68
2γ + 2 Jets + $\not\!\!E_T$ +X	0.66	1	1.04 ± 0.86
2 e + 1μ +X	0.71	1	1.08 ± 0.36

C.2. Distribution scans

C.2.1. Sum of transverse momenta

Exclusive classes

Event class	p-value	$\tilde{p}$	Region (GeV)	Data	SM $\pm \sigma_{sys}$
1 e + 1μ + 3 Jets + $\not{E}_T$	0.0001	0.0036	780 - 970	4	0.209 ± 0.066
2γ + 1 Jet	7.8e-05	0.0042	190 - 220	8	0.89 ± 0.49
1μ + 2γ + $\not{E}_T$	0.0006	0.0075	270 - 300	1	0 ± 0.00075
4μ	0.0017	0.0083	110 - 140	1	0.00171 ± 0.00054
1γ + 3 Jets	0.00044	0.015	220 - 280	7	0.59 ± 0.67
1γ + 5 Jets + $\not{E}_T$	0.0025	0.036	600 - 760	2	0.051 ± 0.046
1μ + 1γ + 1 Jet	0.001	0.036	110 - 150	20	6.8 ± 2.1
3μ	0.0082	0.045	50 - 80	1	0.0039 ± 0.0083
2γ + 3 Jets	0.009	0.05	660 - 750	1	0.0060 ± 0.0079
1μ + 1γ + 3 Jets	0.0087	0.059	220 - 280	1	0.0057 ± 0.0077
2 e + 1μ + $\not{E}_T$	0.0066	0.06	290 - 320	1	0.0066 ± 0.0024
1 e + 1μ + 1γ	0.022	0.062	110 - 140	1	0.018 ± 0.017
3 e + 1 Jet + $\not{E}_T$	0.0085	0.064	350 - 380	1	0.0045 ± 0.0083
1 e + 1μ + 3 Jets	0.0094	0.082	260 - 320	3	0.24 ± 0.28
1μ + 8 Jets + $\not{E}_T$	0.018	0.085	1220 - 1440	1	0.016 ± 0.011
1 e + 1μ + 1 Jet + $\not{E}_T$	0.0027	0.095	610 - 670	3	0.18 ± 0.15
1γ + 6 Jets + $\not{E}_T$	0.021	0.096	1230 - 1420	1	0.015 ± 0.017
2γ + $\not{E}_T$	0.014	0.1	160 - 190	1	0.0140 ± 0.0070
1γ	0.0067	0.12	230 - 260	9	1.5 ± 1.7
1 e + 2μ + 1 Jet + $\not{E}_T$	0.024	0.15	380 - 410	1	0.017 ± 0.021
2 e + 2 Jets + $\not{E}_T$	0.0059	0.16	260 - 340	11	4.05 ± 0.79
1 e + 1μ + 5 Jets + $\not{E}_T$	0.042	0.17	690 - 810	1	0.042 ± 0.019
1μ + 1γ + $\not{E}_T$	0.0076	0.17	80 - 130	16	33.7 ± 5.1
1γ + 2 Jets + $\not{E}_T$	0.0051	0.17	440 - 500	31	12.9 ± 4.9
3μ + 1 Jet + $\not{E}_T$	0.021	0.18	200 - 230	1	0.015 ± 0.019
1γ + 1 Jet + $\not{E}_T$	0.009	0.18	620 - 820	21	7.7 ± 3.8
1γ + 4 Jets + $\not{E}_T$	0.01	0.18	960 - 1100	5	0.74 ± 0.71
2μ + 2 Jets + $\not{E}_T$	0.0046	0.18	260 - 520	31	16.8 ± 2.4
2μ + 1 Jet + $\not{E}_T$	0.0037	0.19	190 - 860	55	33.7 ± 4.2
2γ	0.0076	0.2	110 - 140	3	0.33 ± 0.17
2μ + 5 Jets + $\not{E}_T$	0.04	0.2	510 - 620	1	0.040 ± 0.02
2μ + $\not{E}_T$	0.0056	0.2	190 - 450	11	4.19 ± 0.58
3 e	0.033	0.21	60 - 90	1	0.018 ± 0.033
2 e + 1 Jet + $\not{E}_T$	0.0053	0.23	240 - 270	11	3.91 ± 0.86
2μ + 2 Jets	0.0063	0.24	480 - 690	0	5.31 ± 0.71
2μ + 1γ + 2 Jets	0.051	0.24	230 - 270	1	0.051 ± 0.026
2μ + 4 Jets	0.038	0.25	340 - 430	2	0.301 ± 0.058
1 e + 2μ + $\not{E}_T$	0.05	0.26	230 - 260	1	0.042 ± 0.038
1 e + 4 Jets + $\not{E}_T$	0.027	0.3	1200 - 1450	3	0.56 ± 0.26
1 e + 3 Jets	0.042	0.31	910 - 1030	6	1.6 ± 1.3
1 e + 7 Jets	0.091	0.31	450 - 580	1	0.01 ± 0.12
2 e + 3 Jets + $\not{E}_T$	0.029	0.31	540 - 630	3	0.64 ± 0.15

Continued on next page...

Event class	p-value	$\tilde{p}$	Region (GeV)	Data	SM $\pm \sigma_{sys}$
1μ + 5 Jets	0.028	0.32	750 - 1060	3	0.53 ± 0.32
2 e + $\not{E}_T$	0.023	0.32	560 - 590	1	0.009 ± 0.026
1μ + 2 Jets + $\not{E}_T$	0.0083	0.33	970 - 2140	0	5.15 ± 0.85
1μ + 6 Jets + $\not{E}_T$	0.056	0.35	490 - 690	3	0.84 ± 0.17
1μ + 1γ + 3 Jets + $\not{E}_T$	0.041	0.35	600 - 690	1	0.038 ± 0.026
1 e + 1μ + $\not{E}_T$	0.04	0.38	450 - 480	1	0.021 ± 0.040
2 e + 2 Jets	0.013	0.4	1330 - 1450	1	0.008 ± 0.012
1 e + 2μ + 1 Jet	0.12	0.46	170 - 200	1	0.09 ± 0.10
2γ + 1 Jet + $\not{E}_T$	0.064	0.47	310 - 340	1	0.024 ± 0.072
2μ + 4 Jets + $\not{E}_T$	0.13	0.48	550 - 830	2	0.63 ± 0.12
2 e + 4 Jets + $\not{E}_T$	0.13	0.52	460 - 550	1	0.139 ± 0.061
1γ + 5 Jets	0.084	0.54	1240 - 1420	1	0.038 ± 0.094
2μ + 3 Jets + $\not{E}_T$	0.053	0.54	700 - 790	2	0.361 ± 0.075
1μ + 3 Jets + $\not{E}_T$	0.017	0.54	1380 - 1580	2	0.16 ± 0.10
1 e + 5 Jets	0.22	0.54	1060 - 1240	1	0.11 ± 0.27
1 e + 5 Jets + $\not{E}_T$	0.053	0.57	390 - 680	13	6.8 ± 2.0
1 e + 1γ + 3 Jets + $\not{E}_T$	0.13	0.57	380 - 440	1	0.124 ± 0.086
1 e + 1μ + 4 Jets	0.19	0.6	520 - 610	1	0.03 ± 0.26
1μ + 4 Jets + $\not{E}_T$	0.037	0.63	920 - 1160	6	2.27 ± 0.54
1 e + 1 Jet + $\not{E}_T$	0.061	0.64	780 - 840	4	1.15 ± 0.72
2 e + 3 Jets	0.049	0.64	360 - 480	0	3.10 ± 0.40
1 e + 1μ + 2 Jets	0.18	0.64	520 - 580	1	0.06 ± 0.23
1 e + 1γ + 2 Jets + $\not{E}_T$	0.12	0.64	280 - 340	2	0.44 ± 0.42
1 e + 1γ + 1 Jet	0.16	0.65	540 - 600	1	0.05 ± 0.21
1 e + 1μ + 4 Jets + $\not{E}_T$	0.22	0.65	580 - 670	1	0.258 ± 0.088
1μ + 1γ + 2 Jets + $\not{E}_T$	0.13	0.65	340 - 400	2	0.37 ± 0.51
1μ + 3 Jets	0.056	0.66	550 - 680	11	5.6 ± 1.6
1μ + $\not{E}_T$	0.023	0.66	190 - 250	25	39.0 ± 3.5
1γ + $\not{E}_T$	0.13	0.69	340 - 420	2	0.53 ± 0.36
1μ + 1 Jet + $\not{E}_T$	0.024	0.69	730 - 910	0	3.93 ± 0.64
2μ + 1γ + 1 Jet	0.098	0.7	110 - 140	1	0.085 ± 0.078
1γ + 1 Jet	0.27	0.7	980 - 1040	1	0.31 ± 0.19
1μ + 1 Jet	0.019	0.71	390 - 470	3	9.6 ± 1.1
2 e + 1γ	0.096	0.73	130 - 3620	0	2.58 ± 0.69
2μ + 3 Jets	0.049	0.73	320 - 430	1	4.96 ± 0.71
1 e + 6 Jets + $\not{E}_T$	0.17	0.75	450 - 2090	0	1.86 ± 0.46
2γ + 2 Jets	0.16	0.75	610 - 670	1	0.02 ± 0.23
1 e + $\not{E}_T$	0.022	0.77	250 - 280	12	4.9 ± 1.8
1μ + 2 Jets	0.11	0.78	1000 - 1130	1	0.05 ± 0.12
2 e + 1 Jet	0.031	0.79	440 - 2920	1	5.66 ± 0.93
1μ	0.18	0.81	190 - 250	2	0.75 ± 0.24
1μ + 5 Jets + $\not{E}_T$	0.074	0.82	390 - 520	0	2.87 ± 0.73
1 e + 2 Jets + $\not{E}_T$	0.3	0.83	1260 - 1380	1	0.36 ± 0.20
1 e + 1γ + 1 Jet + $\not{E}_T$	0.085	0.84	280 - 310	3	0.97 ± 0.33
1μ + 1γ + 1 Jet + $\not{E}_T$	0.075	0.84	340 - 370	2	0.39 ± 0.24
2 e	0.059	0.85	360 - 410	2	0.29 ± 0.25
2μ	0.072	0.86	220 - 2950	3	7.5 ± 1.1

Continued on next page...

Event class	p-value	$\tilde{p}$	Region (GeV)	Data	SM $\pm \sigma_{sys}$
2μ + 1 Jet	0.07	0.88	370 - 2610	7	13.3 ± 2.0
1 e + 1μ + 2 Jets + $\not{E}_T$	0.092	0.92	500 - 580	4	1.61 ± 0.46
2 e + 1γ + 1 Jet	0.25	0.93	140 - 2250	0	1.47 ± 0.42
1μ + 1γ + 2 Jets	0.28	0.97	260 - 320	1	0.34 ± 0.13
2 e + 4 Jets	0.38	1	340 - 1790	0	1.01 ± 0.27
1 e + 2 Jets	–	–	880 - 970	4	1.4 ± 1.4
1 e + 1 Jet	–	–	780 - 840	2	0.63 ± 0.68
1 e + 3 Jets + $\not{E}_T$	–	–	1180 - 1300	2	0.79 ± 0.47
1γ + 4 Jets	–	–	1190 - 1360	1	0.19 ± 0.27
1 e	–	–	620 - 650	0	0.000106 ± 8.3e-05
1 e + 1γ	–	–	630 - 680	0	0.0159 ± 0.0095
1 e + 1γ + $\not{E}_T$	–	–	250 - 420	0	0.77 ± 0.27
1 e + 1γ + 2 Jets	–	–	530 - 650	0	0.078 ± 0.034
1 e + 1γ + 3 Jets	–	–	300 - 400	0	0.096 ± 0.029
1 e + 1μ	–	–	260 - 560	0	0.101 ± 0.025
1 e + 1μ + 1 Jet	–	–	340 - 370	0	0.081 ± 0.037
1 e + 2μ	–	–	390 - 430	0	0.00119 ± 0.00057
1 e + 4 Jets	–	–	1600 - 3400	0	0.030 ± 0.022
1γ + 2 Jets	–	–	1030 - 1270	0	1.63 ± 0.63
1γ + 3 Jets + $\not{E}_T$	–	–	1740 - 1890	0	0.043 ± 0.017
1μ + 1γ	–	–	180 - 1240	0	0.79 ± 0.28
1μ + 4 Jets	–	–	1040 - 1310	0	0.078 ± 0.022
2γ + 2 Jets + $\not{E}_T$	–	–	1670 - 2920	0	0.00044 ± 0.00018
2μ + 1γ	–	–	170 - 330	0	0.81 ± 0.27

Inclusive classes

Event class	p-value	$\tilde{p}$	Region (GeV)	Data	SM $\pm \sigma_{sys}$
2γ + 1 Jet +X	0.0001	0.0069	190 - 220	8	0.93 ± 0.50
1 e + 1μ + 1 Jet + $\not{E}_T$ +X	0.00014	0.01	610 - 730	6	0.62 ± 0.24
4μ +X	0.002	0.011	110 - 140	1	0.00202 ± 0.00061
1 e + 1μ + 3 Jets + $\not{E}_T$ +X	0.0009	0.023	780 - 970	4	0.38 ± 0.11
1μ + 8 Jets +X	0.0076	0.026	1270 - 1510	1	0.0053 ± 0.0064
2μ + $\not{E}_T$ +X	0.00039	0.027	190 - 470	55	29.4 ± 3.9
1μ + 2γ + $\not{E}_T$ +X	0.0037	0.029	260 - 290	1	0 ± 0.0047
2γ +X	0.00077	0.037	120 - 150	13	3.1 ± 1.4
1γ + 4 Jets + $\not{E}_T$ +X	0.0021	0.048	960 - 1100	7	1.02 ± 0.80
1γ + $\not{E}_T$ +X	0.0011	0.054	380 - 420	19	5.1 ± 2.7
2γ + 3 Jets +X	0.013	0.064	660 - 750	1	0.009 ± 0.011
2μ + 1 Jet + $\not{E}_T$ +X	0.00093	0.072	190 - 1280	103	64 ± 8.2
1γ + 3 Jets +X	0.0026	0.073	220 - 280	8	1.3 ± 1.0
1γ + 5 Jets + $\not{E}_T$ +X	0.0055	0.073	600 - 760	2	0.097 ± 0.049
3μ +X	0.0094	0.074	70 - 150	4	0.78 ± 0.15
2 e + 1 Jet + $\not{E}_T$ +X	0.0014	0.079	200 - 250	27	11.0 ± 2.9
3 e + 1 Jet + $\not{E}_T$ +X	0.012	0.08	360 - 390	1	0.0105 ± 0.0087
2γ + $\not{E}_T$ +X	0.0034	0.082	240 - 270	3	0.10 ± 0.22
1μ + 8 Jets + $\not{E}_T$ +X	0.018	0.084	1220 - 1440	1	0.016 ± 0.011

Continued on next page...

Event class	p-value	$\tilde{p}$	Region (GeV)	Data	SM $\pm \sigma_{sys}$
1 e + 1μ + 2 Jets + $\not\!\!E_T$ +X	0.003	0.1	720 - 840	4	0.48 ± 0.22
1γ + 6 Jets + $\not\!\!E_T$ +X	0.022	0.11	1230 - 1420	1	0.017 ± 0.017
1μ + 2γ +X	0.023	0.11	190 - 220	1	0.006 ± 0.027
3 e + $\not\!\!E_T$ +X	0.02	0.11	260 - 290	1	0.019 ± 0.010
1 e + 1μ + 3 Jets +X	0.0075	0.12	510 - 810	7	1.90 ± 0.61
1γ + 2 Jets + $\not\!\!E_T$ +X	0.0043	0.13	260 - 320	49	21.8 ± 8.0
1μ + 1γ + $\not\!\!E_T$ +X	0.005	0.14	100 - 130	15	34.4 ± 5.6
1γ + 1 Jet + $\not\!\!E_T$ +X	0.0043	0.15	560 - 660	42	18.3 ± 6.7
2 e + 2 Jets + $\not\!\!E_T$ +X	0.0049	0.17	260 - 320	10	3.35 ± 0.72
3μ + 1 Jet + $\not\!\!E_T$ +X	0.026	0.17	200 - 230	1	0.02 ± 0.021
2 e + 1μ + $\not\!\!E_T$ +X	0.026	0.18	310 - 340	1	0.025 ± 0.014
1μ + 7 Jets +X	0.046	0.18	1160 - 1370	1	0.043 ± 0.030
2μ + 2 Jets + $\not\!\!E_T$ +X	0.0051	0.18	300 - 670	39	22.4 ± 3.2
1μ + 7 Jets + $\not\!\!E_T$ +X	0.052	0.2	1210 - 1420	1	0.054 ± 0.021
3 e +X	0.034	0.22	60 - 90	1	0.019 ± 0.033
1 e + 1μ + 1γ +X	0.06	0.22	90 - 120	1	0.061 ± 0.027
1 e + 2μ + $\not\!\!E_T$ +X	0.031	0.23	230 - 290	2	0.23 ± 0.14
3 e + 1 Jet +X	0.023	0.23	330 - 360	1	0.018 ± 0.018
1 e + 1μ + $\not\!\!E_T$ +X	0.0096	0.25	320 - 350	5	1.16 ± 0.32
1μ + 4 Jets + $\not\!\!E_T$ +X	0.008	0.25	1060 - 1210	5	1.12 ± 0.27
1 e + 1μ + 5 Jets + $\not\!\!E_T$ +X	0.059	0.25	690 - 810	1	0.059 ± 0.032
2μ + 5 Jets + $\not\!\!E_T$ +X	0.054	0.25	510 - 620	1	0.056 ± 0.024
2 e + 1μ +X	0.047	0.26	200 - 230	1	0.049 ± 0.015
1γ + 4 Jets +X	0.021	0.26	760 - 1240	15	5.7 ± 2.9
2μ + 1γ + 2 Jets +X	0.061	0.26	230 - 270	1	0.063 ± 0.029
1μ + 1 Jet +X	0.0047	0.26	450 - 510	12	27.5 ± 3.8
2μ + 4 Jets + $\not\!\!E_T$ +X	0.032	0.28	490 - 580	2	0.27 ± 0.06
1 e + 1μ + 1 Jet +X	0.016	0.28	400 - 480	7	2.02 ± 0.93
1γ + 3 Jets + $\not\!\!E_T$ +X	0.014	0.29	820 - 1060	16	6.0 ± 2.9
3μ + 1 Jet +X	0.052	0.29	160 - 190	1	0.052 ± 0.028
1 e + 2 Jets + $\not\!\!E_T$ +X	0.016	0.3	890 - 980	0	5.6 ± 1.7
2μ +X	0.0093	0.32	240 - 270	1	7.03 ± 0.85
2γ + 1 Jet + $\not\!\!E_T$ +X	0.023	0.34	410 - 450	2	0.04 ± 0.23
1μ + 4 Jets +X	0.017	0.35	940 - 1140	6	1.72 ± 0.65
2γ + 2 Jets +X	0.031	0.35	590 - 670	2	0.04 ± 0.27
1 e + 2μ + 1 Jet + $\not\!\!E_T$ +X	0.05	0.35	390 - 420	1	0.039 ± 0.041
1μ + 1γ + 1 Jet +X	0.012	0.36	110 - 150	24	11.9 ± 3.1
2μ + 3 Jets + $\not\!\!E_T$ +X	0.022	0.37	700 - 790	3	0.58 ± 0.11
1 e + 4 Jets +X	0.071	0.37	1140 - 1300	3	0.64 ± 0.62
2μ + 4 Jets +X	0.043	0.38	340 - 520	4	1.27 ± 0.20
2 e + 1 Jet +X	0.0069	0.38	440 - 1060	4	13.4 ± 1.9
2μ + 5 Jets +X	0.11	0.39	560 - 680	1	0.113 ± 0.033
1 e + 1μ + 2 Jets +X	0.019	0.4	440 - 710	11	4.4 ± 1.4
1 e + 1μ + 5 Jets +X	0.1	0.41	630 - 750	1	0.107 ± 0.052
1 e + 1μ + 4 Jets +X	0.07	0.44	580 - 690	2	0.33 ± 0.27
1 e + 7 Jets +X	0.095	0.45	450 - 580	1	0.01 ± 0.12
1 e + 1μ + 4 Jets + $\not\!\!E_T$ +X	0.074	0.45	580 - 700	2	0.44 ± 0.12

Continued on next page...

Event class	p-value	$\tilde{p}$	Region (GeV)	Data	SM $\pm \sigma_{sys}$
1 e + 1γ + 2 Jets + $\not\!\!E_T$ +X	0.047	0.46	280 - 340	3	0.63 ± 0.42
2 e + 1γ +X	0.035	0.48	130 - 3620	0	3.83 ± 0.97
2 e + 4 Jets + $\not\!\!E_T$ +X	0.14	0.49	460 - 550	1	0.15 ± 0.06
2 e + 2 Jets +X	0.013	0.5	270 - 330	38	23.2 ± 3.5
1μ + 1γ + 3 Jets + $\not\!\!E_T$ +X	0.069	0.51	570 - 660	1	0.068 ± 0.040
2 e + 3 Jets + $\not\!\!E_T$ +X	0.052	0.51	540 - 630	3	0.81 ± 0.18
3μ + $\not\!\!E_T$ +X	0.23	0.51	160 - 190	1	0.262 ± 0.072
1γ + 6 Jets +X	0.094	0.52	1140 - 1340	1	0.05 ± 0.10
1 e + 2μ +X	0.14	0.53	230 - 260	1	0.14 ± 0.11
1μ + 6 Jets +X	0.068	0.53	600 - 1150	0	2.90 ± 0.65
2 e + $\not\!\!E_T$ +X	0.024	0.54	300 - 560	0	4.09 ± 0.86
1μ + 5 Jets +X	0.035	0.54	1000 - 1180	3	0.65 ± 0.23
1γ + 5 Jets +X	0.085	0.55	1000 - 1300	3	0.81 ± 0.58
1 e + 2μ + 1 Jet +X	0.11	0.56	340 - 370	1	0.091 ± 0.086
1 e + 1γ + 3 Jets + $\not\!\!E_T$ +X	0.13	0.57	380 - 440	1	0.136 ± 0.086
1μ + 6 Jets + $\not\!\!E_T$ +X	0.085	0.57	490 - 690	3	1.0 ± 0.21
1 e + 4 Jets + $\not\!\!E_T$ +X	0.088	0.58	1200 - 1450	3	0.98 ± 0.35
1μ + 1γ + 3 Jets +X	0.11	0.62	510 - 600	1	0.123 ± 0.039
2 e +X	0.01	0.67	290 - 360	0	4.78 ± 0.62
1 e + 3 Jets + $\not\!\!E_T$ +X	0.098	0.67	1140 - 1260	4	1.59 ± 0.61
2μ + 1 Jet +X	0.029	0.68	430 - 530	4	10.5 ± 1.3
1 e + 1γ + 1 Jet + $\not\!\!E_T$ +X	0.06	0.71	370 - 400	2	0.33 ± 0.22
1μ + 1γ + 1 Jet + $\not\!\!E_T$ +X	0.043	0.72	320 - 360	4	1.02 ± 0.62
1 e + 5 Jets + $\not\!\!E_T$ +X	0.081	0.73	390 - 520	5	2.07 ± 0.74
1 e + 1 Jet + $\not\!\!E_T$ +X	0.071	0.74	1000 - 1060	2	0.38 ± 0.23
1μ + 5 Jets + $\not\!\!E_T$ +X	0.057	0.75	1150 - 1330	2	0.37 ± 0.14
1μ + 1γ +X	0.1	0.75	200 - 230	3	1.07 ± 0.35
1μ + 3 Jets + $\not\!\!E_T$ +X	0.043	0.75	1380 - 1580	2	0.29 ± 0.16
2μ + 1γ + 1 Jet +X	0.097	0.76	110 - 140	1	0.085 ± 0.077
1 e + 1γ + 3 Jets +X	0.21	0.77	320 - 380	1	0.22 ± 0.13
1 e + $\not\!\!E_T$ +X	0.068	0.78	430 - 470	7	3.2 ± 1.0
2μ + 2 Jets +X	0.034	0.78	170 - 200	19	11.1 ± 1.8
1μ + 1γ + 2 Jets +X	0.13	0.78	280 - 340	3	1.05 ± 0.63
2 e + 3 Jets +X	0.065	0.82	360 - 420	0	2.84 ± 0.46
1γ +X	0.3	0.82	580 - 610	1	0.35 ± 0.19
2 e + 1γ + 1 Jet +X	0.14	0.82	140 - 2250	0	2.08 ± 0.52
1μ +X	0.12	0.84	370 - 480	4	1.84 ± 0.36
2μ + 3 Jets +X	0.076	0.86	260 - 320	7	3.54 ± 0.50
1 e + 1γ + 1 Jet +X	0.19	0.87	540 - 600	1	0.12 ± 0.22
1 e + 1μ +X	0.15	0.88	260 - 7000	0	2.06 ± 0.56
1μ + 1 Jet + $\not\!\!E_T$ +X	0.056	0.9	1030 - 1420	6	2.57 ± 0.54
1μ + 2 Jets +X	0.088	0.91	800 - 1080	5	9.9 ± 1.2
1μ + 3 Jets +X	0.16	0.93	960 - 1100	4	2.02 ± 0.62
2μ + 1γ +X	0.2	0.93	170 - 4410	0	1.74 ± 0.47
1μ + $\not\!\!E_T$ +X	0.1	0.97	490 - 550	4	1.70 ± 0.39
2 e + 4 Jets +X	0.3	0.98	520 - 2900	0	1.21 ± 0.21
1μ + 2 Jets + $\not\!\!E_T$ +X	0.2	1	1000 - 1240	2	4.44 ± 0.79

Continued on next page...

Event class	p-value	$\tilde{p}$	Region (GeV)	Data	SM $\pm \sigma_{sys}$
1 e + 1 Jet +X	–	–	840 - 920	5	2.1 ± 1.4
1 e + 3 Jets +X	–	–	1070 - 1210	5	2.0 ± 1.3
1 e +X	–	–	490 - 520	1	0.35 ± 0.33
1 e + 1γ +X	–	–	650 - 710	0	0.027 ± 0.015
1 e + 1γ + $\not{E}_T$ +X	–	–	230 - 270	0	0.99 ± 0.35
1 e + 1γ + 2 Jets +X	–	–	470 - 630	0	0.52 ± 0.19
1 e + 2 Jets +X	–	–	1270 - 1430	0	0.81 ± 0.38
1 e + 5 Jets +X	–	–	1120 - 1490	0	0.84 ± 0.41
1 e + 6 Jets +X	–	–	400 - 520	0	0.203 ± 0.058
1γ + 1 Jet +X	–	–	1020 - 1080	0	0.84 ± 0.36
1γ + 2 Jets +X	–	–	1150 - 1310	0	1.92 ± 0.75
1μ + 1γ + 2 Jets + $\not{E}_T$ +X	–	–	440 - 520	0	0.338 ± 0.082
2γ + 2 Jets + $\not{E}_T$ +X	–	–	1750 - 5080	0	0.00058 ± 0.00023

C.2.2. Combined mass

Exclusive classes

Event class	p-value	$\tilde{p}$	Region (GeV)	Data	SM $\pm \sigma_{sys}$
1 e + 1μ + 3 Jets + $\not{E}_T$	0.0001	0.0048	780 - 970	4	0.209 ± 0.064
1γ + 3 Jets	5.4e-05	0.0062	280 - 400	31	8.3 ± 3.5
1μ + 2γ + $\not{E}_T$	0.004	0.016	280 - 290	1	0.0029 ± 0.0033
1μ + 1γ + 1 Jet	0.00039	0.025	90 - 120	5	0.29 ± 0.33
3μ	0.0031	0.036	80 - 140	2	0.079 ± 0.016
1μ + 1γ + 3 Jets	0.002	0.037	280 - 300	1	0 ± 0.0025
1 e + 5 Jets	0.00051	0.038	540 - 580	4	0.11 ± 0.24
3 e + 1 Jet + $\not{E}_T$	0.0028	0.045	370 - 380	1	0.0016 ± 0.0026
1γ + 5 Jets + $\not{E}_T$	0.0021	0.045	600 - 760	2	0.051 ± 0.040
2 e + 1μ + $\not{E}_T$	0.0023	0.047	310 - 320	1	0.0022 ± 0.0013
4μ	0.0066	0.047	200 - 210	1	0.0067 ± 0.0015
1 e + 1μ + 1γ	0.0094	0.055	120 - 130	1	0.0069 ± 0.0077
2μ + 2 Jets	0.00049	0.061	170 - 220	20	6.9 ± 1.7
1μ + 8 Jets + $\not{E}_T$	0.013	0.08	1220 - 1360	1	0.0108 ± 0.0088
1γ + 6 Jets + $\not{E}_T$	0.019	0.084	1230 - 1290	1	0.015 ± 0.016
2γ + $\not{E}_T$	0.0062	0.11	180 - 190	1	0.0059 ± 0.0035
2γ + 3 Jets	0.008	0.11	840 - 880	1	0.0060 ± 0.0065
2 e	0.00011	0.12	240 - 280	17	3.9 ± 1.6
1 e + 1μ + 1 Jet + $\not{E}_T$	0.0022	0.12	610 - 670	3	0.18 ± 0.14
2μ + 5 Jets + $\not{E}_T$	0.015	0.15	580 - 620	1	0.013 ± 0.011
2γ + 1 Jet	0.0027	0.16	320 - 340	4	0.44 ± 0.25
1 e + 1μ + 5 Jets + $\not{E}_T$	0.025	0.16	730 - 770	1	0.021 ± 0.017
1μ + 1γ + $\not{E}_T$	0.0047	0.16	90 - 140	17	37.0 ± 5.6
1μ + 4 Jets	0.0035	0.17	520 - 600	18	5.3 ± 2.9
1 e + 2μ + 1 Jet + $\not{E}_T$	0.012	0.18	380 - 390	1	0.007 ± 0.011
2 e + 1 Jet + $\not{E}_T$	0.003	0.18	200 - 260	20	8.4 ± 1.9
1γ + $\not{E}_T$	0.0043	0.19	150 - 190	28	9.4 ± 5.2
2μ + 3 Jets + $\not{E}_T$	0.0075	0.19	700 - 730	2	0.123 ± 0.037

Continued on next page...

Event class	p-value	$\tilde{p}$	Region (GeV)	Data	SM $\pm \sigma_{sys}$
2 e + 2 Jets + $\not\!\!E_T$	0.0044	0.22	240 - 320	10	3.30 ± 0.71
2 e + 1 Jet	0.0019	0.23	320 - 330	17	6.9 ± 1.0
2μ + 2 Jets + $\not\!\!E_T$	0.0042	0.23	260 - 520	31	16.6 ± 2.4
1γ + 2 Jets + $\not\!\!E_T$	0.0043	0.24	380 - 400	18	5.9 ± 2.8
1 e + 2μ + $\not\!\!E_T$	0.017	0.25	230 - 240	1	0.007 ± 0.018
2μ + 4 Jets	0.016	0.25	370 - 400	1	0.0150 ± 0.0098
3μ + 1 Jet + $\not\!\!E_T$	0.071	0.26	220 - 230	1	0.061 ± 0.055
1 e + 1γ + 1 Jet	0.0041	0.28	280 - 360	20	4.8 ± 4.1
1γ + 4 Jets + $\not\!\!E_T$	0.0076	0.28	960 - 1100	5	0.74 ± 0.62
2μ + 1 Jet + $\not\!\!E_T$	0.0048	0.28	220 - 860	43	25.6 ± 3.2
2μ + 1γ + 2 Jets	0.027	0.3	250 - 270	1	0.021 ± 0.022
1 e + 4 Jets + $\not\!\!E_T$	0.01	0.31	1250 - 1300	2	0.10 ± 0.10
2 e + 3 Jets + $\not\!\!E_T$	0.015	0.31	540 - 600	3	0.49 ± 0.12
1 e + 1μ + 3 Jets	0.015	0.33	750 - 780	1	0.005 ± 0.016
1γ + 1 Jet + $\not\!\!E_T$	0.0082	0.34	620 - 820	21	7.6 ± 3.8
1μ + 1γ + 3 Jets + $\not\!\!E_T$	0.02	0.34	600 - 630	1	0.016 ± 0.015
2 e + $\not\!\!E_T$	0.015	0.34	560 - 570	1	0.007 ± 0.015
1 e + 1μ + $\not\!\!E_T$	0.017	0.36	450 - 460	1	0.007 ± 0.018
1μ + 5 Jets	0.019	0.36	1000 - 1120	3	0.48 ± 0.23
2μ + 1γ + 1 Jet	0.015	0.36	120 - 130	1	0.006 ± 0.017
2μ + $\not\!\!E_T$	0.0094	0.37	330 - 450	3	0.40 ± 0.12
2μ + 4 Jets + $\not\!\!E_T$	0.04	0.39	830 - 870	1	0.033 ± 0.030
1 e + 2μ	0.03	0.39	240 - 250	1	0.024 ± 0.023
1μ + 1γ + 2 Jets	0.026	0.4	500 - 520	1	0.012 ± 0.026
1μ + $\not\!\!E_T$	0.0083	0.44	280 - 300	7	2.1 ± 0.43
1μ + 2 Jets	0.032	0.46	1040 - 2070	0	4.4 ± 1.5
1 e + 1γ	0.023	0.47	220 - 230	5	0.7 ± 1.0
2 e + 1γ	0.024	0.48	240 - 250	1	0.019 ± 0.019
2γ	0.013	0.48	90 - 140	4	0.73 ± 0.37
1 e + 1μ	0.045	0.52	140 - 150	5	1.3 ± 1.1
1μ + 2 Jets + $\not\!\!E_T$	0.0098	0.53	910 - 2140	1	7.1 ± 1.0
1μ + 6 Jets + $\not\!\!E_T$	0.055	0.53	490 - 690	3	0.83 ± 0.16
2 e + 4 Jets + $\not\!\!E_T$	0.064	0.55	520 - 550	1	0.066 ± 0.028
2γ + 1 Jet + $\not\!\!E_T$	0.033	0.57	410 - 420	1	0.013 ± 0.036
1 e + 1γ + $\not\!\!E_T$	0.023	0.58	50 - 60	1	0.003 ± 0.028
1μ + 1γ + 1 Jet + $\not\!\!E_T$	0.02	0.58	200 - 220	5	1.41 ± 0.41
1 e + 1γ + 3 Jets + $\not\!\!E_T$	0.1	0.6	380 - 400	1	0.083 ± 0.088
1 e + 2μ + 1 Jet	0.093	0.61	340 - 350	1	0.067 ± 0.086
1 e + 1γ + 3 Jets	0.038	0.61	570 - 600	1	0.016 ± 0.040
1 e + 1μ + 1 Jet	0.036	0.62	340 - 380	5	0.7 ± 1.3
1 e + 7 Jets	0.11	0.63	1080 - 1150	1	0.01 ± 0.15
2μ	0.019	0.66	120 - 140	84	61.2 ± 6.8
3 e	0.11	0.66	90 - 100	1	0.08 ± 0.11
1 e + 1 Jet + $\not\!\!E_T$	0.05	0.66	1160 - 1180	1	0.008 ± 0.061
1 e + 5 Jets + $\not\!\!E_T$	0.053	0.69	390 - 680	13	6.8 ± 2.0
1 e + 3 Jets + $\not\!\!E_T$	0.06	0.7	1180 - 1220	2	0.34 ± 0.22
1μ + 4 Jets + $\not\!\!E_T$	0.024	0.71	1060 - 1160	3	0.56 ± 0.20

Continued on next page...

Event class	p-value	$\tilde{p}$	Region (GeV)	Data	SM $\pm \sigma_{sys}$
1 e + 1μ + 4 Jets + $\not\!\!E_T$	0.088	0.71	580 - 610	1	0.091 ± 0.045
2 e + 2 Jets	0.013	0.72	270 - 330	24	13.5 ± 1.9
1μ + 3 Jets + $\not\!\!E_T$	0.018	0.73	1380 - 1580	2	0.179 ± 0.095
1 e + 1μ + 4 Jets	0.079	0.75	690 - 730	1	0.01 ± 0.10
2μ + 1 Jet	0.018	0.76	220 - 230	51	34.6 ± 4.1
1μ + 1γ + 2 Jets + $\not\!\!E_T$	0.098	0.78	340 - 400	2	0.36 ± 0.38
1γ + 3 Jets + $\not\!\!E_T$	0.048	0.78	320 - 340	2	0.18 ± 0.28
1μ + 1 Jet + $\not\!\!E_T$	0.021	0.79	550 - 910	11	21.6 ± 2.8
2γ + 2 Jets	0.073	0.83	290 - 310	1	0.003 ± 0.095
1 e + 1μ + 2 Jets + $\not\!\!E_T$	0.047	0.83	520 - 540	2	0.33 ± 0.10
1γ + 4 Jets	0.063	0.84	560 - 600	3	0.18 ± 0.83
1 e + 1γ + 1 Jet + $\not\!\!E_T$	0.066	0.85	390 - 400	1	0.060 ± 0.047
2γ + 2 Jets + $\not\!\!E_T$	0.075	0.86	480 - 500	1	0.001 ± 0.099
1μ + 5 Jets + $\not\!\!E_T$	0.066	0.89	1210 - 1270	1	0.062 ± 0.045
1 e + 1γ + 2 Jets + $\not\!\!E_T$	0.087	0.89	440 - 460	1	0.046 ± 0.093
1γ + 5 Jets	0.083	0.9	1360 - 1420	1	0.034 ± 0.093
1 e + 2 Jets + $\not\!\!E_T$	0.15	0.91	1040 - 1100	2	0.57 ± 0.44
1μ + 1γ	0.077	0.92	100 - 140	4	9.2 ± 1.7
1γ + 1 Jet	0.17	0.93	1290 - 1320	1	0.08 ± 0.21
1 e + 6 Jets + $\not\!\!E_T$	0.17	0.93	450 - 2090	0	1.86 ± 0.47
2μ + 3 Jets	0.072	0.93	380 - 550	1	4.49 ± 0.70
1μ + 1 Jet	0.19	0.94	620 - 680	0	1.77 ± 0.51
1 e + 1μ + 2 Jets	0.1	0.94	710 - 740	1	0.03 ± 0.13
1 e + 1γ + 2 Jets	0.079	0.94	840 - 1110	3	0.07 ± 0.98
2 e + 3 Jets	0.076	0.94	480 - 510	2	0.447 ± 0.095
1 e + $\not\!\!E_T$	0.026	0.99	250 - 260	6	1.5 ± 1.1
2μ + 1γ	0.23	1	100 - 120	0	1.54 ± 0.39
2 e + 1γ + 1 Jet	0.25	1	150 - 2100	0	1.47 ± 0.41
2 e + 4 Jets	0.38	1	400 - 2980	0	1.01 ± 0.25
1γ + 2 Jets	–	–	610 - 640	48	23.4 ± 9.6
1 e + 1 Jet	–	–	1230 - 1260	3	0.2 ± 1.6
1 e + 2 Jets	–	–	2080 - 2440	0	0.47 ± 0.32
1 e + 3 Jets	–	–	1970 - 2030	0	0.19 ± 0.16
1 e + 4 Jets	–	–	310 - 340	0	0.180 ± 0.089
1μ + 3 Jets	–	–	1200 - 2010	0	3.5 ± 1.2

Inclusive classes

Event class	p-value	$\tilde{p}$	Region (GeV)	Data	SM $\pm \sigma_{sys}$
2γ +X	0.00012	0.013	100 - 140	17	3.9 ± 1.6
3μ +X	0.00068	0.015	80 - 140	4	0.367 ± 0.076
1γ + 3 Jets +X	0.0003	0.03	260 - 400	35	11.2 ± 4.6
1 e + 1μ + 1 Jet + $\not\!\!E_T$ +X	0.00038	0.03	610 - 710	5	0.47 ± 0.21
1 e + 1μ + 3 Jets + $\not\!\!E_T$ +X	0.00083	0.047	780 - 970	4	0.377 ± 0.098
3 e + 1 Jet + $\not\!\!E_T$ +X	0.0031	0.049	370 - 380	1	0.0025 ± 0.0023
1μ + 2γ + $\not\!\!E_T$ +X	0.0047	0.055	280 - 290	1	0.0032 ± 0.0041
2μ + $\not\!\!E_T$ +X	0.00057	0.055	130 - 450	92	53.1 ± 8.0

Continued on next page...

Event class	p-value	$\tilde{p}$	Region (GeV)	Data	SM $\pm \sigma_{sys}$
4μ +X	0.0083	0.056	200 - 210	1	0.0084 ± 0.0019
1μ + 1 Jet +X	0.00056	0.061	530 - 560	3	16.3 ± 2.6
2μ + 1 Jet + $\not\!\!E_T$ +X	0.00067	0.066	200 - 310	61	34.3 ± 4.5
1μ + 8 Jets + $\not\!\!E_T$ +X	0.013	0.075	1220 - 1360	1	0.0108 ± 0.0088
2μ + 2 Jets +X	0.00067	0.083	170 - 220	22	8.3 ± 1.8
1γ + 5 Jets + $\not\!\!E_T$ +X	0.0053	0.085	600 - 760	2	0.097 ± 0.043
1μ + 8 Jets +X	0.012	0.085	1970 - 2070	1	0.0107 ± 0.0083
1γ + 4 Jets + $\not\!\!E_T$ +X	0.0015	0.087	960 - 1100	7	1.02 ± 0.71
2 e + 1μ + $\not\!\!E_T$ +X	0.0053	0.087	310 - 320	1	0.0023 ± 0.0055
1γ + 6 Jets + $\not\!\!E_T$ +X	0.019	0.094	1230 - 1290	1	0.015 ± 0.016
1 e + 2μ + $\not\!\!E_T$ +X	0.0043	0.095	230 - 260	2	0.080 ± 0.049
3 e + $\not\!\!E_T$ +X	0.011	0.099	220 - 230	1	0.0113 ± 0.0033
3 e + 1 Jet +X	0.0051	0.12	640 - 660	1	0.0005 ± 0.0061
1μ + 2γ +X	0.011	0.13	190 - 200	1	0.003 ± 0.013
3μ + 1 Jet +X	0.0086	0.13	180 - 190	1	0.0024 ± 0.0097
2γ + 3 Jets +X	0.0082	0.13	840 - 880	1	0.0060 ± 0.0068
1 e + 2μ +X	0.0065	0.13	220 - 270	3	0.29 ± 0.18
1 e + 1μ + 1γ +X	0.012	0.14	120 - 130	1	0.0110 ± 0.0081
2 e +X	0.00021	0.15	240 - 260	15	3.4 ± 1.4
1μ + 1γ + 1 Jet +X	0.0019	0.15	90 - 100	4	0.26 ± 0.31
1μ + 1γ + $\not\!\!E_T$ +X	0.0028	0.15	90 - 140	19	44.8 ± 7.5
2 e + 1 Jet + $\not\!\!E_T$ +X	0.0018	0.15	200 - 260	29	13.2 ± 2.8
1μ + 7 Jets +X	0.017	0.16	1960 - 2050	1	0.016 ± 0.011
2μ + 2 Jets + $\not\!\!E_T$ +X	0.003	0.19	300 - 360	17	7.2 ± 1.1
2γ + $\not\!\!E_T$ +X	0.0059	0.19	210 - 220	2	0.01 ± 0.11
1μ + 7 Jets + $\not\!\!E_T$ +X	0.027	0.2	1210 - 1280	1	0.027 ± 0.014
2μ + 5 Jets +X	0.015	0.2	1330 - 1390	1	0.0144 ± 0.0086
2μ + 5 Jets + $\not\!\!E_T$ +X	0.021	0.21	580 - 620	1	0.018 ± 0.014
2μ + 4 Jets + $\not\!\!E_T$ +X	0.015	0.21	520 - 580	2	0.177 ± 0.043
1 e + 1μ + 4 Jets +X	0.0079	0.22	1010 - 1060	2	0.06 ± 0.10
2γ + 2 Jets +X	0.0045	0.22	670 - 850	3	0.13 ± 0.24
2γ + 1 Jet +X	0.0039	0.23	320 - 340	4	0.49 ± 0.26
1 e + 1μ + 5 Jets + $\not\!\!E_T$ +X	0.03	0.24	730 - 770	1	0.027 ± 0.020
1γ + $\not\!\!E_T$ +X	0.006	0.24	250 - 270	19	5.1 ± 3.9
2 e + 2 Jets + $\not\!\!E_T$ +X	0.0045	0.24	240 - 320	11	3.84 ± 0.81
2μ +X	0.005	0.27	410 - 430	3	0.31 ± 0.11
1γ + 1 Jet + $\not\!\!E_T$ +X	0.0043	0.27	280 - 290	51	21.9 ± 8.8
1μ + 5 Jets +X	0.0062	0.29	1300 - 1360	4	0.64 ± 0.22
1γ + 2 Jets + $\not\!\!E_T$ +X	0.0062	0.3	240 - 320	53	24.7 ± 9.0
1 e + 1μ + 2 Jets + $\not\!\!E_T$ +X	0.0078	0.32	700 - 840	4	0.65 ± 0.28
1γ + 5 Jets +X	0.011	0.32	1770 - 1920	2	0.06 ± 0.14
2 e + 1μ +X	0.025	0.33	250 - 260	1	0.025 ± 0.011
2γ + 1 Jet + $\not\!\!E_T$ +X	0.013	0.33	410 - 440	2	0.03 ± 0.17
1 e + 2μ + 1 Jet +X	0.018	0.33	340 - 370	2	0.14 ± 0.14
1 e + 2μ + 1 Jet + $\not\!\!E_T$ +X	0.024	0.35	380 - 390	1	0.016 ± 0.021
3μ + 1 Jet + $\not\!\!E_T$ +X	0.071	0.35	220 - 230	1	0.061 ± 0.055
2μ + 1γ + 2 Jets +X	0.029	0.35	250 - 270	1	0.024 ± 0.022

Continued on next page...

Event class	p-value	$\tilde{p}$	Region (GeV)	Data	SM $\pm \sigma_{sys}$
1μ + 1γ + 3 Jets + $\not{E}_T$ +X	0.024	0.38	600 - 630	1	0.022 ± 0.015
1 e + 4 Jets + $\not{E}_T$ +X	0.012	0.38	280 - 300	2	0.02 ± 0.16
1μ + 6 Jets +X	0.017	0.38	700 - 750	2	0.19 ± 0.06
3 e +X	0.018	0.38	250 - 260	1	0.013 ± 0.015
1 e + 1μ + 5 Jets +X	0.028	0.4	1080 - 1130	1	0.021 ± 0.023
2μ + 1γ + 1 Jet +X	0.015	0.41	120 - 130	1	0.006 ± 0.017
2 e + 3 Jets + $\not{E}_T$ +X	0.024	0.42	540 - 600	3	0.58 ± 0.14
1γ + 3 Jets + $\not{E}_T$ +X	0.013	0.43	820 - 1060	16	6.0 ± 2.8
1 e + 1γ + 1 Jet +X	0.0071	0.46	280 - 320	14	4.1 ± 2.4
2μ + 4 Jets +X	0.03	0.47	370 - 400	1	0.029 ± 0.016
1 e + 1γ +X	0.019	0.48	220 - 240	12	3.1 ± 2.8
1μ + 4 Jets + $\not{E}_T$ +X	0.011	0.49	1060 - 1210	5	1.10 ± 0.45
2μ + 3 Jets + $\not{E}_T$ +X	0.021	0.49	700 - 790	3	0.56 ± 0.10
1γ + 6 Jets +X	0.032	0.5	1950 - 2040	1	0.003 ± 0.039
1 e + 5 Jets +X	0.022	0.51	2510 - 2980	2	0.05 ± 0.21
1γ + 4 Jets +X	0.017	0.52	1480 - 1540	3	0.32 ± 0.34
2 e + 1 Jet +X	0.0057	0.53	320 - 330	20	9.8 ± 1.4
3μ + $\not{E}_T$ +X	0.11	0.53	170 - 180	1	0.121 ± 0.057
1μ + $\not{E}_T$ +X	0.013	0.55	280 - 330	15	7.38 ± 0.96
1 e + 1γ + $\not{E}_T$ +X	0.018	0.56	50 - 70	3	0.46 ± 0.24
2 e + 4 Jets + $\not{E}_T$ +X	0.064	0.58	520 - 550	1	0.066 ± 0.027
1 e + 1μ + 4 Jets + $\not{E}_T$ +X	0.076	0.58	580 - 700	2	0.44 ± 0.12
2 e + $\not{E}_T$ +X	0.019	0.59	560 - 570	1	0.013 ± 0.017
2 e + 2 Jets +X	0.0086	0.6	510 - 550	13	5.51 ± 0.99
2 e + 3 Jets +X	0.022	0.6	720 - 750	3	0.57 ± 0.10
1 e + 2 Jets + $\not{E}_T$ +X	0.02	0.6	890 - 980	0	5.3 ± 1.7
1 e + 1μ + 1 Jet +X	0.032	0.63	300 - 320	9	3.5 ± 1.5
1μ + 4 Jets +X	0.023	0.63	940 - 1090	23	11.8 ± 3.5
1γ + 1 Jet +X	0.027	0.64	760 - 780	13	5.0 ± 2.6
1 e + 1γ + 3 Jets + $\not{E}_T$ +X	0.11	0.64	380 - 400	1	0.089 ± 0.091
1 e + 1μ + 3 Jets +X	0.029	0.64	750 - 1050	5	1.54 ± 0.47
1μ + 1γ + 3 Jets +X	0.06	0.64	280 - 300	1	0.009 ± 0.075
1μ + 1γ + 2 Jets +X	0.03	0.66	500 - 520	2	0.12 ± 0.23
1 e + 4 Jets +X	0.07	0.66	2290 - 2860	2	0.24 ± 0.35
1μ + 1γ + 2 Jets + $\not{E}_T$ +X	0.04	0.67	520 - 540	1	0.030 ± 0.033
2 e + 1γ +X	0.039	0.68	240 - 250	1	0.038 ± 0.022
1μ + 5 Jets + $\not{E}_T$ +X	0.035	0.68	1150 - 1270	2	0.28 ± 0.10
1μ + 1γ +X	0.028	0.7	30 - 40	2	7.9 ± 1.5
1 e + 3 Jets + $\not{E}_T$ +X	0.044	0.71	1140 - 1220	4	1.15 ± 0.49
1μ + 6 Jets + $\not{E}_T$ +X	0.082	0.71	1170 - 1230	1	0.086 ± 0.034
1μ + 3 Jets +X	0.027	0.71	1530 - 2010	0	4.5 ± 1.3
1 e + 1 Jet + $\not{E}_T$ +X	0.037	0.72	1000 - 1040	2	0.24 ± 0.18
1 e + 1γ + 3 Jets +X	0.059	0.76	450 - 480	1	0.049 ± 0.047
2γ + 2 Jets + $\not{E}_T$ +X	0.075	0.77	480 - 500	1	0.001 ± 0.099
1 e + 7 Jets +X	0.12	0.78	1080 - 1150	1	0.03 ± 0.15
1 e + 1μ + $\not{E}_T$ +X	0.042	0.82	450 - 460	1	0.041 ± 0.024
2 e + 4 Jets +X	0.11	0.82	640 - 680	1	0.120 ± 0.059

Continued on next page...

Event class	p-value	$\tilde{p}$	Region (GeV)	Data	SM $\pm \sigma_{sys}$
1 e + 1μ + 2 Jets +X	0.049	0.84	710 - 740	2	0.31 $\pm$ 0.17
2μ + 1γ +X	0.072	0.88	80 - 90	7	3.34 $\pm$ 0.85
1μ + 1γ + 1 Jet + $\not\!\!E_T$ +X	0.057	0.89	200 - 220	5	1.88 $\pm$ 0.60
1 e + 5 Jets + $\not\!\!E_T$ +X	0.074	0.89	640 - 680	4	1.34 $\pm$ 0.67
1 e + 1μ +X	0.14	0.9	280 - 370	0	2.23 $\pm$ 0.71
1μ + 3 Jets + $\not\!\!E_T$ +X	0.045	0.9	1380 - 1580	2	0.31 $\pm$ 0.14
1μ + 2 Jets +X	0.069	0.9	1390 - 2070	2	6.3 $\pm$ 1.2
1 e + 1γ + 2 Jets + $\not\!\!E_T$ +X	0.1	0.91	440 - 460	1	0.075 $\pm$ 0.096
1μ + 2 Jets + $\not\!\!E_T$ +X	0.047	0.91	1000 - 1120	0	3.19 $\pm$ 0.52
1 e + $\not\!\!E_T$ +X	0.081	0.92	360 - 370	3	0.88 $\pm$ 0.45
1 e + 2 Jets +X	0.21	0.93	2180 - 2230	1	0.10 $\pm$ 0.25
1μ + 1 Jet + $\not\!\!E_T$ +X	0.056	0.94	1030 - 1420	5	1.91 $\pm$ 0.50
2μ + 1 Jet +X	0.039	0.95	350 - 370	26	16.8 $\pm$ 2.2
1 e + 1γ + 1 Jet + $\not\!\!E_T$ +X	0.088	0.95	360 - 400	2	0.44 $\pm$ 0.25
1 e + 1γ + 2 Jets +X	0.1	0.96	840 - 930	2	0.09 $\pm$ 0.56
2 e + 1γ + 1 Jet +X	0.14	0.98	150 - 3030	0	2.08 $\pm$ 0.52
2μ + 3 Jets +X	0.081	0.99	880 - 960	3	0.98 $\pm$ 0.21
1 e + 1 Jet +X	–	–	1230 - 1260	5	1.6 $\pm$ 2.4
1 e + 3 Jets +X	–	–	2150 - 2210	1	0.19 $\pm$ 0.48
1 e + 6 Jets +X	–	–	700 - 850	0	0.42 $\pm$ 0.09
1γ + 2 Jets +X	–	–	80 - 130	0	0.084 $\pm$ 0.028

C.2.3. Missing transverse energy

Exclusive classes

Event class	p-value	$\tilde{p}$	Region (GeV)	Data	SM $\pm \sigma_{sys}$
1μ + 2γ + $\not\!\!E_T$	0.00088	0.005	90 - 120	1	0 $\pm$ 0.0011
2μ + 1 Jet + $\not\!\!E_T$	0.00062	0.016	50 - 80	21	8.5 $\pm$ 1.2
2μ + 2 Jets + $\not\!\!E_T$	0.0013	0.028	30 - 90	36	18.6 $\pm$ 2.5
2μ + 3 Jets + $\not\!\!E_T$	0.0026	0.042	60 - 90	6	1.27 $\pm$ 0.23
1γ + 5 Jets + $\not\!\!E_T$	0.017	0.057	10 - 40	3	0.41 $\pm$ 0.27
2 e + 1μ + $\not\!\!E_T$	0.019	0.064	100 - 130	1	0.0183 $\pm$ 0.0094
1μ + 8 Jets + $\not\!\!E_T$	0.017	0.069	20 - 50	1	0.016 $\pm$ 0.010
1γ + 1 Jet + $\not\!\!E_T$	0.0061	0.074	120 - 270	6	1.32 $\pm$ 0.53
1 e + 1μ + 3 Jets + $\not\!\!E_T$	0.0064	0.076	130 - 170	3	0.351 $\pm$ 0.091
3 e + 1 Jet + $\not\!\!E_T$	0.027	0.078	10 - 40	1	0.025 $\pm$ 0.016
1μ + 1γ + $\not\!\!E_T$	0.0085	0.095	30 - 60	20	40.3 $\pm$ 6.4
1 e + 3 Jets + $\not\!\!E_T$	0.0023	0.12	170 - 280	0	6.7 $\pm$ 1.1
1γ + 6 Jets + $\not\!\!E_T$	0.052	0.13	40 - 70	1	0.049 $\pm$ 0.033
2μ + 5 Jets + $\not\!\!E_T$	0.045	0.14	10 - 40	1	0.046 $\pm$ 0.019
1μ + 3 Jets + $\not\!\!E_T$	0.0036	0.15	140 - 170	0	6.8 $\pm$ 1.5
1 e + 2μ + $\not\!\!E_T$	0.04	0.15	80 - 110	1	0.037 $\pm$ 0.025
1 e + 1μ + $\not\!\!E_T$	0.029	0.16	230 - 260	1	0.005 $\pm$ 0.035
2μ + 4 Jets + $\not\!\!E_T$	0.037	0.19	60 - 90	2	0.292 $\pm$ 0.071
2γ + $\not\!\!E_T$	0.11	0.19	10 - 40	1	0.12 $\pm$ 0.042
3μ + 1 Jet + $\not\!\!E_T$	0.084	0.2	10 - 40	1	0.080 $\pm$ 0.055

Continued on next page...

Event class	p-value	$\tilde{p}$	Region (GeV)	Data	SM $\pm \sigma_{sys}$
2γ + 1 Jet + $\not\!\!E_T$	0.13	0.21	10 - 40	2	0.51 ± 0.37
1γ + $\not\!\!E_T$	0.019	0.21	180 - 210	2	0.186 ± 0.097
1 e + 1μ + 5 Jets + $\not\!\!E_T$	0.072	0.21	70 - 100	1	0.075 ± 0.026
1 e + 2μ + 1 Jet + $\not\!\!E_T$	0.19	0.32	40 - 70	1	0.19 ± 0.14
1γ + 3 Jets + $\not\!\!E_T$	0.093	0.34	200 - 230	1	0.01 ± 0.12
1 e + 1μ + 4 Jets + $\not\!\!E_T$	0.093	0.34	120 - 150	1	0.098 ± 0.032
1μ + 1γ + 3 Jets + $\not\!\!E_T$	0.23	0.41	70 - 100	1	0.17 ± 0.26
2 e + $\not\!\!E_T$	0.12	0.42	130 - 160	1	0.133 ± 0.058
1 e + 1γ + 3 Jets + $\not\!\!E_T$	0.22	0.43	10 - 40	1	0.21 ± 0.20
1 e + 1μ + 1 Jet + $\not\!\!E_T$	0.047	0.44	180 - 250	2	0.31 ± 0.16
2 e + 4 Jets + $\not\!\!E_T$	0.18	0.45	10 - 40	1	0.202 ± 0.049
1μ + 1 Jet + $\not\!\!E_T$	0.021	0.52	210 - 270	2	8.2 ± 1.5
2 e + 3 Jets + $\not\!\!E_T$	0.11	0.54	70 - 100	2	0.56 ± 0.17
1 e + 1γ + $\not\!\!E_T$	0.11	0.58	60 - 1610	1	4.06 ± 0.93
1μ + 6 Jets + $\not\!\!E_T$	0.098	0.58	150 - 180	1	0.102 ± 0.047
1 e + $\not\!\!E_T$	0.035	0.63	170 - 260	8	3.47 ± 0.73
1μ + 4 Jets + $\not\!\!E_T$	0.045	0.68	110 - 140	1	5.10 ± 0.77
1 e + 5 Jets + $\not\!\!E_T$	0.09	0.7	100 - 550	0	2.50 ± 0.44
2 e + 1 Jet + $\not\!\!E_T$	0.14	0.74	80 - 140	1	3.67 ± 0.72
1 e + 1γ + 1 Jet + $\not\!\!E_T$	0.13	0.75	50 - 80	4	1.78 ± 0.69
1μ + 2 Jets + $\not\!\!E_T$	0.056	0.75	270 - 690	0	3.05 ± 0.57
1μ + $\not\!\!E_T$	0.037	0.76	210 - 250	3	0.68 ± 0.23
1 e + 6 Jets + $\not\!\!E_T$	0.17	0.76	30 - 450	0	1.86 ± 0.46
1 e + 1 Jet + $\not\!\!E_T$	0.056	0.76	200 - 230	11	6.01 ± 0.99
1μ + 5 Jets + $\not\!\!E_T$	0.082	0.79	60 - 90	7	3.48 ± 0.84
1 e + 4 Jets + $\not\!\!E_T$	0.087	0.81	210 - 240	2	0.48 ± 0.15
2μ + $\not\!\!E_T$	0.14	0.81	60 - 7000	3	6.30 ± 0.87
1 e + 2 Jets + $\not\!\!E_T$	0.061	0.82	230 - 260	5	1.95 ± 0.54
1 e + 1μ + 2 Jets + $\not\!\!E_T$	0.31	0.94	150 - 180	1	0.38 ± 0.12
1μ + 1γ + 1 Jet + $\not\!\!E_T$	0.28	0.94	90 - 370	0	1.36 ± 0.41
2 e + 2 Jets + $\not\!\!E_T$	0.315	0.97	100 - 130	1	0.40 ± 0.10

Inclusive classes

Event class	p-value	$\tilde{p}$	Region (GeV)	Data	SM $\pm \sigma_{sys}$
2μ + 1 Jet + $\not\!\!E_T$ +X	7.2e-05	0.0032	60 - 90	34	14.0 ± 2.1
2μ + 3 Jets + $\not\!\!E_T$ +X	0.00059	0.012	60 - 90	8	1.69 ± 0.30
1μ + 2γ + $\not\!\!E_T$ +X	0.0076	0.018	90 - 120	1	0 ± 0.0096
2μ + $\not\!\!E_T$ +X	0.00069	0.021	40 - 90	79	46.9 ± 5.9
2μ + 2 Jets + $\not\!\!E_T$ +X	0.00091	0.024	30 - 90	46	24.6 ± 3.3
1μ + 8 Jets + $\not\!\!E_T$ +X	0.017	0.062	20 - 50	1	0.016 ± 0.010
1γ + 5 Jets + $\not\!\!E_T$ +X	0.011	0.07	20 - 50	4	0.64 ± 0.38
3 e + 1 Jet + $\not\!\!E_T$ +X	0.032	0.093	10 - 40	1	0.030 ± 0.019
1 e + 1μ + 3 Jets + $\not\!\!E_T$ +X	0.0081	0.12	110 - 170	5	1.13 ± 0.28
1γ + 6 Jets + $\not\!\!E_T$ +X	0.056	0.13	40 - 70	1	0.054 ± 0.034
2 e + 1 Jet + $\not\!\!E_T$ +X	0.0077	0.13	10 - 40	38	19.5 ± 5.1
1 e + 1μ + $\not\!\!E_T$ +X	0.0099	0.15	230 - 260	2	0.113 ± 0.088

Continued on next page...

Event class	p-value	$\tilde{p}$	Region (GeV)	Data	SM $\pm \sigma_{sys}$
2μ + 5 Jets + $\not{E}_T$ +X	0.057	0.18	10 - 40	1	0.059 ± 0.023
3μ + 1 Jet + $\not{E}_T$ +X	0.084	0.19	10 - 40	1	0.080 ± 0.056
2 e + 1μ + $\not{E}_T$ +X	0.061	0.2	80 - 110	1	0.062 ± 0.029
3 e + $\not{E}_T$ +X	0.099	0.21	10 - 40	1	0.104 ± 0.030
1γ + 1 Jet + $\not{E}_T$ +X	0.015	0.23	210 - 270	3	0.44 ± 0.21
1γ + 2 Jets + $\not{E}_T$ +X	0.029	0.29	70 - 100	16	7.2 ± 2.9
1γ + $\not{E}_T$ +X	0.01	0.3	200 - 230	3	0.36 ± 0.20
2μ + 4 Jets + $\not{E}_T$ +X	0.06	0.31	60 - 90	2	0.389 ± 0.086
1 e + 2μ + $\not{E}_T$ +X	0.13	0.32	80 - 110	1	0.129 ± 0.086
1 e + 1μ + 5 Jets + $\not{E}_T$ +X	0.1	0.34	70 - 100	1	0.107 ± 0.032
1 e + 1μ + 1 Jet + $\not{E}_T$ +X	0.032	0.36	150 - 190	5	1.58 ± 0.48
2γ + $\not{E}_T$ +X	0.1	0.37	90 - 120	1	0.01 ± 0.13
1 e + 3 Jets + $\not{E}_T$ +X	0.017	0.37	180 - 210	0	4.30 ± 0.66
1 e + 1μ + 2 Jets + $\not{E}_T$ +X	0.029	0.39	150 - 180	3	0.63 ± 0.16
1γ + 3 Jets + $\not{E}_T$ +X	0.099	0.41	200 - 230	1	0.02 ± 0.13
1μ + 7 Jets + $\not{E}_T$ +X	0.15	0.43	20 - 50	1	0.167 ± 0.045
3μ + $\not{E}_T$ +X	0.19	0.44	10 - 40	1	0.207 ± 0.063
1μ + 1γ + 3 Jets + $\not{E}_T$ +X	0.25	0.47	70 - 100	1	0.21 ± 0.26
1 e + 1μ + 4 Jets + $\not{E}_T$ +X	0.12	0.47	120 - 150	1	0.124 ± 0.055
2 e + 4 Jets + $\not{E}_T$ +X	0.22	0.51	10 - 40	1	0.245 ± 0.060
1μ + 3 Jets + $\not{E}_T$ +X	0.025	0.53	270 - 330	4	1.05 ± 0.23
1 e + 1γ + 3 Jets + $\not{E}_T$ +X	0.23	0.57	10 - 40	1	0.23 ± 0.20
1 e + 5 Jets + $\not{E}_T$ +X	0.05	0.6	100 - 550	0	3.28 ± 0.74
1μ + 5 Jets + $\not{E}_T$ +X	0.046	0.61	90 - 150	0	3.37 ± 0.76
1 e + 6 Jets + $\not{E}_T$ +X	0.13	0.66	40 - 450	0	2.19 ± 0.53
1 e + 1 Jet + $\not{E}_T$ +X	0.041	0.7	170 - 200	16	26.4 ± 3.2
2 e + 3 Jets + $\not{E}_T$ +X	0.16	0.7	30 - 90	6	3.56 ± 0.67
1μ + 6 Jets + $\not{E}_T$ +X	0.15	0.73	150 - 180	1	0.161 ± 0.042
1μ + 4 Jets + $\not{E}_T$ +X	0.063	0.74	110 - 140	2	6.7 ± 1.5
2 e + $\not{E}_T$ +X	0.15	0.79	130 - 160	3	1.30 ± 0.35
1 e + 4 Jets + $\not{E}_T$ +X	0.087	0.82	140 - 210	1	4.35 ± 0.87
1μ + 1γ + 1 Jet + $\not{E}_T$ +X	0.17	0.87	90 - 550	0	1.94 ± 0.56
1 e + $\not{E}_T$ +X	0.14	0.93	270 - 300	1	3.56 ± 0.61
1μ + 2 Jets + $\not{E}_T$ +X	0.15	0.93	220 - 250	8	5.00 ± 0.76
1 e + 2 Jets + $\not{E}_T$ +X	0.15	0.96	230 - 260	6	3.42 ± 0.76
2 e + 2 Jets + $\not{E}_T$ +X	0.33	0.96	70 - 100	0	1.10 ± 0.30
1 e + 1γ + $\not{E}_T$ +X	0.32	0.97	110 - 650	0	1.23 ± 0.41
1μ + $\not{E}_T$ +X	0.14	0.98	390 - 7000	0	2.08 ± 0.50
1μ + 1 Jet + $\not{E}_T$ +X	0.17	0.99	280 - 350	8	5.25 ± 0.77

Bibliography

[1] P. A. Biallass, "Commissioning of the CMS Muon Detector and Development of Generic Search Strategies for New Physics", 2009. PhD Thesis; http://web.physik.rwth-aachen.de/~hebbeker/theses/biallass_phd.pdf.

[2] C. Hof, "Implementation of a Model-Independent Search for New Physics with the CMS Detector Exploiting the World-Wide LHC Computing Grid", 2009. PhD Thesis; http://web.physik.rwth-aachen.de/~hebbeker/theses/hof_phd.pdf.

[3] T. Hebbeker, "A Global Comparison between L3 Data and Standard Model Monte Carlo – a first attempt", *L3 note 2305* (1998). http://web.physik.rwth-aachen.de/~hebbeker/l3note_2305.pdf.

[4] H1 Collaboration, "A general search for new phenomena in ep scattering at HERA", *Phys. Lett. B* **602** (2004) 14. doi:10.1016/j.physletb.2004.09.057.

[5] D0 Collaboration, "Search for new physics in e-mu-X data at D0 using SLEUTH: A quasi-model-independent search strategy for new physics", *Phys. Rev. D* **62** (2000) 092004. doi:10.1103/PhysRevD.62.092004.

[6] D0 Collaboration, "Quasi-model-independent search for new physics at large transverse momentum", *Phys. Rev. D* **64** (2001) 012004. doi:10.1103/PhysRevD.64.012004.

[7] CDF Collaboration, "Model-independent and quasi-model-independent search for new physics at CDF", *Phys. Rev. D* **78** (2007) 012002. doi:10.1103/PhysRevD.78.012002.

[8] CDF Collaboration, "Global search for new physics with 2.0 fb^{-1} at CDF", *Phys. Rev. D* **79** (2009), no. 1, 011101. doi:10.1103/PhysRevD.79.011101.

[9] S. Weinberg, "A Model of Leptons", *Phys. Rev. Lett. 19, 1264* (1967). http://prola.aps.org/abstract/PRL/v19/i21/p1264_1.

[10] S. Glashow, J. Iliopoulos, and L. Maiani, "Weak Interactions with Lepton-Hadron Symmetry", *Phys. Rev. D 2, 1285* (1970). http://prola.aps.org/abstract/PRD/v2/i7/p1285_1.

[11] A. Salam and J. Ward, "Gauge Theory of Elementary Interactions", *Phys. Rev. 136, B763* (1964). http://prola.aps.org/abstract/PR/v136/i3B/pB763_1.

[12] D. J. Gross and F. Wilczek, "Asymptotically Free Gauge Theories. I", *Phys. Rev. D* **8** (1973) 3633–3652. doi:10.1103/PhysRevD.8.3633.

[13] F. Halzen and A. Martin, "Quarks and Leptons: An introduction course in modern particle physics". John Wiley & Sons, 1984. ISBN 0-471-88741-2.

[14] Z. Maki, M. Nakagawa, and S. Sakata, "Remarks on the Unified Model of Elementary Particles", *Progress of Theoretical Physics* **28** (1962), no. 5, 870–880. doi:10.1143/PTP.28.870.

[15] B. Pontecorvo, "Neutrino Experiments and the Problem of Conservation of Leptonic Charge", *Soviet Journal of Experimental and Theoretical Physics* **26** (1968) 984.

[16] R. Davis, D. S. Harmer, and K. C. Hoffman, "Search for Neutrinos from the Sun", *Phys. Rev. Lett.* **20** (1968) 1205–1209. doi:10.1103/PhysRevLett.20.1205.

[17] N. Cabibbo, "Unitary Symmetry and Leptonic Decays", *Phys. Rev. Lett.* **10** (1963) 531–533. doi:10.1103/PhysRevLett.10.531.

[18] M. Kobayashi and T. Maskawa, "CP-Violation in the Renormalizable Theory of Weak Interaction", *Progress of Theoretical Physics* **49** (1973), no. 2, 652–657. doi:10.1143/PTP.49.652.

[19] http://pdglive.lbl.gov/listings1.brl.

[20] W. de Boer, "Results on R from PEP, PETRA, TRISTAN and SLC",.

[21] V. Branchina, M. Consoli, R. Fiore et al., "Combined fit to R and data from the CERN collider LEP", *Phys. Rev. D* **46** (1992) 75–83. doi:10.1103/PhysRevD.46.75.

[22] A. Martin, W. Stirling, R. Thome et al., "Parton distributions for the LHC", *Eur.Phys.J.C63:189-285* (2009). doi:10.1140/epjc/s10052-009-1072-5.

[23] J. M. Campbell, J. W. Huston, and W. J. Stirling, "Hard interactions of quarks and gluons: a primer for LHC physics", *Rep. Prog. Phys.* **70** (2007), no. 1, 89. doi:doi:10.1088/0034-4885/70/1/R02.

[24] F. Zwicky, "On the Masses of Nebulae and of Clusters of Nebulae", *ApJ, 86, 217* (1937). http://dx.doi.org/10.1086/143864.

[25] G. H. et.al., "Five-Year Wilkinson Microwave Anisotropy Probe (WMAP) Observations: Data Processing, Sky Maps, and Basic Results", *The Astrophysical Journal Supplement Series* (2008). http://arxiv.org/abs/0803.0732.

[26] B. Lee, C. Quigg, and H. Thacker, "Weak interactions at very high energies: The role of the Higgs-boson mass", *Phys. Rev. D 16, 1519* (1977). http://link.aps.org/abstract/PRD/v16/p1519.

[27] CMS Collaboration, "Combination of SM Higgs Searches", *CMS PAS* **CERN CDS 1406347** (2011).

[28] (SNO Collaboration) Collaboration, "Measurement of the Rate of charged current Interactions Produced by 8B Solar Neutrinos at the Sudbury Neutrino Observatory", *Phys. Rev. Lett.* **87** (2001) 071301. doi:10.1103/PhysRevLett.87.071301.

[29] P. Langacker, "The Physics of Heavy Z' Gauge Bosons", arXiv:0801.1345.

[30] U. Baur, M. Spira, and P. Zerwas, "Excited-quark and -lepton production at hadron colliders", *Phys. Rev. D* **42** (1990) 815–824. doi:10.1103/PhysRevD.42.815.

[31] S. Martin, "A Supersymmetry Primer", (2006). http://arxiv.org/abs/hep-ph/9709356.

[32] U. Amaldi, W. de Boer, and H. Fürstenau, "Comparison of grand unified theories with electroweak and strong coupling constants measured at LEP", *Physics Letters B* **260** (1991), no. 3–4, 447 – 455. doi:10.1016/0370-2693(91)91641-8.

[33] H. Pieta, "Discovery Potential of MSUGRA-Supersymmetry in the muon+Jet+MET Channel at CMS", 2008. Diploma Thesis; http://web.physik.rwth-aachen.de/~hebbeker/theses/pieta_diploma.pdf.

[34] https://twiki.cern.ch/twiki/bin/view/CMSPublic/LumiPublicResults2010.

[35] https://twiki.cern.ch/twiki/bin/view/CMS/PileupInformation?rev=4#2010_Pileup_Scenarios.

[36] "LHC Design Report, Volume 1". http://doc.cern.ch/cernrep/2004/2004-003-v1/2004-003-v1.html.

[37] "LHC Design Report, Volume 2". http://doc.cern.ch/cernrep/2004/2004-003-v2/2004-003-v2.html.

[38] "LHC Design Report, Volume 3". http://doc.cern.ch/cernrep/2004/2004-003-v3/2004-003-v3.html.

[39] CMS Collaboration, "The CMS experiment at the CERN LHC", *JINST* **3** (2008) S08004. doi:10.1088/1748-0221/3/08/S08004.

[40] http://fsp102-cms.de/.

[41] CMS collaboration, "The Electromagnetic Calorimeter - Technical Design Report", (1997). CERN/LHCC 97-33 - http://cmsdoc.cern.ch/cms/TDR/ECAL/ecal.html.

[42] CMS collaboration, "The Hadron Calorimeter Project - Technical Design Report", (1997). CERN/LHCC 97-31 - http://cmsdoc.cern.ch/cms/TDR/HCAL/hcal.html.

[43] CMS Collaboration, "Performance of muon identification in pp collisions at s**0.5 = 7 TeV", *CMS PAS* **CERN CDS 1279140** (2010).

[44] CMS collaboration, "Track reconstruction in the CMS Tracker", (2010). https://twiki.cern.ch/twiki/bin/view/CMS/TrackingPOGTrackerRecoNote.

[45] R. Frühwirth, "Application of Kalman filtering to track and vertex fitting", *Nucl. Instrum. Meth. A 262, 444* (1987). http://dx.doi.org/10.1016/0168-9002(87)90887-4.

[46] G. A. et al, "Muon Reconstruction in the CMS Detector", (2009). http://cms.cern.ch/iCMS/jsp/db_notes/noteInfo.jsp?cmsnoteid=CMS%20AN-2008/097.

[47] CMS collaboration, "Review of clustering algorithms and energy corrections in ECAL", (2010). http://cms.cern.ch/iCMS/jsp/db_notes/noteInfo.jsp?cmsnoteid=CMS%20IN-2010/008.

[48] CMS Collaboration, "Electron reconstruction and identification at sqrt(s)=7 TeV", *CMS PAS* **CERN CDS 1299116** (2010).

[49] CMS Collaboration, "Reconstruction of Electrons with the Gaussian-Sum Filter in the CMS Tracker at the LHC",.

[50] CMS Collaboration, "Particle-Flow Event Reconstruction in CMS and Performance for Jets, Taus and MET", *CMS PAS* **CERN CDS 1194487** (2009).

[51] M. Cacciari, G. P. Salam, and G. Soyez, "The anti- k t jet clustering algorithm", *Journal of High Energy Physics* **2008** (2008), no. 04, 063. doi:10.1088/1126-6708/2008/04/063.

[52] CMS Collaboration, "Jet Energy Corrections determination at 7 TeV", *CMS PAS* **CERN CDS 1308178** (2010).

[53] S. V. der Meer, "Calibration of the effective beam height in the ISR", *ISR Note* **CERN CDS 296752** (1968).

[54] CMS Collaboration, "Measurement of CMS Luminosity", *CMS PAS* **CERN CDS 1279145** (2010).

[55] TOTEM Collaboration, "First measurement of the total proton-proton cross section at the LHC energy of sqrt(s) = 7 TeV",.

[56] T. Sjostrand, S. Mrenna, and P. Z. Skands, "PYTHIA 6.4 Physics and Manual", *JHEP* **0605** (2006) 026, arXiv:hep-ph/0603175. doi:10.1088/1126-6708/2006/05/026.

[57] J. Alwall et al., "MadGraph/MadEvent v4: The New Web Generation", *JHEP* **09** (2007) 028, arXiv:0706.2334. doi:10.1088/1126-6708/2007/09/028.

[58] M. L. Mangano, M. Moretti, F. Piccinini et al., "ALPGEN, a generator for hard multiparton processes in hadronic collisions", *JHEP* **07** (2003) 001, arXiv:hep-ph/0206293. doi:10.1088/1126-6708/2003/07/001.

[59] S. Agostinelli, J. Allison, K. Amako et al., "G4–a simulation toolkit", *Nuclear Instruments and Methods in Physics Research A* **506** (2003), no. 3, 250 – 303. doi:DOI: 10.1016/S0168-9002(03)01368-8.

[60] J. Allison, K. Amako, J. Apostolakis et al., "Geant4 developments and applications", *Nuclear Science, IEEE Transactions on* **53** (2006), no. 1, 270–278. doi:10.1109/TNS.2006.869826.

[61] https://twiki.cern.ch/twiki/bin/viewauth/CMS/StandardModelCrossSections.

[62] R. Gavin, Y. Li, F. Petriello et al., "FEWZ 2.0: A code for hadronic Z production at next-to-next-to-leading order", *Computer Physics Communications* **182** (2011), no. 11, 2388 – 2403, arXiv:1011.3540. doi:10.1016/j.cpc.2011.06.008.

[63] N. Kidonakis, "Higher-order corrections to top-antitop pair and single top quark production", 2009.

[64] J. M. Campbell and R. K. Ellis, "An update on vector boson pair production at hadron colliders", *Phys. Rev.* **D60** (1999) 113006, arXiv:hep-ph/9905386. doi:10.1103/PhysRevD.60.113006.

[65] CMS Collaboration, "Measurement of the Inclusive Upsilon production cross section in pp collisions at sqrt(s)=7 TeV", *Phys. Rev. D* **83** (Jun, 2011) 112004, arXiv:1012.5545. doi:10.1103/PhysRevD.83.112004.

[66] O. Charaf, B. Clerbaux, V. Dero, A. Gay, G. De Lentdecker,Sh. Elgammal, A. Gay, S. Harper, J. Jackson, P. Marage, Ph. Miné, D. Newbold, E. Olaiya,C. Shepherd-Themistocleous, L. Thomas, V. Timciuc, P. Vanlaer, "Search for High-Mass Resonances Decaying to Electron Pairs in the CMS Experiment", 2010. http://cms.cern.ch/iCMS/jsp/db_notes/noteInfo.jsp?cmsnoteid=CMS%20AN-2010/318.

[67] A. Gueth,T. Hebbeker, K. Hoepfner, S. Thueer, T. Bose, E. C. Jarrin, D. Sperka, C. Leonidopoulos, C. D. Pardos, S. G. Lopez, J. Hauser, C. Jarvis, "Search for W' in the muon channel in pp Collisions at sqrt(s) = 7 TeV", 2010. http://cms.cern.ch/iCMS/jsp/db_notes/noteInfo.jsp?cmsnoteid=CMS%20AN-2010/315.

[68] CMS Collaboration, "Tracking and Primary Vertex Results in First 7 TeV Collisions", *CMS PAS* **CERN CDS 1279383** (2010).

[69] J. P. Chou, S. Eno, S. Kunori, S. Sharma, J. Wang, "Anomalous HB/HE Noise at Startup: Characteristics and Rejection Algorithms", 2010. http://cms.cern.ch/iCMS/jsp/db_notes/noteInfo.jsp?cmsnoteid=CMS%20IN-2010/006.

[70] https://twiki.cern.ch/twiki/bin/view/CMS/ExoticaMuons?rev=29.

[71] https://twiki.cern.ch/twiki/bin/view/CMS/HEEPElectronID?rev=51.

[72] https://twiki.cern.ch/twiki/bin/view/CMS/PhotonID?rev=31.

[73] https://twiki.cern.ch/twiki/bin/view/CMS/JetID?rev=74#Documentation.

[74] CMS Collaboration, "Measurement of the Inclusive Jet Cross Section in pp Collisions at $\sqrt{s} = 7$ TeV", *Phys. Rev. Lett.* **107** (2011) 132001. doi:10.1103/PhysRevLett.107.132001.

[75] R. D. Cousins, J. T. Linnemann, and J. Tucker, "Evaluation of three methods for calculating statistical significance when incorporating a systematic uncertainty into a test of the background-only hypothesis for a Poisson process", *NIM: A* **595** (2008), no. 2, 480 – 501. doi:DOI: 10.1016/j.nima.2008.07.086.

[76] S. A. Schmitz, "Model Unspecific Search for New Physics with High pT Photons in CMS", 2009. Diploma Thesis; http://web.physik.rwth-aachen.de/~hebbeker/theses/schmitz_diploma.pdf.

[77] M. Olschewski, "Study of Alternative Statistical Methods for a Model Unspecific Search in CMS", 2009. Diploma Thesis; http://web.physik.rwth-aachen.de/~hebbeker/theses/olschewski_diploma.pdf.

[78] C. Collaboration, "Absolute luminosity normalizations", *CMS DPS* **CERN CDS 1335668** (2011).

[79] CMS Collaboration, "Measurement of the W and Z inclusive production cross sections at sqrts=7 TeV with the CMS experiment at the LHC", *CMS PAS EWK-10-005* **CERN CDS 1337017** (2011).

[80] J. Pumplin, D. Stump, R. Brock et al., "Uncertainties of predictions from parton distribution functions II: the Hessian method", *Phys.Rev.D65:014013* (2001). doi:10.1103/PhysRevD.65.014013.

[81] H.-L. Lai, J. Huston, Z. Li et al., "Uncertainty induced by QCD coupling in the CTEQ global analysis of parton distributions", arXiv:1004.4624.

[82] A. Martin, W. Stirling, R. Thorne et al., "Uncertainties on aS in global PDF analyses and implications for predicted hadronic cross sections", *The European Physical Journal C - Particles and Fields* **64** (2009) 653–680. doi:10.1140/epjc/s10052-009-1164-2.

[83] F. Demartin, S. Forte, E. Mariani et al., "The impact of PDF and alphas uncertainties on Higgs Production in gluon fusion at hadron colliders", arXiv:1004.0962.

[84] R. D. Ball, L. D. Debbio, S. Forte et al., "A first unbiased global NLO determination of parton distributions and their uncertainties", arXiv:1002.4407.

[85] A. Vicini. http://www.hep.ucl.ac.uk/pdf4lhc/PDF4LHC_practical_guide.pdf.

[86] S. Alekhin, S. Alioli, R. D. Ball et al., "The PDF4LHC Working Group Interim Report", arXiv:1101.0536.

[87] M. Botje, J. Butterworth, A. Cooper-Sarkar et al., "The PDF4LHC Working Group Interim Recommendations", arXiv:1101.0538.

[88] CMS Collaboration, "Search for excited leptons in pp Collisions at sqrt(s)=7 TeV", 2011. doi:10.1016/j.physletb.2011.09.021.

[89] CMS Collaboration, "Search for Large Extra Dimensions in the Diphoton Final State at the Large Hadron Collider", 2011. Submitted to JHEP.

[90] CMS collaboration, "Search for new physics with same-sign isolated dilepton events with jets and missing transverse energy at the LHC", *Journal of High Energy Physics* **2011** (2011) 1–47. doi:10.1007/JHEP06(2011)077.

[91] CMS Collaboration, "Model Unspecific Search for New Physics in pp Collisions at sqrt(s) = 7 TeV", *CMS PAS* **CERN CDS 1360173** (2011).

[92] CMS Collaboration, "Search for Resonances in the Dilepton Mass Distribution in *pp* Collisions at $\sqrt(s) = 7$ TeV", *Journal of High Energy Physics* **2011** (2011) 1–35, arXiv:1103.0981. doi:10.1007/JHEP05(2011)093.

[93] D. Newbold, R. Walton O. Charaf, B. Clerbaux S. Harper, C. Shepherd-Themistocleous, "Electron ID at High Energies", 2008. http://cms.cern.ch/iCMS/jsp/db_notes/noteInfo.jsp?cmsnoteid=CMS%20AN-2008/045.

[94] O. Charaf et. al., "Search for high mass resonances decaying into an electron pair in CMS at 10 TeV with 100/pb", 2009. http://cms.cern.ch/iCMS/jsp/db_notes/noteInfo.jsp?cmsnoteid=CMS%20AN-2009/097.

[95] S. Harper, "Study of shower shape variable s_eta_eta for electron ID", 2008. Talk given in EGamma meeting: https://indico.cern.ch/conferenceDisplay.py?confId=27560.

[96] S. Bolognesi, M.A. Borgia, R. Castello, C. Mariotti, , M. De Mattia, T. Dorigo, "Calibration of track momentum using dimuon resonances in CMS", 2010. http://cms.cern.ch/iCMS/jsp/db_notes/noteInfo.jsp?cmsnoteid=CMS%20AN-2010/059.

[97] S. Baffioni, C. Charlot, F. Ferri, D. Futyan, P. Meridiani, I. Puljak, C. Rovelli, R. Salerno, Y. Sirois, "Electron reconstruction in CMS", 2006. http://cms.cern.ch/iCMS/jsp/db_notes/noteInfo.jsp?cmsnoteid=CMS%20NOTE-2006/040.

[98] R. Ciesielski H. Held, P. Schieferdecker M. Zielinski, "Jet Energy Resolutions Derived from QCD Simulation for the Analysis of First sqrt(s)=7 TeV Collision Data", 2010. http://cms.cern.ch/iCMS/jsp/db_notes/noteInfo.jsp?cmsnoteid=CMS%20AN-2010/121.

[99] Finn Rebassoo, Sarah Eno, "MET resolution vs. sumEt in Minimum Bias 7 TeV events", 2010. http://cms.cern.ch/iCMS/jsp/db_notes/noteInfo.jsp?cmsnoteid=CMS%20AN-2010/142.

Acknowledgements

There are many people who made this work possible and I like to thank all of them. I will list some of them and I will for sure forget a lot of them, but that is not because I do not value them and their work. The list is in random order and without any particular hierarchy, just as you come to my mind.

I had a lot of fun, fruitful discussions and a great time working in close collaboration with: Paul Papacz, Stefan Schmitz, Mark Olschewski, Carsten Hof, Erik Dietz-Laursonn, Michael Brodski, Debbie Duchardt, Arnd Meyer, Kerstin Hoepfner, Markus Merschmeyer, Daniel Teyssier, Philipp Biallass.

A special thanks goes to my supervisor Prof. Dr. Thomas Hebbeker, who gave just the right mixture of freedom and guidance for years of both fun and productive work. I also like to thank Prof. Dr. Christopher Wiebusch for reviewing my thesis.

And then there are the countless people who did a lot of work and help me a lot: All current and past members of the CMS group of this institute. Those who kept the computers running, namely Andreas Nowack, Thomas Kress, Michael Bontenackels and Oleg Tsigenov. The CMS collaboration and particularly the EXOTICA physics group, and the PXL development team.

And last but not least I like to thank those who supported me at all times, my parents and Nicole, my love.